

Aus dem Institut/der Klinik für Neuropathologie  
der Medizinischen Fakultät Charité – Universitätsmedizin Berlin

DISSERTATION

**”Manipulating microglia in Alzheimer’s disease”**

zur Erlangung des akademischen Grades  
Doctor of Philosophy (PhD)

im Rahmen des  
International Graduate Program Medical Neurosciences

vorgelegt der Medizinischen Fakultät  
Charité – Universitätsmedizin Berlin

von

Gina Dji-In Eom

*aus Seoul, Südkorea*

Datum der Promotion: 4.9.2015 .....

## Table of Contents

Abstract	iii.
Introduction	p.1
1. <i>Alzheimer's disease</i>	
2. Clinical aspects of the disease	
2.1 <i>Epidemiology</i>	
2.2 <i>Genetic Risk factors</i>	
2.3 <i>Demographic factors</i>	
2.4 <i>Diagnosis</i>	
2.5 <i>Heritable forms of AD</i>	
3. <i>Disease etiology</i>	
3.1 <i>Pathophysiology</i>	
3.2 <i>Amyloid cascade hypothesis</i>	
3.3 <i>A<math>\beta</math> Production</i>	
4. <i>Murine models of AD</i>	
5. <i>Current and future treatment options in AD</i>	
5.1 <i>Current treatment options</i>	
5.2 <i>Experimental treatments relying on the amyloid hypothesis</i>	
5.3 <i>AN1972</i>	
5.4 <i>After AN1972</i>	
6. Neuroimmunological aspects of AD	
6.1 <i>Tissue resident macrophages</i>	
6.2 <i>Brain resident mononuclear phagocyte systems</i>	
6.3 <i>Microglia in AD</i>	
6.4 <i>Inflammatory environment in AD</i>	
6.5 <i>Microglia in AD immunotherapy</i>	
6.6 <i>Models &amp; tools for investigating microglia</i>	
Hypothesis and aim of this study	p.26
Methods	p.27
Materials, Tools, Software	p.43
Results	p.48
1. <i>Prevention study</i>	
2. <i>Interventional immunotherapy</i>	
3. <i>Antibody dosing studies</i>	
4. <i>Microglial depletion</i>	
5. <i>Effect of microglial depletion on neuronal physiology</i>	
6. <i>The role of microglia on AD immunotherapy</i>	

Discussions	p.86
Summary	p.105
References	p. 116
Statement	p. 119
Curriculum Vitae	p. 117
Publications	p.120
Acknowledgments	p.121

## **Abstract**

Despite some setbacks in clinical trials, vaccination strategies targeting beta-amyloid (A $\beta$ ) continue to be the most promising therapeutics for the treatment of Alzheimer's disease (AD). As the mechanism of antibody mediated A $\beta$  plaque reduction is not known, we compared the therapeutic efficacy of passive vaccination against A $\beta$  in a mouse model of AD in the presence or absence of microglia. Notably, we unequivocally identify these brain intrinsic immune cells as key mediators of antibody-triggered A $\beta$  clearance. The present experimental set up allows for the first time a cell-specific depletion of microglia in an in vivo A $\beta$  vaccination setting. In this way our findings will help to appropriately clarify results retrieved from ongoing A $\beta$  vaccination trials and aid the design of improved treatment strategies.

## **Zusammenfassung**

Angesichts der neu veröffentlichten Ergebnisse bezüglich der Stabilisierung der kognitiven Fähigkeiten von AD Patienten durch A $\beta$  Impfungen, ist es von großer Bedeutung, die Mechanismen der passiven Immunisierung weiter zu untersuchen und verstehen zu lernen.

Wir haben ein Behandlungsprotokoll etabliert, welches uns erlaubt, zeitgleich in gealterte AD-Mäusen Mikroglia zu depletieren und passiv zu immunisieren.

In dieser Monographie identifizieren wir eindeutig, dass diese Gehirn intrinsische Immunzellen als wichtige Mediatoren der Antikörper ausgelösten A $\beta$ -Klärung funktionieren.

Im Rahmen neu gewonnener Erkenntnisse hinsichtlich des Wirkungsmechanismus könnten in den nächsten Schritten durch etwaige Modifikation der Behandlung unerwünschte Nebenwirkungen vermieden werden.

## Introduction

### 1. *Alzheimer's disease*

Perhaps the most notoriously reputed form of dementia in popular culture, Alzheimer's disease (AD) has devastated over thirty million individuals and their families world-wide, and these numbers are rapidly spiraling upwards (1). Since its initial case report published by Alois Alzheimer over a century ago in 1906, the eponymous disease (AD) leaves the patient with little hope for a recovery. Put differently, in spite of incremental findings that have advanced our understanding of the disease, and in spite of more than 500 experimental treatments that have been proposed and tried (2–4), AD is still considered a terminal illness. To date, there is still no efficacious treatment or a cure.

Societal cost for the afflicted patient extends well beyond the requisite 24/7 round-about care at the late stage of the disease; it also takes a heavy social, emotional and physical toll on family members and caretakers (such as burnout from the patient's total dependence, and depression from social isolation) (1).

Needless to say, AD presents itself as a great health burden and is considered one of the greatest economic taxations in the 21<sup>st</sup> century(1,2) in the developed world. This is particularly attributed to the fact that the demographic composite in the first world is of an increasingly aging population. In the United States alone, it is predicted to tally up a medical bill of over 260billion dollars (180billion Euros) in year 2012(5).

For the patient, symptoms are detrimental on both the physiological and psychological level – most often starting gradually. These include impaired memory, confusion, emotional apathy, restlessness, altered and later on impaired behaviour, and language deterioration(2,5). Not uncommon is a personality alteration in the patient, and such a socially devastating element of the disease is exactly which paints it with a certain reputation and notoriety.

Over 99%(2) of AD cases are sporadic, meaning they do not have any faithful or predictable familial (vertical transmission) component. Most cases are typically diagnosed at a late stage in life (>65), while only a small percentage of individuals inherit AD like symptoms termed

familial Alzheimer's disease (FAD) via an autosomal dominant inheritance of a pathological genetic mutation, which usually manifests an onset much earlier in life (35-40 on average)(2). Early onset AD cases are mostly of this genetic form. Unless explicitly mentioned, the term 'AD' within the context of this thesis will refer to sporadic, late-onset forms of AD. FAD will be explicitly referred to as such.

## *2.1 Epidemiology*

The greatest risk factor for AD is age, the highest prevalence being in economically developed regions of North America and Western Europe where people generally have the longest lifespan (1). The rate and prevalence for dementia increases exponentially with age, with the most significant jump seen at the age of > 60 and 70 (1). It is thought that depending on a particular region's socioeconomic climate, different risk factors contribute differently to survival and to the prevalence and incidence of the disease(5). Segregating these various contributing factors is difficult and often context dependent on the particularities of the specific region. It is known that the incidence of AD is lower in less developed countries, but this is likely due to a shorter lifespan from other life threatening diseases which occur earlier on in life; in other words, other health threats supersede a chance for developing AD in these regions(5).

## *2.2 Genetic Risk factors:*

In addition to age (a non-genetic determinant of AD), the presence of  $\epsilon 4$  allele of the apolipoprotein E (ApoE) is a strong genetic risk factor for late-onset AD (6). Conversely, the  $\epsilon 2$  allele is associated with a lower risk factor for developing AD(7). The ApoE gene codes for the protein apolipoprotein E, which plays a role in lipid catabolism and its role in the brain is still an enigmatic question(8).

The exact mechanism behind this genotype effect on AD is unclear and is under active investigation. It is currently known that specific ApoE genotypes significantly influence the A $\beta$  economy – in terms of its production, catabolism, accumulation and clearance from the brain – by directing the process of fibrillogenesis of A $\beta$  peptides and thus influence the aggregation kinetics(9,10). There is also evidence that different ApoE genotypes affect clearance

mechanisms in the brain and the integrity of the vasculature(11). In relation to this, CAA and associated microhemorrhage are thought to be affected by ApoE types as well(11).

There is unequivocal gene dosing evidence that a significant percentile of AD patients possess at least one allele of ApoE4(12). In heterozygotes, the risk of the disease is 3 times higher for developing AD than non carriers; in homozygotes, the risk is 15 times higher(13). Influence related to glucose metabolism dysregulation via this ApoE4 allele has also been suggested(14), implicating metabolic demand in relations to AD. Taken together, this active field of investigation is still searching for more supporting evidence and data(8).

More recently, other genetic risk factors have been identified. Genome wide analysis studies (GWAS) have enabled powerful population based genetic analyses utilizing centrally archived material and data sets such as the Brain Bank in the United Kingdom(15). Such coordinated efforts of collecting between hundreds and thousands of subject samples have enabled statistical analyses with high P-values. These types of studies have identified a new series of risk variants associated with low risk, such as complement receptor 1 (CR1)(16) and TREM2(17,18).

Using this GWAS analysis with an expanded search algorithm, analysis of an Icelandic population has revealed that there is a protective mutation “against AD”, of which a carrier is much less likely to acquire AD(19). When looking for rare allele variants of the APP gene with a significant effect on the risk for Alzheimer’s disease, Kari Stefansson and his colleagues found a coding mutation in the APP gene (A673T) that conferred a significant reduction in the prevalence of AD and also cognitive decline(19). In vitro there seems to be a 40% reduction of A $\beta$  in vitro production(19).

Likewise approaches were used by two independent studies to identify a low prevalence risk variant of TREM2 as a major risk factor for late-onset AD(17)(18). TREM2 is a marker found mainly on tissue-resident myeloid cells, with known functions including phagocytosis of bacterial material, and downstream effector molecules being involved in immunomodulation. It is hypothesized that a specific activation state of brain-resident microglia is modulated by

TREM2, highly influencing AD pathology by determining brain microenvironment and susceptibility, for example by affecting A $\beta$  accumulation.

### *2.3 Demographic factors:*

Eventhough twice as many women currently live with AD, there is no conclusive evidence as to whether there is greater risk of developing AD by being a woman. Women simply live longer(5), which explains their greater proportion of the AD patient pool as age remains the greatest risk factor for AD.

There is also no known ethnicity skewing, although the disease is underdiagnosed in minorities such as African (or African American) populations living in Western nations (US or Europe).

Interestingly, years of education seems to be a major negative risk factor for AD as well as other dementias, suggesting that a certain level of cognitive training might be beneficial in preventing AD (20). It has been shown that resting state accumulation of metabolic demand results in a sloppy/slothy clearance, whereas the active redirection into other brain centers of energy demand results in lower A $\beta$  accumulation(21).

Underlying conditions such as high blood pressure & diabetes have been shown to increase risk for AD, and these conditions tend to be more prevalent in lower socioeconomic groups (1,5).

### *2.4 Diagnosis:*

Neurologists are now able to diagnose AD with a high accuracy(22). Diagnosis is based on taking thorough medical history, as well as a thorough report from a close companion on their observed changes of the patient. Mental status testing is performed, as well as physical and neurological examination. Although the practice of diagnosing AD used to rely heavily on differential exclusions, more recently it has started to rely heavily on the history taking particularly through the informant, which has significantly driven up the recent diagnostic accuracy(22). Table 1 summarizes the typical symptoms observed that help make the diagnosis of a patient.

The Alzheimer's Association, a non-profit American health organization in conjunction with the NINDS/NIA (National Institute of Aging) continuously update the diagnostic criteria in a timely fashion incorporating recent clinical research findings in order to improve diagnostic accuracy and establish earlier, more reliable detection of the disease.

To date, the 1984 diagnostic criteria established are under review, and new Diagnostic Criteria have been recommended in 2011 (23). The diagnostic criteria (1984 modified last in 2007) include detectable cognitive impairment parameters established via neuropsychological examination, and the possibility of imaging in order to establish definite diagnosis.

Only with the recent onset of imaging techniques has it been possible to diagnose someone definitely while the patient is still alive. Fluorbetapir and its predecessor Pittsburgh Compound B label amyloid plaques in the brain, visualized with PET imaging. Historically, only post mortem histology has allowed for a definite diagnosis.

A $\beta$  plaques can now be detected by means of brain imaging in patients, through a fluorescent, C<sup>11</sup>-radiolabelled amyloid-binding agent Pittsburgh compound B (PiB) detectable by PET scan(24), which is available for research studies. The FDA has approved a F<sup>18</sup>-labelled PiB-derivative compound in April 2012 called florbetapir (Lilly), which due to a longer half life allows for a clearer detection of amyloid load in the brain(25).

### *2.5 Heritable forms of AD*

As stated previously, FAD is a rare form of AD, and almost unequivocally all cases occur in the form of early onset form of AD. Whilst the symptoms presented closely mimic sporadic Alzheimer's disease, a clear heritable autosomal dominant mutations have been shown to be the cause of AD. The genes associated with FAD are genes with high penetrants encoding amyloid precursor protein (APP), or APP modifying proteins presenilin 1, and presenilin 2 (2).

<b>Clinical stages</b>	<b>Typical signs &amp; symptoms</b>
<b>Very mild cognitive decline</b>	The person experiences memory lapses but this is not obvious to the neurologist upon medical examination. Companions do not notice any changes.
<b>Mild cognitive decline</b>	Increasing problems with memory, for example remembering the names of newly met people. Short term memory decline such as remembering what a person just said. Trouble with planning or organizing, which progressively gets worse. Misplacing objects of value with increasing frequency.
<b>Moderate cognitive decline</b>	Person can no longer live on their own. Forgetfulness worsens to the point where one's personal history becomes unclear. Confusion, inability to perform mental arithmetics, complex tasks such as organizing or meeting deadlines become very difficult. At this point usually mood changes become apparent.
<b>Severe cognitive decline</b>	Loss of awareness of surroundings, requiring help in daily activities such as meals or hygiene.

Table 1 Clinical stages of AD and corresponding typical signs and symptom. Source: Alzheimer's association 2012 report (5)

### 3.1 Pathophysiology

AD is marked with pathophysiological hallmarks distinct from other diseases of dementia. These include accumulation of senile extracellular plaques in specific regions (hippocampus, endorhinal cortex, and later the neocortex), with subsequent intraneuronal tangle formation, and ultimate atrophy of brain (white) matter. A definite diagnosis of AD is done by confirmation of A $\beta$  plaque accumulation and intraneuronal tangles post-mortem, or more recently by amyloid imaging as mentioned above.

An early detection of abnormally high levels of A $\beta$  accumulating in the brain accompanied by its decreased detection in cerebrospinal fluid (CSF) is thought to be a key initiator of the disease (26).

The A $\beta$  plaques are often described to be heterogeneous in their morphology, and this is also reflected in some of their histological profiles. Loosely aggregated plaques are sometimes described as “cottonwool plaques” due to their relatively large diameter and rather fluffy appearance, lacking a dense amyloid core. Core plaques stain in a denser fashion for amyloid and are generally also denser in appearance. In patient material, often a darkly stained region in the centre of a plaque is identifiable as the plaque core.

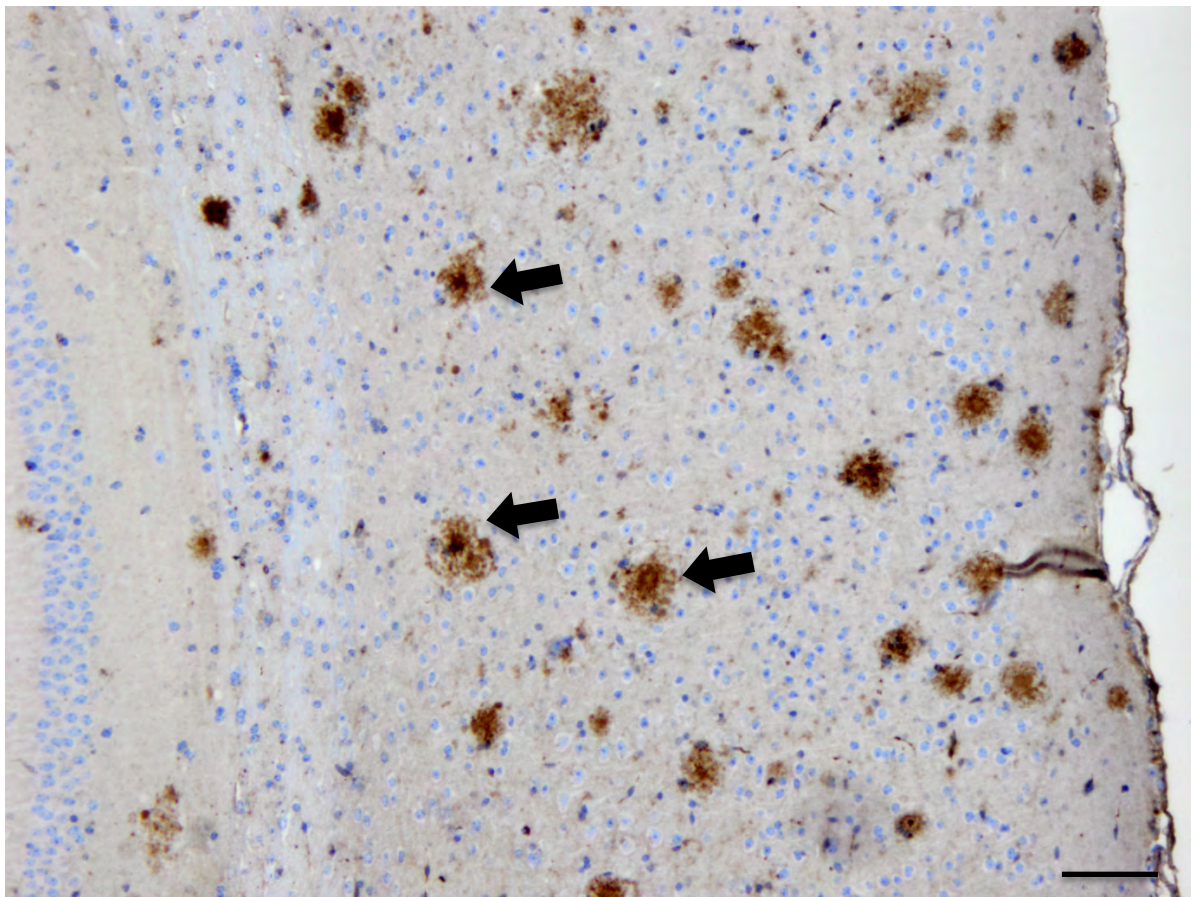


Figure 1 Representative immunohistochemistry stain for A $\beta$  in APPS1 mice in the cortex. Dense cores are seen surrounded by more loosely aggregated A $\beta$  in many plaques. Scale bar = 50um.

A $\beta$  plaques are surrounded by astrocytes and microglia forming a “wall” around the plaques, and these glial cells display a reactive morphology, with thickened processes.

It is thought that the sequestration of A $\beta$  into these senile plaques that cause a sharp decrease in its clearance rate, as a seeding process is initiated. Subsequently intraneuronal tangles occur, which consists of abnormally phosphorylated tau-protein. Phosphorylated tau protein can be detected in CSF samples in AD patients, but this event usually occurs after the alternation in A $\beta$  levels in the brain and in the CSF(26).

Both events (senile plaque formation and intraneuronal tangles) usually occur many years before onset of cognitive alterations. It is important to note that A $\beta$  accumulation as plaques is currently the earliest known alteration in the disease course of AD.

Although senile plaques are mainly composed of A $\beta$  peptides of different lengths (27), including pyroglutinated A $\beta$  thought to be exclusively found in these plaques, what other potential peptides or substances comprises a senile plaque is an ongoing field of research. However, the majority of the component of senile plaques is A $\beta$  (as shown biochemically, genetically, pathologically).

How exactly A $\beta$  accumulation in the brain leads to neurofibrillary tangles is a topic of mere speculation(28), since little evidence has come forward to shed light on this important question. Moreover, various theories on the mechanism of neuronal death by means of A $\beta$  accumulation have been proposed with accompanying research evidence, but there is currently no concrete consensus for a definite process. Thus, our knowledge on the pathophysiology by which Alzheimer's disease leads to the symptomatic memory loss, especially how neurodegeneration occurs, is still at its infancy.

What we know from the genotypes of FAD patients is that APP mutations are definite causes for the disease at least in this particular type of AD, and that this is the determining factor for the subsequent pathological hallmark events. Notably the early rise in A $\beta$  accumulation in the brain by way of plaque formation has now been confirmed with biomarker detection in these patients in a pattern that is strikingly similar to that of sporadic AD cases(29). It is also known from these patients that the APP mutation or a component of APP processing (PSEN mutations) is sufficient to cause subsequent pathological events of AD including

neurofibrillary tangle accumulation intraneuronally, as well as neurodegeneration (brain atrophy (26)).

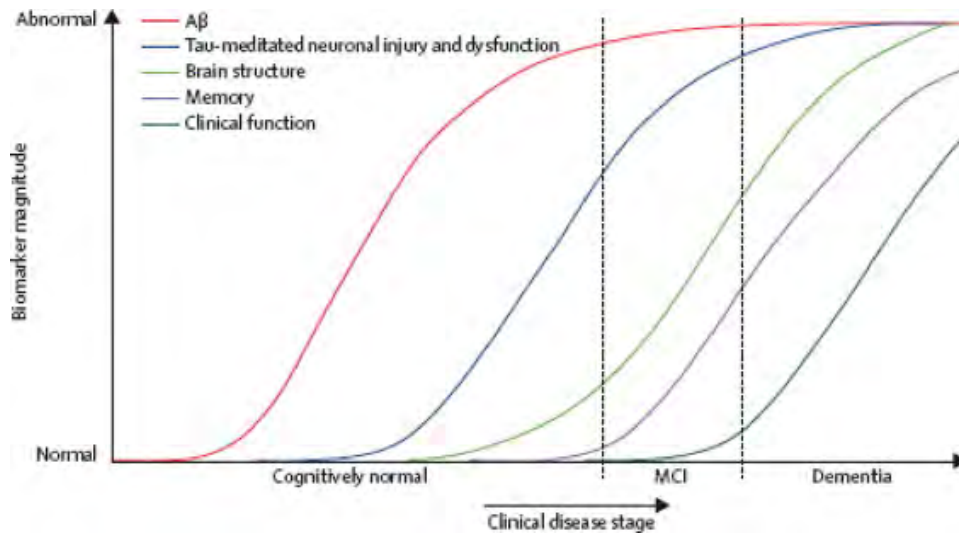


Figure 2 Model of dynamic biomarker appearance in the pathological progression in AD. Source: Jack C et al 2010 (26). MCI= mild cognitive impairment. Depiction of observed biomarkers in sequence of pathological events seen and measured in AD patients.

### 3.2 Amyloid cascade hypothesis

The amyloid cascade hypothesis is currently the most widely accepted hypothesis on disease manifestation, and it places A $\beta$  accumulation as the key initiator of subsequently observed pathophysiology in AD. According to this hypothesis, the disease unfolds slowly and progressively over a course of years – and more often decades (Figure 2).

The hypothesis states that as A $\beta$  accumulates in the brain and throws brain homeostasis off balance, it triggers a multifaceted cascade of physiological responses and reactions, which ultimately lead to the observed neuronal death (brain atrophy) and cognitive decline.

Downstream events from A $\beta$  accumulation are controversial. There is supporting evidence that A $\beta$  conformation plays an important role in altering synaptic plasticity, ultimately altering memory functions (30). We also know that APP, the parent protein of A $\beta$  has a role early on in development in engaging certain death receptors only found in axons(31). We furthermore know that A $\beta$  is a reactive sterile inflammatory trigger for immune and glial cells

– including microglia and astrocytes in the brain(32). The release of proinflammatory cytokines such as TNFalpha, IL1b and reactive oxygen species may further contribute to neuronal damage (32,33). Much more research has to be done to either validate or elucidate alternatives to these proposed mechanisms of damage to the brain. Figure 3 depicts a current hypothetical model of the cascade.

There is also supporting epidemiological evidence for the amyloid cascade hypothesis: the fact that the genotype of APP (the parent protein of A $\beta$ ) is an important risk factor and being able to either confer an aggressive type of early onset AD (FAD) or in the aforementioned “protective” genotype of this protein(19) even confer lower risk of developing AD seems to suggest that it is a major trigger for the disease.

Furthermore, impaired clearance of beta-amyloid(34) showed that AD patients clear A $\beta$  30% less effectively, contributing to a build-up of A $\beta$  plaques and further rendering support for the amyloid hypothesis(34).

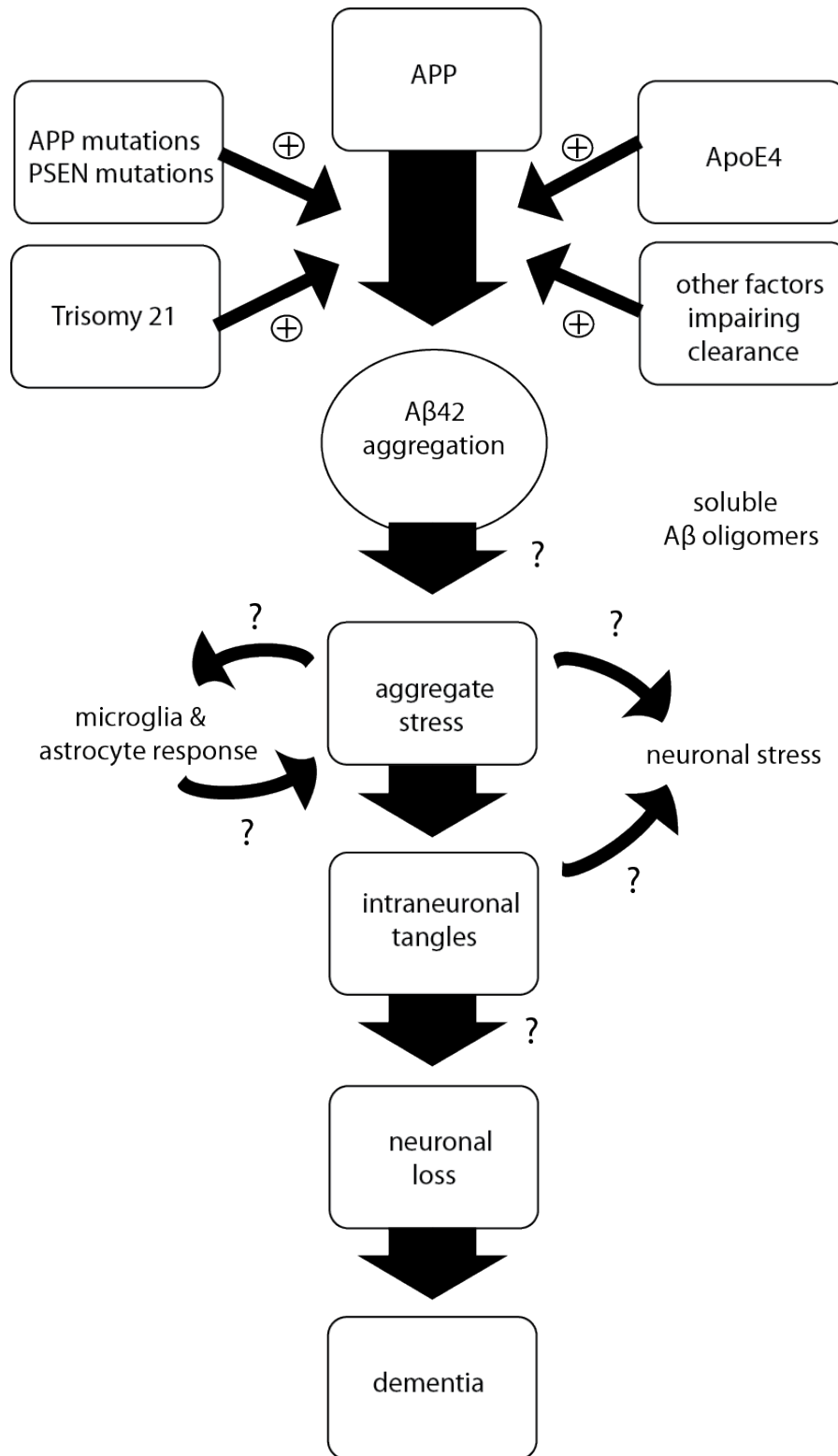


Figure 3 Amyloid cascade hypothesis as postulated by Selkoe D and colleagues(30). APP processing can be influenced by genetic mutations in members of the processing cascade, and an imbalance of Aβ is regarded as the initiating event of AD. Downstream events of Aβ misfolding and aggregation is the formation of intraneuronal tangles, neuronal death and ultimately dementia in patients.

### *3.3 A $\beta$ Production:*

A $\beta$  production is a normal physiological process which occurs by the sequential proteolytic cleavage of its transmembrane parent protein APP(31). The two key enzymes involved in the cleavage of APP are called beta secretase and gamma secretase. These two enzymes produce the beta-cut and the gamma-cut (Figure 4), which release the hydrophobic and amyloidogenic A $\beta$  portion of the parent protein, as well as two other cleavage products (AICD and sAPP $\beta$ ).

APP can also be processed in a “non” amyloidogenic route through a series of cleavage enzymes known as alpha secretase, producing the alpha-cut, and gamma secretase (Figure 4). One of the products of the non-amyloidogenic route, sAPP $\alpha$ , has been shown in several studies to be lowered in AD(35), suggesting that this pathway is perhaps downregulated or impaired in the disease.

Recently, A $\beta$  has been the major focus on AD research due to the fact that it has been shown to be produced at “normal” levels when comparing AD patients to controls, however it is the clearance rate of A $\beta$  that has been shown to be impaired(34). Between A $\beta$  subspecies A $\beta$ 38 to 42, A $\beta$ 42 is known to be the most aggregation-prone. This is reflected in this study(34) where there is a greater impairment of A $\beta$ 42 clearance in AD patients.

Endogenous APP function is not described very well as of yet, although it’s known that it’s expressed highly in development and there is evidence of involvement in cell survival, neurite outgrowth, synaptogenesis, plasticity, memory, neurogenesis, cell adhesion, and neuroprotection(31). However, murine models of APP gene knock-outs show only a very modest phenotype, rather being compensated by APLP 1 and 2(36).

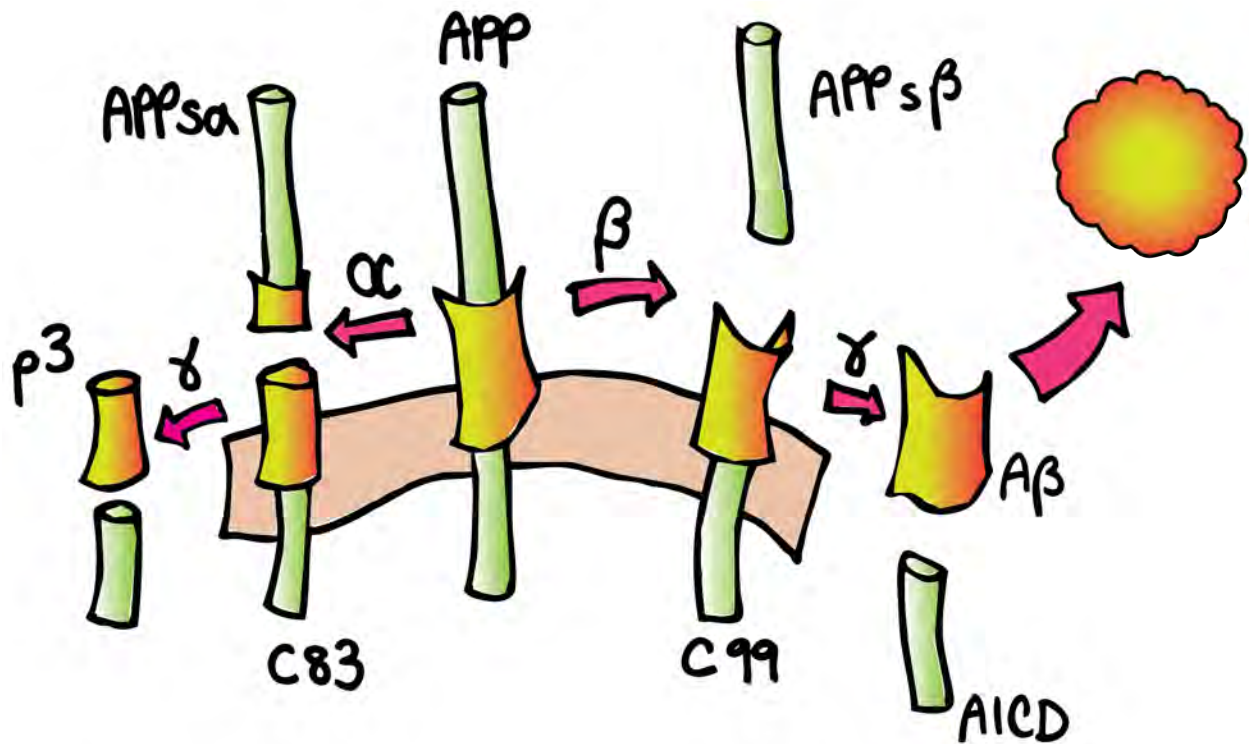


Figure 4 APP cleavage pathways(2) involving difference enzymes. Two cleavage pathways are depicted, the alpha cut producing p3 and AICD, whereas the  $\beta$  and  $\gamma$  cut produce AICD and A $\beta$ , which has its hydrophobic domains exposed, more likely to seek likewise hydrophobic counterparts for aggregation into plaques.

#### 4. Murine models of AD

There is a dearth of a natural murine model for AD, as the disease seems to be specific to higher evolved species with a relatively longer lifespan(37).

Familial forms of AD have faithfully recapitulated the pathology and clinical symptoms of sporadic AD, hence the definite genetic mutation found in FAD have been used as a tool to introduce AD-like pathology into the murine model(37).

The most commonly used model is a transgenic mouse harbouring the Swedish mutation (APP 671KM/NL) that is found in a Swedish family of FAD(37,38). These transgenic (tg) human (hu) APPsw mice end up with A $\beta$  plaques in the brain parenchyma (often recapitulating the areas where AD patients also have the greatest build up of plaques – such as the cingulate cortex, hippocampus and neocortex (39)).

There are at least 25 known genetic mutations in APP that cause FAD, and over 170 for either PSEN1 or PSEN2 (coding for presenilin 1 or 2, respectively)(37). Coexpression of APP with a PSEN1 mutation (“APPPS1”) results in a rapid acceleration of A $\beta$  plaques, and increases the amyloid burden in these mice. Importantly, it also skews the A $\beta$ 42 to 40 ratio greatly towards more aggregate-prone A $\beta$ 42.

Murine models of AD currently recapitulate only some facets of the disease. While an APPPS1 mouse can faithfully recapitulate cerebral amyloidosis, it does not result in neurofibrillary tangles, nor is there significant enough neuronal loss to see any overt brain atrophy of that of AD patients(39).

Currently some murine models also address neurofibrillary tangle formation by creating triple transgenic lines with a mutation in the tau gene, as well as transgenic APP and PS1 mutations(40).

However, there is currently no known familial AD form which harbours this tau mutation, and thus data obtained from this taupathy model is considered to be translationally questionable(37,41).

Furthermore, the fact that the pathogenic huAPP transgene alone does not result in downstream neurofibrillary tangle formation or overt neuronal loss (whereas in FAD patients these event occur faithfully), beckons the question as to whether the mouse is an appropriate host system to study the disease in.

Nonetheless, it can be argued that paradoxically there is an advantage to studying cerebral amyloidosis in an “isolated” setting. Since it is becoming more and more accepted that A $\beta$  is a key initiator of events, studying the physiological events unfolding during A $\beta$  plaque build up may render valuable information and new therapeutic avenues.

Taken into consideration all the caveats of the translational animal models, it is currently considered a gold standard to utilize several murine models of AD to confirm the robustness of a finding.

### 5.1 Current treatment options

The diagnosed patient is left with few options: current treatments on the market have shown modest response to improving cognitive symptoms at best, and recent studies even cast doubts on their efficacy. There is currently cure.

Drug name	Drug type	Approved for	FDA approved	EMA approved
Donepezil	Cholinesterase inhibitors	All stages of AD	1996	
Galantamine	Cholinesterase inhibitors	Mild to moderate	2001	2000*
Memantine	NMDA receptor agonist	Moderate to severe	2003	2002*
Rivastigmine	Cholinesterase inhibitor	Mild to moderate	2000	1997*
Tacrine**	Cholinesterase inhibitor	Mild to moderate	1993	

Table 2 Currently approved drugs used in treatment for AD patients (December 2012). Source: Alzheimer's Association 2012 report and EMA 2012 report.

\* delays in some EU member countries

\*\* rarely prescribed today due to association with more serious side effects compared to other drugs in this class

### 5.2 Experimental treatments relying on the amyloid hypothesis

Numerous lines of experimental treatments continue to enter clinical trial phase after showing efficacy in animal models of AD. A significant portion of these has relied on components of the amyloid hypothesis as therapeutic targets(3). These include gamma secretase inhibitors, beta secretase inhibitors, and antibodies against beta-amyloid to offset the amyloidogenic pathway in general. However, success has been marginal in all of these trials.

High hopes had been placed on gamma secretase inhibitors, however in August 2010 the

most coveted drug of that class, Semagacestat, was discontinued abruptly due to unexpected results – the large cohort of thousands of patients who were enrolled in this trial showed on average an increased decline in cognitive function and were faced with a greater risk of skin cancer when compared to placebo treated AD patients (42).

Beta secretase inhibitors started to enter Phase II of clinical trials as of August 2012 (43).

Other treatment strategies have been NSAIDs and IVIg to immunomodulate the disease. Company Baxter's IVIg treatment Gammagard has shown a three-year stabilization in cognition in treated patients when compared to placebo treated controls, however there was no amelioration in cognition and their clinical endpoints failed to be met (44).

### 5.3 AN1972

Dale Schenk and colleagues showed that it was possible to immunize against A $\beta$  by injecting the peptide with an adjuvant to murine models of amyloidosis(45). Active immunization has the clear advantage of conferring memory of the immune system, continuing to raise a steady immune response against its unwanted target in the body.

These young AD mice were vaccinated at the early age of 6 weeks and the brain was analysed for pathology much later at 11 months. Actively immunized mice when compared to control mice showed significantly lowered A $\beta$  load in the brain (45).

Immediately following this surprising report, a rush to bring this treatment to patients was implemented in a multinational active vaccination trial known as AN1972. 300 patients were injected with adjuvant (QS21) containing emulsion of synthetic A $\beta$ 42, and compared to placebo treated controls patients(28,46).

In 2002, the trial had to be halted abruptly as 6% of the patients (18 out of 300) developed aseptic meningoencephalitis as well as leukoencephalopathy(46).

Much speculation has been made around the reasoning of this side effect, and it has been

proposed that the C-terminal region of A $\beta$ 42 elicits a human T cell response, whereas the N-terminal portion is more likely to be B-cell responsive(47).

#### *5.4 After AN1972*

Second generation active and passive immunization strategies have rolled out since the initial setback of AN1972 with modifications to the protocol to avoid these unwanted side effects observed in the initial trial (Table 3).

Several of these newer treatment candidates failed to meet their endpoints past Phase II and have been terminated early. Two examples of these prematurely halted experimental drugs are GSK933776A from GlaxoSmithKline (48) and Ponezumab from Pfizer (<http://clinicaltrials.gov/ct2/results?term=PF-04360365>).

Furthermore, Solanezumab (Lilly) and Bapineuzumab (Pfizer/Janssen), both of human isotype IgG1 against A $\beta$ aa16-24 and A $\beta$ aa 1-5 respectively, had concluded Phase III of clinical trials in 2012(3,4). Bapineuzumab had modified its treatment protocol after discovering dose dependent frequency of vascular related imaging abnormalities, discontinuing its highest treatment dose(49). Although these imaging abnormalities were not accompanied by significant or distinct symptoms (there were some reports of headache and confusion), it was still deemed necessary to err on the side of caution(49).

In September 2012 it was revealed that although there was target engagement in Bapineuzumab (for example, a significant decrease in phosphorylated tau in CSF) the drug failed to meet its endpoints and thus was discontinued. The manufacturer Janssen/Pfizer has rolled out a related antibody, AAB-003, where the hinge region (Fc) of the antibody has been mutated at three points, claiming to engage microglial Fc receptor and C1q to lower affinities(48). Vasogenic edema observed in the higher doses of Bapineuzumab is hoped to be thwarted by making these modifications.

In the same spirit, another company has manufactured an anti A $\beta$  antibody of isotype IgG4, which is thought to engage to the target with lower affinity, procuring a dampened microglial response(50).

Solanezumab (Lilly) also did not meet its target end points after their Phase III trial, however a post-acquisition analysis conducted by university researchers revealed that there was a significantly slowing of cognitive decline in the mild-cognitively impaired patients, but not in the moderately impaired cohort(51).

Drug name	Company	Type of Drug	Trial Phase	Comments
CAD106	Novartis	A $\beta$ 1-6 + virus-like-particle (VLP)	III	active
Affitope AD02	Affiris	Mimitope A $\beta$ 1-6	II	active/mimitope
UB311	United Biomedical	A $\beta$ 1-14	II	active
ACC-001+QS21	Wyeth	A $\beta$ 1-7+ carrier	II	active
Crenezumab	AC Immune /Genentech (Roche)	IgG4	II	passive enrolled for API
Gantenerumab	Roche	IgG1	II	passive enrolled for DIAN
Solanezumab	Lilly	IgG1	III did not meet target endpoints	passive enrolled for DIAN and A4
AAB 003	Pfizer/Janssen	IgG1 against A $\beta$ 1-6 + 3 mutations of the heavy chain hc constant region	II	passive

Table 3 A $\beta$ -targeting immunotherapies in clinical trial (up to date on January 2013). DIAN, A4, API are new collaborative Alzheimer's prevention trials. DIAN works with FAD patients on a multinational level and is thought to involve hundreds of patients per trial arm. A4 administers A $\beta$  antibodies to one thousand healthy individuals who have signs of amyloid deposition but no signs of cognitive impairment. API works with a Colombian FAD family living around Medellin in treating them a decade before predicted onset of disease.

### 6.1 Tissue resident macrophages

Our physiological system has adapted and evolved mechanisms able to respond to insults onto a specific region rapidly and efficiently. Tissue resident macrophages throughout the body have been shown to be the first responders in the event of an insult, acquiring an activated phenotype, and recruiting further downstream immune reactions(52–54). For

instance, during a respiratory infection, alveolar macrophages secrete a significantly higher amount of respiratory burst compared to other macrophages(55,56). They are also highly specialized to rapidly recruit neutrophils and blood borne macrophages for a full-blown immune response. Paradoxically, they are kept extremely quiescent in a non-diseased setting. Therefore, alveolar macrophages are unique in that they are capable of undergoing extreme ranges of activation states(56).

Tissue resident macrophages have not been acquired at the same time throughout all organs. In fact, during embryogenesis the hematopoietic compartment migrates onto different juncture points: in the murine system, it migrates from the yolk sac to the liver, and from the liver to the bone marrow(54). These stages are thought to be part of a maturation program of the hematopoietic system(54).

Since tissue resident macrophages are acquired at different stages throughout development depending on the tissue, each compartment has recently shown to not necessarily be of same origins. In the case of the brain, formation of the blood brain barrier is an event that thereafter seals off massive cellular infiltration under non-diseased, physiological conditions(54,57,58). Thus, immigration of microglial precursor cells happens before this maturation of the nervous system. Recent ontological studies have identified that microglia arise from primitive macrophage precursors in the yolk sac and migrate into the neural tissue region of the embryo. The same pool of primitive precursor cells gives rise to Kupffer cells, but other tissue resident myeloid cells arise from a more mature precursor cell type in the murine setting(54,57).

Postnatally, hematopoietic precursors are thought not to contribute in replenishing the CNS parenchyma with microglia under physiological conditions. Instead it is believed the microglial compartment is self-renewing(54).

<b>Tissue resident macrophages</b>	<b>Host organ</b>	<b>Ontological origin</b>	<b>Known function</b>	<b>Pathology</b>
Microglia	Brain	Yolk sac	neuronal patterning, fluid balance	NeurodegenerationAM(54,59–61)
Osteoclasts	Bone	Bone marrow	bone remodelling;	Osteoporosis, osteopetrosis(60,62)
Kupffer cells	Liver	Yolk sac	Lipid metabolism, toxin removal	fibrosis(59,60)
Alveolar macrophages	Lung	Bone marrow	First line of defense debris removal, lung remodelling(56)	Not found
Red pulp macrophages	Spleen	Bone marrow	Removal of senescent red blood cells	Disrupted iron homeostasis(63)
Marginal metallophilic macrophages	Spleen	Bone marrow	Lymphoid tissue like function, antigen presentation and entrapment	Disrupted cell population in different types of leukemia(64)
Bone marrow macrophages	Bone marrow	Bone marrow	haematopoiesis(62)	leukemia

**Table 4 Tissue resident macrophages and their ontological origin, function in the host tissue, and issues of pathology. This table is not comprehensive of all tissue resident macrophages but rather displays a select prominent populations in order to illustrate their range in specialized function depending on their host environment.**

Besides immunosurveillance, tissue resident myeloid cells take on specialized functions of its host organ, thus also contributing to day-to-day homeostatic maintenance (Table 4).

Functional implications of these heterogeneous origins on the host tissue remain an open question. Whether the macrophages arising from mature hematopoietic compartment (in the bone marrow) is different compared to yolk sac macrophage precursor is not known(59). Are

there functional repertoires of tissue resident macrophages (such as microglia and Kupffer cells) with more primitive origins, that they do not possess? Or are there evolutionary advantages of debris clearing cells from primitive ontologies? There are many open questions in this field.

### *6.2 Brain resident mononuclear phagocyte systems*

The adult brain contains a heterogeneous population of mononuclear phagocytes: these include perivascular macrophages occupying the perivascular space, and microglia, which form the majority of brain resident mononuclear phagocytes and are usually distributed in a non-overlapping fashion in the brain parenchyma(65).

Microglia become activated upon insult and take on a hypertrophic morphologically distinct phenotype. Processes swell up and the cell body becomes amorphous and processes hypertrophy(52).

While microglia were considered to be dormant during a state of good health, it has been recently shown that under physiological conditions, microglial processes survey and sample the parenchymal space in a systemic fashion, protruding and retracting its processes rhythmically and not overlapping with a neighbouring process (66). It was therefore determined that microglia are highly versatile and sensitive to very subtle perturbations in the brain environment and constantly monitor it in a systematic fashion(67). This modern belief drastically departs from the previous notion of microglia “resting” during non-diseased times in the brain.

### *6.3 Microglia in AD*

Microglial cells form a wall around A $\beta$  plaques, and their morphology is distinct from non-plaque associated microglia. Their processes are polarized towards the plaque border and they tend to be thicker.

A highly debated topic of interest is the interaction between the brain resident immune compartment and the accumulated A $\beta$  peptide content in the brain. Theoretically, debris clearing, ie. scavenging function – hallmark functions of the tissue resident mononuclear phagocyte system (MPS) should be involved in clearing the misfolded protein deposits(52). Microglial aptitude to internalize A $\beta$  has been demonstrated *in vitro* and *ex vivo*.

On the other hand, their ability to be polarized/activated to release proinflammatory cytokines/ or any cytokine profile that exacerbates neurotoxicity “inflammation” and damage may be harmful and thus contributing to pathology. Recent evidence has shown that the repetitive structure from fibrillized A $\beta$  activates pattern recognition receptors on microglia, triggering a proinflammatory cascade that exacerbates plaque burden as well as neuronal damage and behavioural outcome in AD mice(68–70).

It has been shown that complement is increased in AD patient brain(71) upon post-mortem histopathological analysis and it has been thought that microglia and astrocytes that take on an abnormal dystrophic morphology and are somehow involved in the complement producing and responsive process. Whether or not complement upregulation in AD brains is harmful or beneficial is still controversial (72).

Thus, microglia propagate inflammation and/or participate in clearance of built-up pathologic protein. These two seemingly contradictory dual roles of the immune compartment in the brain have baffled researchers and have fuelled debates in the community for a long time. It is only recently that evidence has come to light offering elucidating evidence addressing this question in more detail(70,73–76).

#### *6.4 Inflammatory environment in AD*

Increasing evidence points to the possibility that an “overshot” production of inflammatory mediators(17,75) and reactive oxygen species from microglia and the mononuclear phagocyte compartment may drive the chronic inflammatory process through or causing dysfunctionally

programmed microglia (17,77)

Recent studies show that even a peripheral proinflammatory environment may be detrimental for plaque pathology later on and sets up (“primes”) a system more likely to exacerbate plaque burden(73,75).

### *6.5 Microglia in AD immunotherapy*

Immunotherapy in Alzheimer’s disease has moved forward in clinical trials for decades, with setbacks and only modest successes(3,4,28). Nevertheless, the insights that have been revealed from the trials has refined our understanding of the disease and continued to fuel hope for treating the disease with greater efficacy.

In spite of decades of trials involving strategic targeting of A $\beta$  using antibodies, there is a dearth of knowledge on the mechanism of action of the treatment types. Furthermore, there is limited evidence as to how the reported side effects are elicited by this type of treatment.

### *6.6 Models & tools for investigating microglia*

Primary microglia have been used in the past from neonatal brains and kept in culture. In vitro conditions are at times artificial and limited in the applicability of the data gained, as the microenvironment of the in vivo setting is poorly recapitulated. It is in the interest of the experiment therefore to work with primary microglia quickly, or to recreate the microenvironment of the setting of interest, for example by exposing primary microglia to brain slices.

The use of chemicals in order to deplete microglia have also been used. The most common is minocycline, an antibiotic with known immunomodulatory functions. Minocycline has been successful in dampening and downregulating microglial function, reducing its inflammatory reaction when challenged(78). It has, besides its antibiotic function, an additional effect on T and B lymphocytes as well, thus shifting the entire baseline of the immune system(79).

A few studies have used Mac1-saporin to deliver an apoptotic trigger to microglia specifically, however the depletion success is not reported and seems to vary (80). Clodronate

Several murine models exist to study microglial functions in vivo(60). Fractalkine knockout mice(81) have microglia with limited motility compared to wild type microglia. It is possible to study the effect of fractalkine signaling and microglial motility with these mice. However since they have had this gene deleted since birth, it is not possible to exclude that any phenotype observed in the mouse is also dampened by compensatory mechanisms.

Cell specific ablation approaches can now be used on transgenic mice that harbor genetic depletion constructs, such as diphtheria toxin sensitive- or herpes simplex virus thymidine kinase – containing constructs. CD11b-DTR mice are sensitive to diphtheria toxin and the receptor is not expressed anywhere in the body except in CD11b expressing cells(60). To my knowledge there has not been a study to date that has utilized this model in order to deplete microglia, although it has been widely used to ablate other CD11b-positive macrophage compartments in the periphery(60). The disadvantage of treating mice with diphtheria is that they can develop an immunological response against it, thereby skewing the entire immune response inadvertently(82).

Two versions of the CD11b-HSVTK transgenic mouse have been developed in order to ablate microglial cells upon the addition of ganciclovir(83,84). Both reports show a significant depletion of microglial cells and thus are an effective tool to study general microglial function. The off-target effects of ganciclovir are not well characterized and thus have to be well controlled.

It has been speculated that using such a cell ablation approach may cause cytotoxic damage, releasing danger signals(85). While these studies have been performed in cell culture, in vivo monitoring upon GCV exposure is recommended.

Microglial biology is plagued by the lack of a unique receptor or antigen which allows the researcher to discriminate microglia from macrophages via histology, gene signature or

transcriptional profile. While Iba1 is a commonly used histological marker for microglia, peripheral macrophages also stain for Iba1(86).

## **Hypothesis and aim of this study**

Here, I used a therapeutic paradigm in AD mice by which an A $\beta$  targeted antibody was administered in order to remove plaque burden. Simultaneously I ablated microglia in these mice in order to study the functional role of microglia in this treatment class in AD. I sought to address whether A $\beta$  immunotherapy has a mechanistic component that relies on microglia.

Put another way, I sought to address whether plaque removal by this class of treatment can be dependent on microglia, and whether microglia can be prompted to efficiently remove A $\beta$  in vivo.

## Methods and Materials

### *Experimental Mice*

*APPS1* mice transgenically overexpressing the human Swedish (KM670/671NL) APP mutation and a Presenilin 1 mutation under the Thy1 promoter were used for this study(39).

Hemizygous males from each line were mated/crossed to hemizygous *CD11b-HSVTK* females (84) to produce *APPS;TK+* double transgenic or *APPS;TK-* "control" offsprings.

*APP23* mice overexpressing only the human Swedish (KM670/671NL) APP mutation under the Thy1 promoter were used as a second mouse line for this study(87). Hemizygous males from each line were mated/crossed to hemizygous *CD11b-HSVTK (TK)* females to produce *APP23;TK+* double transgenic or *APP23;TK-* "control" offsprings(88). Male mice of this line, due to their known aggressiveness after 12 months of age(89), were kept in individual cages. This mouse line also showed high mortality in both genders after 12 months of age.

All mice were kept in a 12 h/12h dark-light cycle, under controlled temperature and humidity, and allowed food and water *ad libitum*. Mice were age-matched for all experiments, and all experiments were carried out in accordance with the guidelines of the animal welfare and safety regulations of the State/City of Berlin and FELASA (license numbers O0129/09, T0276/07, G0154/08, L0366/11).

Special attention was placed on mouse husbandry of these mice in order to accommodate for the challenging breeding of *TK+* mice(83,84). It is known that *TK+* males are sterile due to their defect in spermatogenesis(90), and in addition we experienced challenges in milk production of the *TK+* mothers.

To address these issues, I implemented the use of CD1 outbred mice into the breeding facility as foster mothers for both of the double transgenic mouse lines. Since CD1 mice are albino, they could easily be distinguished by colour from the transgenic mouse lines on black-6 background. More importantly, the CD1 mice were an outbred strain, displaying greater

characteristics suitable for taking on foreign pups: more docile, less aggressive, more robust in terms of their ability to nurture their offsprings for example in terms of litter size and milk production(91). New litters born to *TK+* mothers were transferred to CD1 mothers who had given birth around the same time. The CD1 offsprings were sacrificed and the litters from the *TK+* mother given to the CD1 foster according to a published protocol(91). Breeding of *TK+* lines were kept hemizygous (*TK+* mothers with wild type or *APP+/-* or *APP23+/-* males). These additional strategies were necessary for yielding a more efficient colony expansion.

### *Genotyping*

Mouse tail or ear biopsies were incubated overnight at 55°C on a shaker in a cocktail of 300 µL tail lysis buffer (10mM Tris HCl pH 9, 50mM KCl, 0.5% NP40%, 0.5% Tween-20) and 0.1 mg/ml proteinase K (Roche). The enzyme was deactivated thereafter by heating the tail samples at 95°C for 15 min, centrifuged at 14000 rpm for 10 min, in order to use 2 µl of the supernatant for genotyping, which was exclusively performed via PCR reactions.

Genotyping of transgenic mouse lines was done to detect the presence or absence of TK and human APP with the primers listed in Table 5. PCRs were performed using a thermocycler PCR machine and the reaction consisted of 20uL total reaction buffer/sample containing primers at 0.375uM each forward and reverse, and 1xGoTaq Green PCR master mix (2x, diluted out with nuclease free H<sub>2</sub>O). Sequences of the PCR primers are shown in Table 5 and the respective optimized PCR programs are shown in Table 6.

Primer	Sequence 5'-3'	T <sub>Annealing</sub> (°C)
HSVTK 5'	GAC TTC CGT GGC TTC TTG CTG C	62
HSVTK 3'	GTG CTG GCA TTA CAG GCG TGA G	62
PS1 5'	CAG GTG CTA TAA GGT CAT CC	58
PS1 3'	ATC ACA GCC AAG ATG AGC CA	58
APP CT 5'	GAA TTC CGA CAT GAC TCA GG	58
APP CT 3'	GTT CTG CTG CTG CAT CTT GGA CA	58

Table 5 Primer sequences used in genotyping APPPS1, APP23, APPS;TK and APP23;TK mice.

Temperature	Duration	Repeat
94°C	2 min	x1
94°C	30 sec	x35
62°C for HSVTK, 58°C for APPCT and PS1	30 sec	
72°C	45 sec	
72°C	5 min	x1
4°C	Unlimited	x1

Table 6 PCR programs used for this project in genotyping mouse strains.

To separate the PCR products, samples were run on a 2% (w/v in 1x TAE) agarose gel with incorporated 0.5ug/mL ethidium bromide at 110 – 120 mV for 25-40 minutes and visualized under UV light at 300-600ms exposure. The APPCT product was approximately 250bp, whereas the HSVTK product was 500bp. The samples were run alongside positive and negative controls as well as water-only controls and a DNA ladder (Easyladder I, Bioline).

#### *Removal of resident microglia*

A microglial removal protocol was adapted from a previous study (ref). Briefly, nucleoside analog ganciclovir was suspended to the desired concentration with sterile filtrated artificial CSF and filled into a miniosmotic pump (for example, Model 2004, Alzet) that was connected to a plastic tubing. The pumps were primed according to manufacturer's instructions (5-48 hours, depending on the model).

The primed pump was then connected to a cannula (Brain infusion kit 3, Alzet), and the drug was delivered to the right lateral ventricle by means of surgically implanting the miniosmotic pump. The pump itself rested in a subcutaneously created pocket along the shoulder blade and back of the animal. Animals were anaesthetized by ketamine/xylacine (60 mg/kg of animal) prior to this procedure. Aged *APP23;TK* mice received about 50% of the regular dosage.

Stereotaxic coordinates from bregma: a/p: -0.2 mm, a/l +1 mm, d/v -3 mm. for the surgical

procedure and kept on a heating mat and hydrated via subcutaneous injection of warm (35°C) lactated Ringer's solution until recovery. The animals received paracetamol up to 5 days after surgery. Successful removal of microglia was confirmed with Iba1 immunohistology.

#### *Anti-A $\beta$ immunotherapy*

In our treatment paradigms, murine IgG was used: either anti-A $\beta$  n-aa. 1-16 specific clone Ab9 of subclass IgG2a  $\kappa$  (QED Bioscience Inc.), or total nonspecific mouse IgG purified from pooled serum (SLM66; Equitech Bio) denoted as "ctrl".

Ab9 was protein G purified by QED Biosciences Inc (Lot 110309, Ascites lot 092209) and suspended with pH 7.4 with PBS and sterile filtrated through a 0.2 $\mu$ m pore size. Control antibody was further repurified in-house via Protein G column (GE Healthcare) with a protocol and buffer compositions comparable to the Ab9 purification process. Endotoxin levels of selected aliquots were confirmed via limulus gel clot assays of sensitivity <0.03 EU/mL (Charles River). Vehicle treatment was PBS at pH 7.3.

#### *Preventative immunotherapy*

Preventative study in *APPS;TK*- mice was carried out in 3-week old mice weaned from their mother at postnatal day 21, genotyped and treated with the murine IgG of either Ab9 or control. The standard treatment dose was 500 $\mu$ g per intraperitoneal injection (approx.17mg/kg).

#### *Interventional immunotherapy*

Interventional immunotherapy was carried out in animals which already had a robust plaque burden as described by the literature. Exact dosing of intraperitoneal injections are shown in Table 6.

Whenever concurrent ganciclovir infusion was present in an experiment, antibodies were injected a few days after recovery from miniosmotic pump implantation. For instance, 19 month old mice from the APP23;TK (+ or -) line received weekly intraperitoneal injections of 500  $\mu$ g murine IgG for 4 weeks, and this treatment started three to five days after ganciclovir infusion.

### *Tissue harvest*

Animals were perfused with 20 mL PBS (pH 7.2) and organs of interest were either snap frozen in liquid nitrogen with the help of 2-methyl butane (Merck) for gentler freezing in case of the brain, or immersion fixed in 4% formalin (Herbeta Berlin).

Formalin-fixed tissues were prepared either for paraffin embedding via alcohol dehydration using a Shandon Histocentre II machine overnight, or prepared for free floating sections by sucrose cryoprotection (30% sucrose in PBS pH 7.4) for subsequent cryosectioning. Exact preparation of tissue for histology relating to a particular experiment is listed on Table Z.

For each in vivo experiment the following tissue was harvested: brain, cervical lymph nodes, blood (for plasma preparation or flow cytometry) in EDTA treated tubes, inguinal and axillary lymph nodes, spleen, kidney, liver, and tail sample (for regentyping). Whenever possible, the organ on the anatomical right hand side was snap-frozen in liquid nitrogen, and the anatomical left organ was formalin-fixed. For some experiments more organs were saved for future analyses.

### *Plasma sampling*

As mentioned above, terminal collection of whole blood into EDTA treated tubes (BD Bioscience) was performed just before systemic perfusion.

From mice before and during treatment which were operated with a miniosmotic pump, blood was sampled by laceration of the tail vein after immobilizing the mouse in a custom-made chamber.

In bleeding mice where grappling was not a challenge, I preferred to use the submandibular bleeding method using a specialized lancet (GoldenRod), as it was less invasive, more humane, and reliably yielded more than 150 uL of blood from the living animal.

Plasma was arvested from coagulated blood which had been incubated at room temperature between 30 to 120 minutes and then centrifuged at 4200 rpm for 15 minutes. The plasma was collected with a pipette and snap frozen for long term storage.

### *Immunocytochemistry:*

*\*\*please note: histological preparation and quantitative analyses of tissue were performed differently depending on the experiment. This was mainly an operational factor, due to the evolving tools and techniques that were being introduced into the lab at the time.*

Formalin fixed tissue was either embedded in paraffin and cut at 5  $\mu\text{m}$  on a microtome (Leica), or 30  $\mu\text{m}$  free floating sections were generated with a cryostat (Leica) after cryoprotection of tissue in 30% sucrose solution. The sections were stored in 24-well plates in a tissue-protective cocktail (28.5% ethylene glycol, 23.8% glycerine (v/v) in 0.1M phosphate buffer at pH 7.4) at 4°C.

Conventional immunohistochemical protocols were utilized for staining with primary antibodies Iba1 (Wako), POD-conjugated Goat anti-Rabbit (Jackson). Briefly, tissues were rinsed 3 times with PBS for 10 minutes each on a shaker, blocked and permeabilized with 10% normal goat serum (AbD Serotec) in 0.3% Triton X-100 buffer for one hour, and then incubated overnight with primary Iba1 antibody at a dilution of 5  $\mu\text{g}/\text{mL}$  at 4°C. Sections were then washed 3 times with PBS for ten minutes each, and secondary antibody added at room temperature for 2-3 hours at a concentration of 50 $\mu\text{g}/\text{mL}$ . After another washing step, the chromogen was reacted with diaminobenzidine (Dako) for a permanent colour development. The sections were rinsed thoroughly with dH<sub>2</sub>O, mounted onto a microscope slide (R. Langenbrinck) and briefly counterstained with hematoxylin before being dehydrated in ascending alcohol series and finally xylol. Sections were coverslipped using a mounting medium (Roti).

If a treatment group had poor Iba1 immunohistochemical staining, postfixation in formalin at 37°C greatly improved the quality. Whenever deemed necessary, citric acid pretreatment (pH 6.5) for 30minutes at 75°C improved the staining further in visualizing microglial morphology.

Immunohistochemistry against A $\beta$  followed the same general protocol as for Iba1, with the primary antibody 4G8 diluted at 1:1000 from stock (Covance), as well as secondary antibodies

POD-conjugated Goat anti-Mouse (Jackson) at 50 ug/mL. Brief counterstaining with hematoxylin also followed conventional staining procedure described above.

Congo red histochemistry was performed on free-floating sections as follows: sections were washed and mounted onto microscope slides and allowed to adhere (air-dried at room temperature for 15-20 minutes). Sections were counterstained with hematoxylin for 5 minutes followed by a 10 minute development under a stream of luke-warm tap water. Sections were subsequently incubated in a pre-treatment solution of freshly prepared 0.02% NaOH, which was added to an overnight prepared 3% NaCl (w/v) solution in 80% denatured ethanol (Herbeta Berlin). Congo red powder (Roti) was strained through a filter paper using the pretreatment solution containing 0.01% NaOH. Sections were incubated in the Congo red dye for 40 minutes at room temperature, washed three times vigorously in 100% denatured ethanol, treated with xylol twice at 3 minutes each and coverslipped.

Iba1 immunohistochemistry, 4G8 immunohistochemistry, and Congo red histochemistry protocols on free-floating sections were established by my colleague Susann Handrick and all protocols for paraffin-staining were carried out and developed by Petra Matylewski in our diagnostics core facility under the guidance of Roland E Kälin and Stefan Prokop.

Novel chemoluminescent probes detecting protofibrillar structures were used to appreciate yet another parameter of A $\beta$  conformation upon antibody treatment in AD mice. pFTAA has been extensively characterised in a recent study (cite) and has been shown to share almost complete similarity to A $\beta$  antibody staining in early stages of cerebral amyloidosis in APPS;TK- mice (cite Nilsson paper), however whether their coverage is different at a later age or in other mouse models is still under active investigation. We utilized pFTAA at a concentration of 1:1000 of stock (from Susann Handrick) in PBS and incubated this solution with washed and mounted sections for 30 minutes. The sections were coverslipped with an aqueous mounting medium and visualized under the FITC filter of the fluorescent microscope. A careful side by side comparison to unstained controls was required due to the high autofluorescence in the FITC fluorescent filter in *APP23;TK+* or *APP23;TK-* mice.

*Immunofluorescence:*

Conventional immunohistochemical and histochemical protocols were utilized for staining with primary antibodies Iba1 (Wako) and 4G8 (Covance) as well as secondary antibodies Alexafluor 488-conjugated goat anti-mouse (Invitrogen), Alexafluor 568-conjugated goat anti-rabbit (Invitrogen). Brief counterstaining with DRAQ5 or DAPI also followed conventional staining procedure.

*Perl's Prussian Blue Stain:*

2.5% Ferric hexacyanoferrate (Merck) was freshly prepared and added at a 1:1 ratio with 2% HCl solution and incubated for 20 minutes at room temperature on every 23<sup>rd</sup> 30µm thick coronal hemisection and briefly counterstained with nuclear fast red (Sigma). Quantification and grading scheme for microhemorrhage was adapted from a previous study in the same mouse model (23) and scored according to a similar system. Grade 1 was a cluster with 1-3 hemosiderin-positive cells; Grade 2, cluster of 4-10 cells; Grade 3, cluster of more than 10 cells. Each brain was analysed by average number of bleeds per section and an average grade was given per bleed. Sample images are shown in Figure 5.

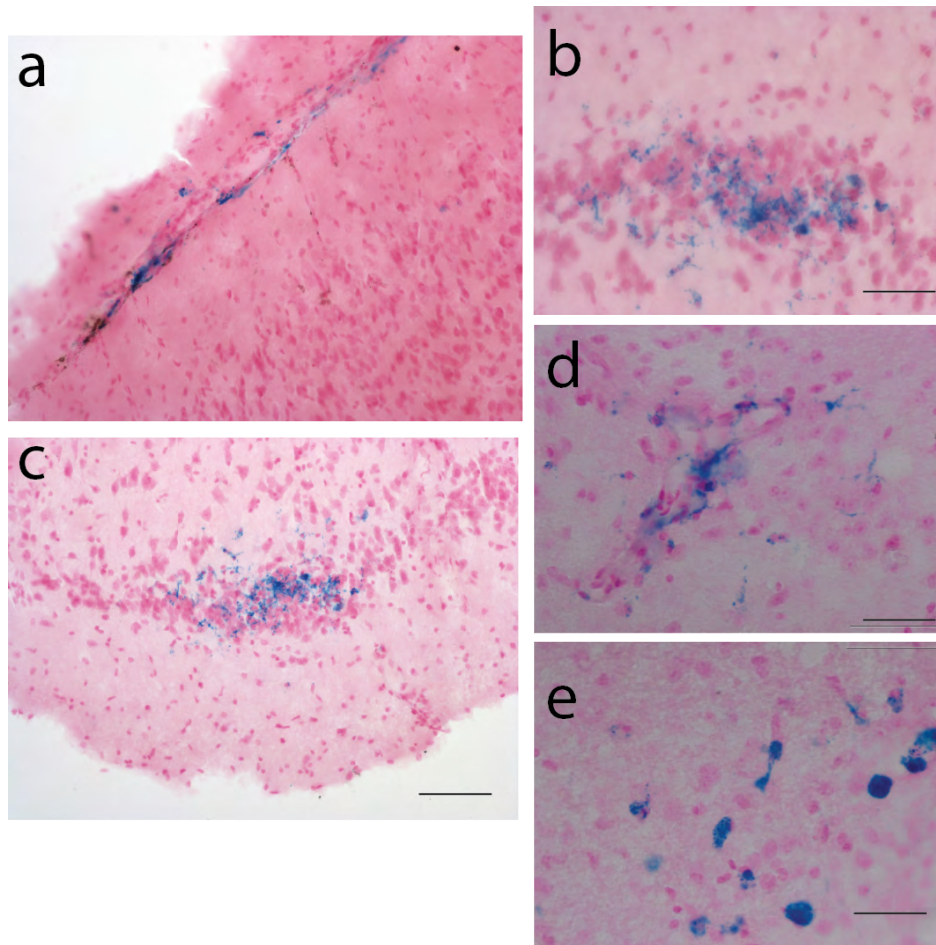


Figure 5 Representative images of microhemorrhages (from a control-treated APP23 mouse shown here) visualized by Perl's Prussian Blue histology under brightfield illumination. a. Vascular association of microhemorrhage was obvious in this cortical region. Scale bar (for a and c) = 50 $\mu$ m. b. diffuse iron stain likely permeating cellular processes. Scale bar (for b and d) = 100  $\mu$ m. c. lower magnification of b. d, e. higher magnification of vascular (d) and cellular (e) association of hemosiderin positivity.

#### *Stereology:*

Stereological methods were used to systematically sample the entire cerebral cortex of the left hemisphere to assess cortical plaque burden and microglial population density. 8-12 coronal brain hemisections spaced 570  $\mu$ m apart were sampled using the Stereo Investigator (MBL) software as described previously(92) for each parameter.

Briefly, plaque burden was assessed in 4G8 stained sections using a two dimensional dissector for area fractionation as a total ratio from the cortical area outlined. I used the help of the area fraction fractionator program and serial section manager of the Stereoinvestigator. Paxinos

mouse atlas was used as a reference for anatomical precision in outlining the cortex.

Population density of microglia was sampled using a three dimensional dissector. Microglial cell bodies were counted after Iba1 IHC and morphologically distinguished from protrusions only or staining artifacts. Cell number was assessed with the optical fractionator method utilizing the work flow from the Stereo Investigator software. Overall population density was computed by taking the estimated population from the mean section thickness and dividing it by the estimated sampling volume. Statistical significance was determined by Schmitz-Hof (1<sup>st</sup> category).

*Semiquantitative assessment of plaque coverage and Abeta coverage in paraffin sections*

In paraffin sections, Cell<sup>^</sup>D software was used to look at phase analysis (area coverage) under the Cy3 filter for amyloid burden, and manually set thresholds in a regular phase analysis in 4G8 immunohistological stains.

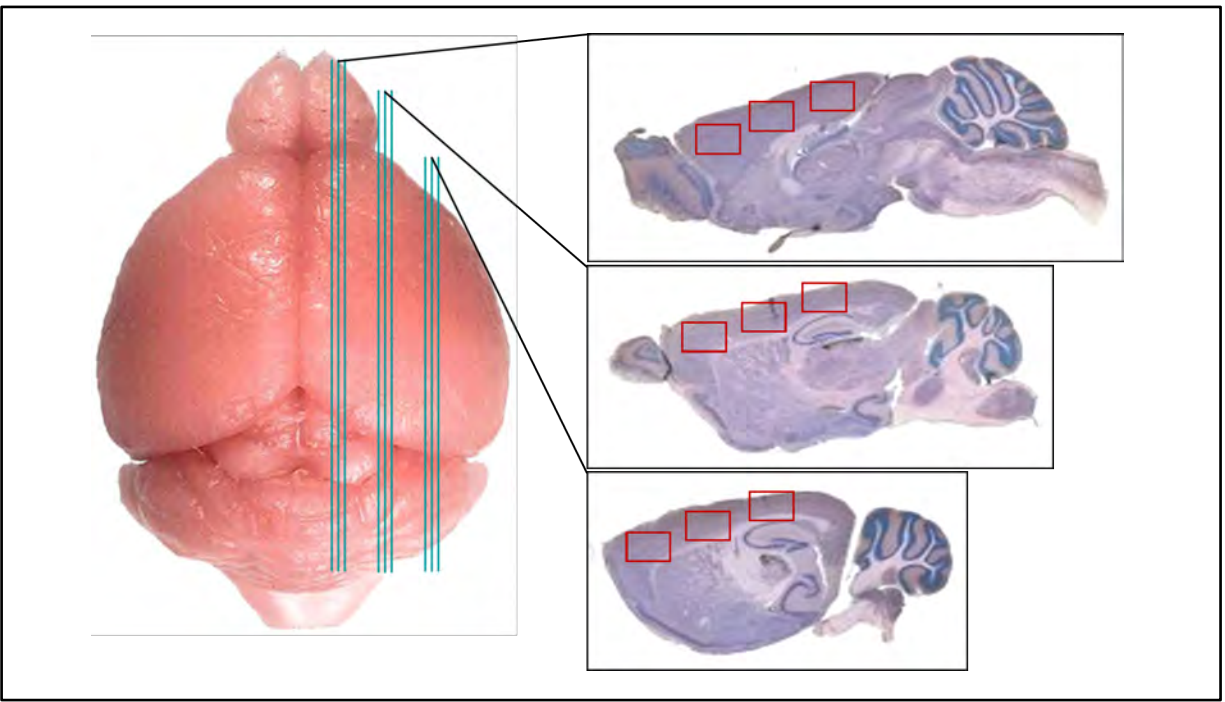


Figure 6 Paraffin cutting scheme used for early immunization studies in APPPS1 mice. 3 sagittal levels were evaluated.

*Paraffin sections:* Fluorescent photos were taken under the Cy3 filter of nine 0.1% Congo red stained sagittal hemisections spaced 1040  $\mu\text{m}$  apart for each brain. 35-36 images were taken along the entire cortical ribbon at 10x magnification with consistent exposure time/camera settings (Olympus BX53). Area coverage of Cy3 positivity was computed by a manually defined colour/ intensity threshold using Cell<sup>^</sup>D Software (Olympus) and computed relative to the total area of the region of interest. Figure 7 shows an overview of regions sampled.

*Free-floating sections:* Fluorescent photos were taken under the Cy3 filter of six 0.1% Congo red stained coronal hemisections spaced 1080  $\mu\text{m}$  apart for each brain. Congo red staining under Cy3 filter yielded a clear picture of positivity with virtually no background, allowing for a precise measurement of amyloid burden (Figure 7). 50-60 images were taken along the entire cortical ribbon at 10x magnification with consistent exposure time/camera settings (Olympus BX53). Area coverage of Cy3 positivity was computed by a manually defined colour/ intensity threshold using Cell<sup>^</sup>D Software (Olympus) and computed relative to the total area of the region of interest.

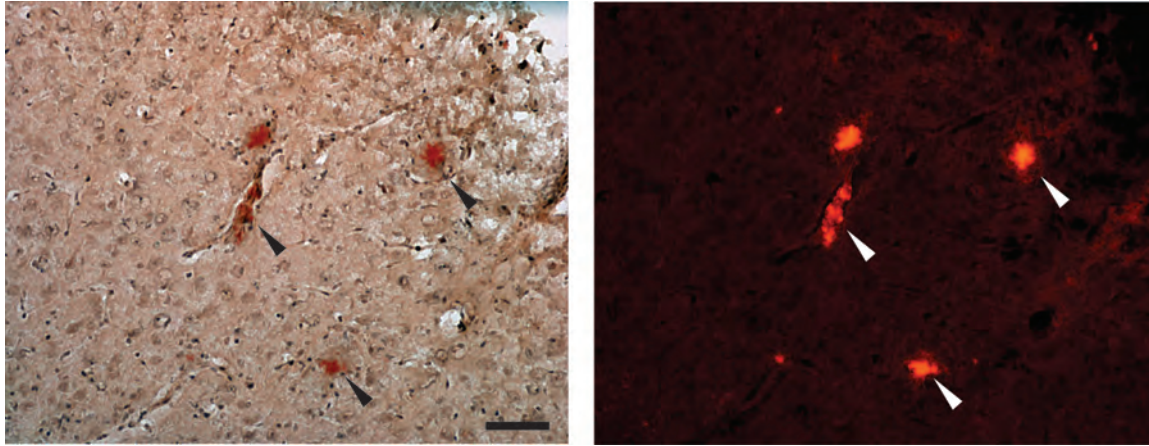


Figure 7 Congophilic structures seen under brightfield and Cy3 filter. A 200-day old APPS;TK- mouse stained for 0.1% Congo red and visualized under brightfield and Cy3 filter (200ms exposure, Gain = 5, offset = -150). Scale bar = 100  $\mu$ m

*Vascular amyloid:* A modified protocol from previous studies was used, where all morphologically identifiable cortical blood vessels from 3-4 Congo red stained sections spaced 1140  $\mu$ m apart were assessed for their amyloid burden. We assigned a vascular grading criteria (Figure 8, Table xxx) to be able to distinguish between the different degrees of angiopathy degrees that was adapted from previous studies in both murine and patient settings(93).

“CAA frequency” refers to all amyloid laden vessels divided by total vessels counted in the entire set of systematically sampled sections. “CAA severity” refers to the score multiplied by number of vessels. The mean for all vessels was taken as CAA severity. “CAA score” was calculated by multiplying CAA frequency with CAA severity.

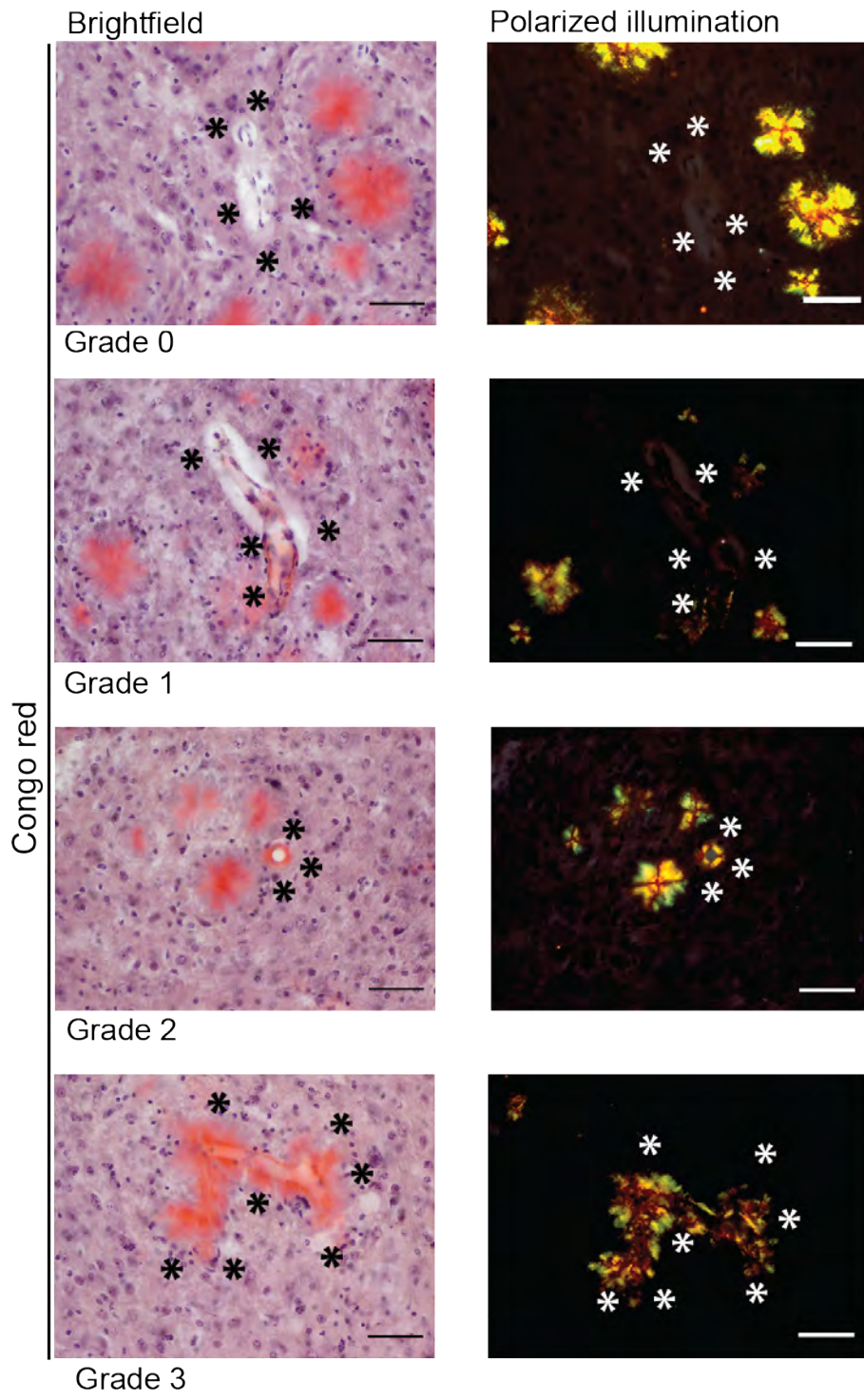


Figure 8 Reference images for CAA scoring used to discriminate different grades of vessel pathology. Left panel brightfield and right panel polarized light. Scale bars: 50um.

Grade	Criteria
0	No Congo red positivity
1	Partial Congo red stain around the circumference, Congo red free areas visible
2	Entire circumference is covered by Congo red, confirmed by birefringence
3	Emanating Congo red positive amyloid, clear birefringence

Table 7 Criteria for CAA grade assignment per vessel.

*A $\beta$  quantitation from fragmented brain extracts.*

Frozen hemibrains were homogenized and proteins extracted in a four-step fractioning fashion modified from an existing protocol(94). Brain proteins were extracted sequentially, by initial homogenization with repeated, rigorous passage through progressively increasingly gauged syringes with protease inhibitor (Roche) containing tris buffered saline (TBS, 150 mg /ml wet weight). Subsequently, ultracentrifugation steps were taken at 100,000 g for 1 hour, after which the pellet was resuspended with stronger detergent 1% Triton X-100. After another ultracentrifugation with the same duration and force, the pellet was resuspended in 2%SDS. The final resuspension post ultracentrifugation was 70% Formic acid, after which the pellet disappeared(94).

Protein concentrations of each homogenate was measured by means of a chromogenic assay (BCA, Pierce) in order to best stipulate the dilutions for subsequent A $\beta$  measurements. As a general rule of thumb, TBS and TritonX-100 homogenates were diluted 1:10, whereas SDS homogenates were diluted 1:1000 or 1:100, and formic acid extracted homogenates were diluted 1:250 with a pH adjustment with 1M Tris-base (pH 9.0).

*A commercially available electrochemiluminescence-linked immunoassay, the MSD 96-well MULTI-SPOT Human (6E10) A $\beta$  Triplex Assay (Meso Scale Discovery) was used for quantifying A $\beta$ 40 and 42 in brain brain homogenates. This assay is currently the gold standard in the field for sensitively measuring A $\beta$  content in tissue, for both clinical and research settings.*

### *Particle size analysis.*

*APP23;TK- or APP23;TK+ mice:* Six A $\beta$ -immunostained sections spaced 1140  $\mu\text{m}$  were photomicrographed using the same camera settings through the neocortex, procuring 30 images per mouse. Plaques in each image were analysed and classified by area ( $\mu\text{m}^2$ ) grouping with the help of CellSens software (Olympus) and manual discrimination from background staining or artifacts.

For the determination of plaque size distribution in 120 and 250 day old *APPPS1* mice 27 defined A $\beta$ -immunostained section through the neocortex were imaged using Cell Sense software (Olympus, Tokyo, Japan)(88). Individual plaques were classified into different plaque size classes (50-500  $\mu\text{m}^2$ , 500-1000  $\mu\text{m}^2$ , 1000-5000  $\mu\text{m}^2$ , 5000-10000  $\mu\text{m}^2$ , 10000-50000  $\mu\text{m}^2$ . Plaques smaller than 70  $\mu\text{m}$  were excluded. In sections with high background, false-positive detection was removed by hand. Each section was checked manually for proper identification of plaque moiety.

*APPS;TK- or APPS;TK+ mice:* Nine A $\beta$ -immunostained (4G8) sagittal paraffin sections spaced 1140  $\mu\text{m}$  were photomicrographed using the same camera settings through the neocortex, procuring 35-36 images. Plaques were classified into size classes (50-500  $\mu\text{m}^2$ , 500-1000  $\mu\text{m}^2$ , 1000-1500  $\mu\text{m}^2$ , 1500-2000  $\mu\text{m}^2$ , 2000-2500  $\mu\text{m}^2$ , 2500-3000  $\mu\text{m}^2$ , 3000-6500  $\mu\text{m}^2$ ). Plaques smaller than 70  $\mu\text{m}$  were excluded. False-positive detection was removed by hand., and each section was checked manually for proper identification of plaque moiety.

### *Statistics:*

Statistical analyses were performed with GraphPad Prism 5.0 or R (15.0).

Assumption of normality was tested both graphically, QQ, and using D'Agostino-Pearson omnibus test as a prerequisite for further analysis with one-way ANOVA.

Post hoc analyses were computed with a Bonferroni *post-hoc* test comparing all groups with one another.



## Materials:

### Materials & tools for in vivo work

Item	Manufacturer
Saline 0.9%	Fresenius Kalbi
Rompun/xylacine	Bayer
Ketamine	Actavis
Descosept	Dr. Schumacher
Bepanten eye and nose cream	Bayer
Contact Pen system VA100 glue	Weicon
Lactated Ringer's solution	B.Braun
Paracetamol	
Heating pad	Beurer
Scalpel	
roundtip applicator	Henry Schein
Prolene polypropylene suture material	Ethicon
Stereotaxic frame for mice	Stoelting
surgical tools (forps, suture holder, fine sharp scissors, blunt tough scissors)	Fine science tools

## Chemical Reagents

Item	Manufacturer
Acetone	Merck
Agarose	Serva
Albumin from bovine serum	Sigma
Chlorform reinst (für RNA Isolierung)	Merck 2431
D+-Saccharose p.a. mind. 99,5%	Carl Roth
EDTA	Sigma
Ethanol 96% rst	Baker
Ethanol abs. z.A	Baker
Ethidium bromide	Merck
Ethylene Glycol	Sigma
ETOH 70%	Herbeta
ETOH 80%	Herbeta
ETOH 96%	Herbeta
ETOH abs. Vergällt	Herbeta
Formaldehyd 4% gepuffert pH7 ·5l	Herbeta
Formic acid	Merck
Glycerine 99,5% w.fr·	Carl Roth
HCl	Herbeta
HCL-Alcohol 3%	Herbeta
Hydrogen peroxide 30%	Merck
Methanol >99,8%	Carl Roth
NaOH tablets	Merck

Na(HPO <sub>4</sub> ) <sub>2</sub>	Sigma
NaCl	Sigma
NaH <sub>2</sub> PO <sub>4</sub>	Sigma
NaOH	Merck
NH <sub>4</sub> Cl Ammonium chloride	AppliChem
PBS	Biochrom
Percoll	GE Healthcare
Potassium chloride	Carl Roth
Propanol, 2	Merck
Protease Complete mini	Roche
Proteinase K	Roche
Rnase ZAP/Away	Carl Roth
Sulfuric acid 95-98%	Merck
SDS	Sigma
Sodium citrate	Calbiochem
Sucrose	Carl Roth
TEA buffer 50x	Appllichem
TEMED	Carl Roth
Tris Base	Carl Roth
Tris HCl 99%	Sigma
Tris-Base	Sigma
Tris-HCl	Sigma
Triton X-100	Sigma
Tween 20	Aldrich
Xylol	Baker

## Software

<b>Program</b>	<b>Manufacturer</b>
Endnote 5.0	Thomson Reuters
Prism 5.0	Graphpad
Cell <sup>^</sup> D	Olympus
Cell Sens	Olympus
Stereoinvestigator	MBL Biosystems
Photoshop CS5	Adobe
Illustrator CS5	Adobe
Microsoft Office 2011	Microsoft
Syngene 2.0	Syngene
Zen 2.0	Carl Zeiss
SPSS 11.5	IBM

## Instruments

<b>Item</b>	<b>Manufacturer</b>
Spectrophotometer Infinite M200	Tecan
Microtome	Leica
Cryostat Microm HM 560	Thermo Scientific
Waterbath	Medax
Electronic balance	Kern & Sohn GmbH
Shaker	neoLab
Microscope Axiostar plus	Zeiss
Microscope BX53	Olympus
Confocal microscope	Zeiss

Thermomixer	Eppendorf
Tabletop centrifuge Fresco 17	Thermo Scientific
Tabletop centrifuge Multifuge 2SR+	Thermo Scientific
Consort EV power supply	Sigma Aldrich
Real Time PCR cyclers	Applied Biosystems
Microwave	Siemens
G: Box gel imaging system	VWR
Hotplate magnetic stirrer L32	Labinco
pH meter Mettler Toledo	Sigma Aldrich
PCR Cycler	Biometra
Incubator Heraeus	Thermo Scientific
FACS Calibur II	BD
Sector Imager (Meso Scale plate reader)	MSD
Ultracentrifuge	Becton Dickinson

## **Results:**

### *1. Prevention study*

In order to prevent or contain/slow down the accumulation of A $\beta$  in the brain, an anti- A $\beta$  antibody injection course was started prior to the onset of plaques in our murine model. In APPPS1 mice, onset of plaque accumulation has been estimated to begin at 4-6 weeks of age(39).

At postnatal day 21-22 (3 weeks of age), APPPS1 mice were weaned from their mother and injected weekly for 13 weeks with 500ug of Ab9 intraperitoneally. Mice were sacrificed at 4 months of age (120 days) at 3 days after their last antibody injection, and tissue was processed for analysis.

Brain analyses for A $\beta$  content was performed by histological and immunohistological examination. Qualitative assessment of immunohistochemistry against A $\beta$  (4G8) revealed no visibly obvious diffuse A $\beta$  at 4 month-old APPPS1 (APPS;TK-) mice either treated with control or Ab9 IgG. However, numerous and clearly identifiable 4G8-immunopositive A $\beta$  plaques were seen in both treatment groups, with a region-specific distribution that was concentrated in the frontal neocortical area and lessened occipitally, whilst completely sparing lower brain structures. Few plaques were seen in the hippocampal area irrespective of treatment (qualitative observation).

Quantitative analysis of A $\beta$ -plaque burden of the treated AD mouse brains revealed no significant difference in percentage of area occupied by the plaques in the neocortex (Figure 9).

Prevention study

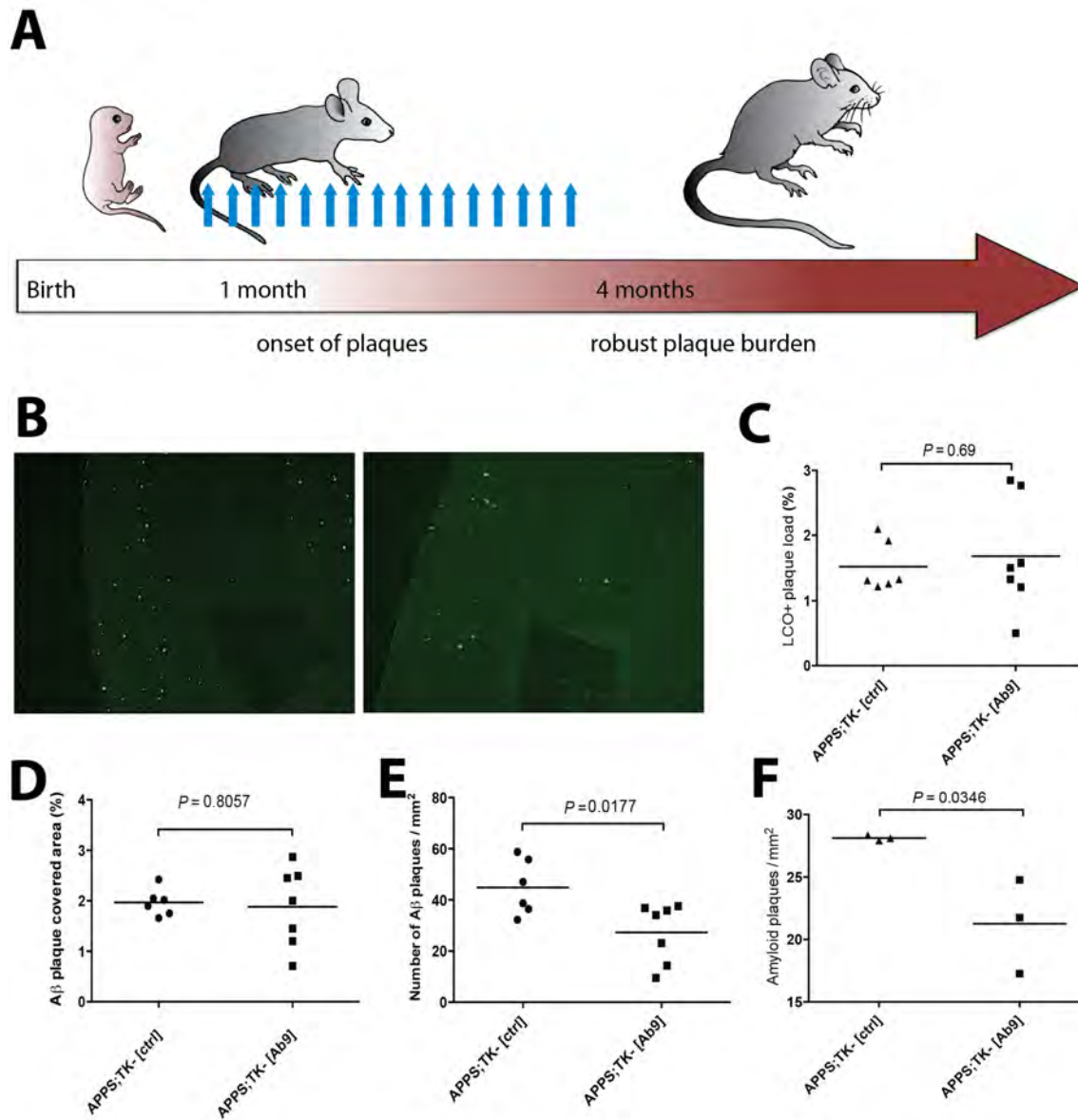


Figure 9 Prevention Study in APPS;TK- mice. 3 week-old APPS;TK- mice were weaned and injected weekly with 500ug of either control IgG [ctrl] or specific [Ab9] ip. a. Scheme of the prevention study. Mice were injected 2-3 weeks before reported onset of plaques in this mouse strain. b. Representative pFTAA-stained images of mouse brains at 120 days. Left panel – control treated. Right panel – Ab9 treated. c. Quantitation of pFTAA-covered area in the brain. d. Quantitation of Abeta plaque covered area. e. Quantitation of Abeta (4G8-positive) plaque population in the neocortex of control or Ab9 treated mice. f. Amyloid burden assessment in the neocortex in control or Ab9 treated mice in the prevention study.

A count of the number of plaques, however, revealed a modest reduction of plaque number by approximately 27% in Ab9 treated mice when compared to the control treated group,  $P < 0.05$ ,  $n = 5-6$  per group (Figure 9). An additional analysis revealed a total increase in size of plaques in the Ab9 treated group (data not shown).

Taking advantage of structural dyes to probe for conformational state of A $\beta$  in treated AD mice enabled additional histological assessments beyond immunohistochemistry (antibody clone-dependent).

Using a newly reported structural chemoluminescent probe - pFTAA - which intercalates to  $\beta$ -pleated sheets (95) and identifies organized structures as early as proto-fibrils in this particular mouse model (APP<sup>PS1</sup>,(39)), a clear distinction was visible in the cortical area occupied by amyloid peptides between Ab9 treated and control IgG treated mice, and quantitative analysis confirmed a significant reduction by 23% in pFTAA covered area ( $P < 0.05$ ) in Ab9 treatment compared to control groups (Figure 9) as well as a significant reduction by 40% ( $P < 0.05$ ) in pFTAA positive number of deposits (Figure 9).

Prevention study

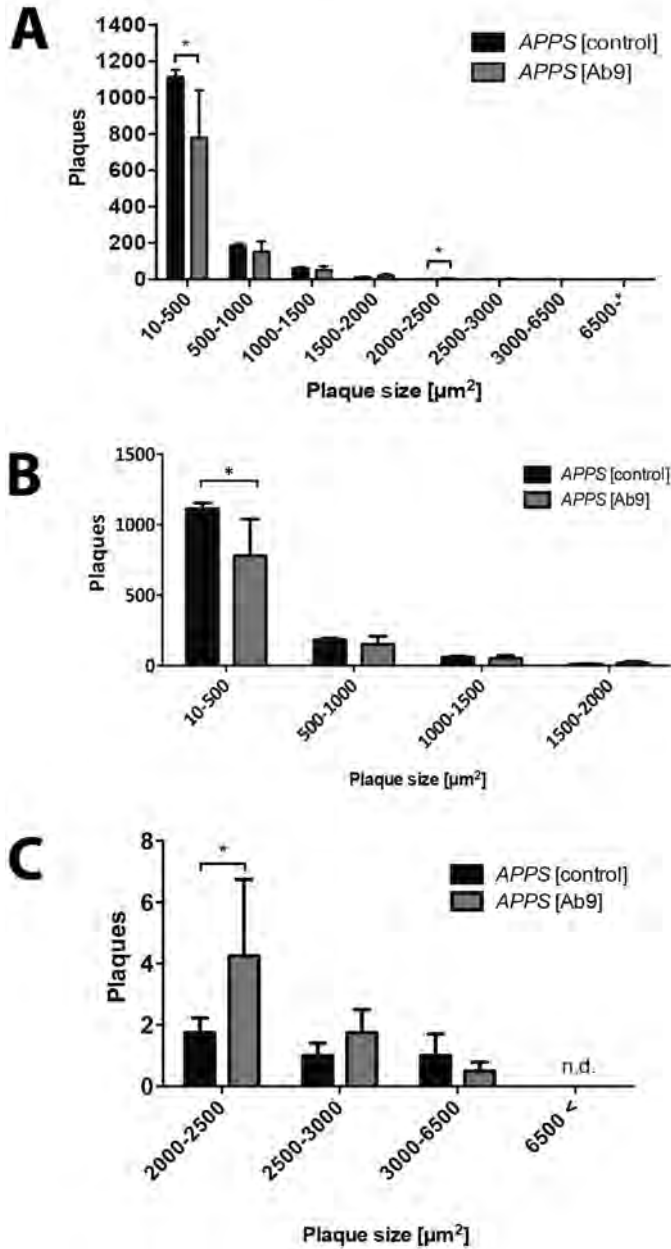


Figure 10 Plaque size analysis of control vs Ab9 treated animals from the prevention trial in APPS;TK- mice (Figure 1). a. overview of plaque size distribution. b a closer view of small plaques. c a closer view of larger plaques.

This observation could also be confirmed using the canonical amyloid dye Congo red, which is one of two accepted amyloid dyes used in diagnostics for detecting amyloid. Congo red positive amyloid burden was significantly reduced in Ab9 treated mice when compared to control treated mice.

Furthermore, the overall amyloid burden was reduced not only in area coverage but also in the number of site of amyloid formation, supporting the notion of a change in amyloid burden.

A detailed analysis of plaque size distribution in the prevention study was undertaken in order to appreciate more subtle morphological changes. In line with the gross Abeta plaque and gross amyloidosis assessment (Figure 9), plaque size classification of 4G8-immunopositive Abeta plaques revealed that there was a shift in Ab9 treated mice compared to control treated mice (Figure 10). There was significant decrease in smaller plaques, whilst there was an increase in larger plaques in Ab9 treated mice when compared to control mice ( $P < 0.05$ ), Figure 10 a-c. Thus, Ab9 treatment as a prophylaxis seems to result in altered Abeta plaque kinetics, while unable to prevent plaque formation completely.

## *2. Interventional immunotherapy*

Whether the specific antibody could reduce plaque burden in full-blown diseased brain in our tg-AD model was investigated. Additionally, the question whether there was therapeutic efficacy in the presence of ganciclovir (a requisite drug treatment for subsequent microglia depletion experiments) was addressed in this study.

Here, 250-day old age and sex matched APPS;TK- mice were injected on a weekly basis with 500ug Ab9 or vehicle (PBS) ip for 8 weeks. Concurrently, for the entirety of the treatment, the animals were treated with intracerebrally with 0.25uL of ganciclovir per hour.

After 8 weeks of treatment, mice were sacrificed and the brain analysed for plaque pathology. There was a visible reduction in the A $\beta$  plaque burden in Ab9 treated group when compared to vehicle controls. Quantitation for A $\beta$  plaque coverage of the neocortex revealed a 30% reduction in the Ab9 treated group, but this effect was not statistically significant. However, there was a significant reduction in the A $\beta$ -plaque population by roughly 25% ( $P = 0.077$ ), as well as a clear, significant 50% reduction in amyloid burden ( $P = 0.0078$ ) and amyloid deposit

sites ( $P = 0.0077$ ).

Intervention study

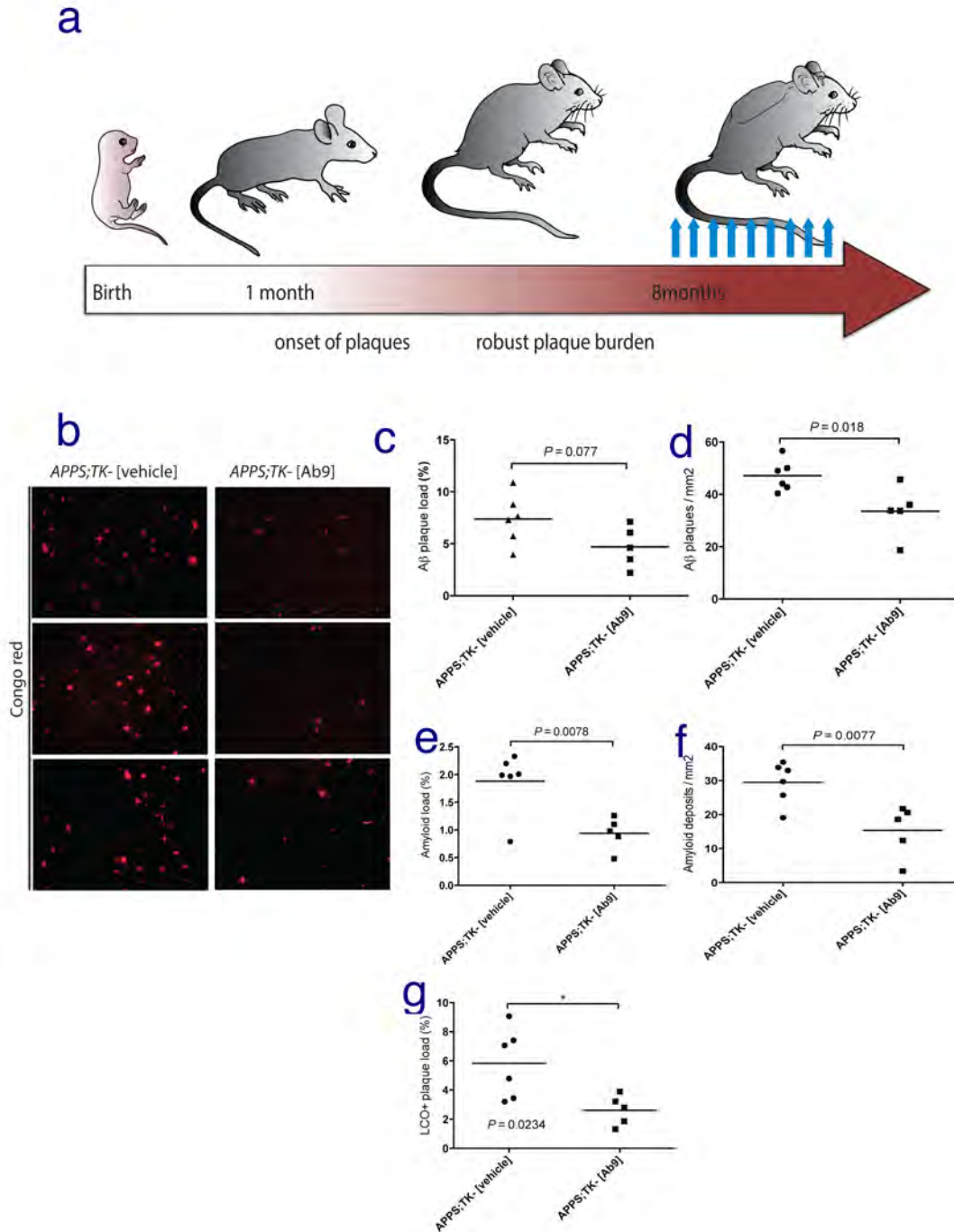


Figure 11 Interventional immunotherapy in APPS1 mice that were aged to 8 months and treated for 8 weeks. **a** scheme of treatment overview **b** representative amyloid images of Congo red staining visualized under Cy3 filter **c,d** quantitation of 4G8 immunohistochemistry in terms of area covered(**c**) and population (**d**). **e, f** quantitation of amyloid burden in terms of (**e**) area covered and (**f**) population. **g**. chemoluminescent analysis of area covered in the cortex.

Novel pentameric thiophene derivatives have been shown to capture a more premature aggregation state with regards to amyloid structures which comprise core plaques(95).

Notably, in Ab9 immunized APPS;TK- mice, qualitative observation revealed a clear reduction in this particular type of pFTAA-positive diffuse plaque species (Figure 11, 40%,  $P < 0.05$ ), revealing clear, crisp borders of remaining plaques upon this histochemical staining. This observation differed drastically from vehicle treated control mice, where “fuzzy” pFTAA positive structures remained (data not shown). Taken together, an 8 week Ab9 treatment was able to reduce plaque burden as a therapeutic intervention model with modest efficacy in APPPS1 mice. Notably, Ab9 reduced plaque burden more effectively as an interventional treatment than when administered preventatively.

As cerebral amyloid angiopathy and microhemorrhages are a pathologic parameter of interest in  $A\beta$ -immunotherapy(96), we performed a histological assessment of vascular alterations related to microhemorrhage and angiopathy. These two parameters have been implicated in vascular imaging alterations in patients in ongoing and previous clinical trials(49). In our treatment set-ups in APPPS1 mice, we have been unable to detect any obvious pathological changes around the vessels (qualitative observation, data not shown) and there were no visible signs of microhemorrhage when compared to a positive control (observation, Figure 12). Thus, we concluded that APPPS1 mice do not have obvious vascular alterations upon Ab9 treatment.

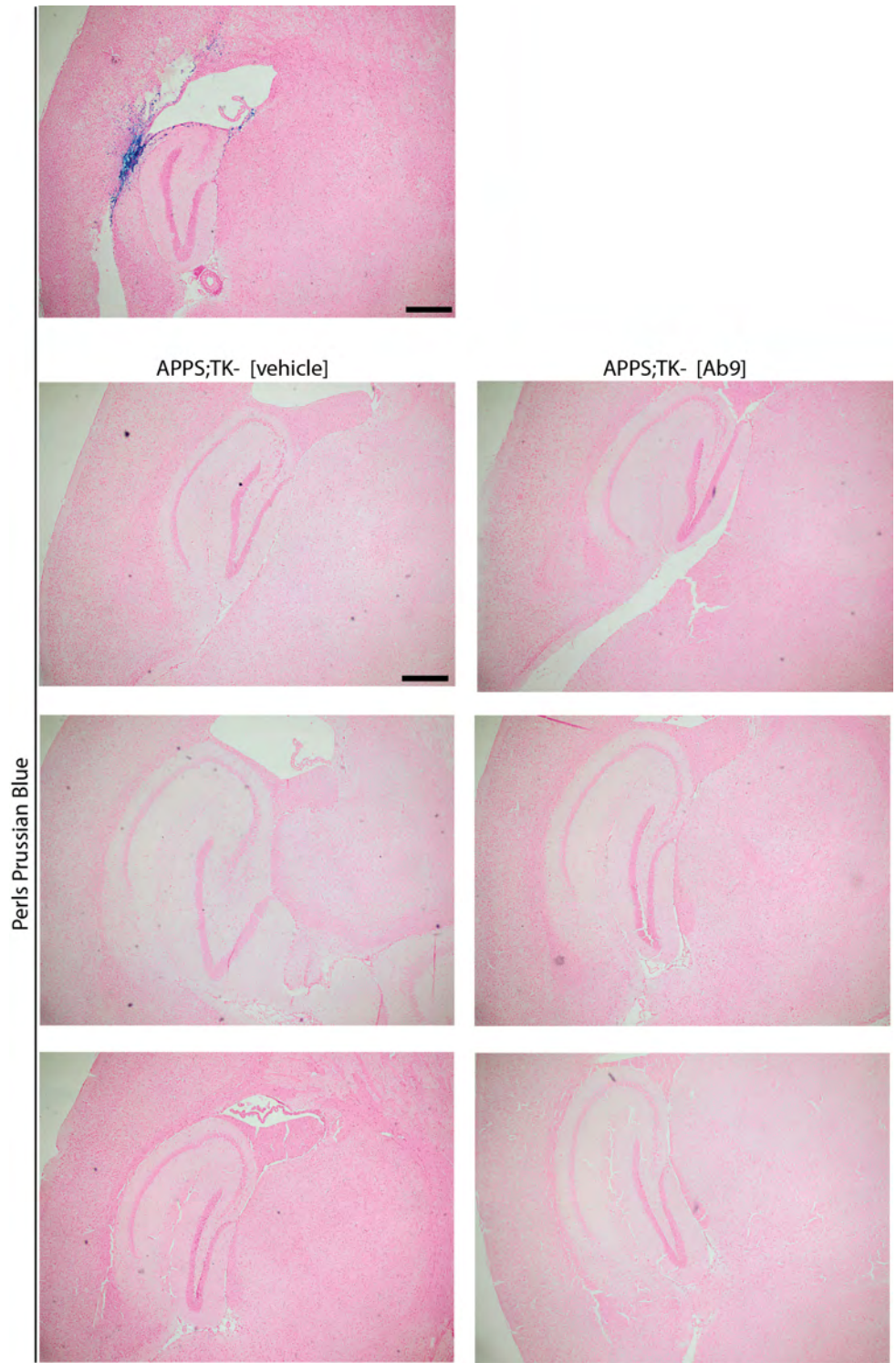


Figure 12 Microhemorrhage assessment in 10.5 mo-old control vs Ab9 - treated APPS;TK- mice

### *3. High dosing for a 4 week treatment in APPS;TK- mice.*

To date there has been no published protocol achieving a microglial depletion beyond 4 weeks in CD11b-HSVTK mice(83,88).

Thus, a treatment protocol resulting in concurrent microglia depletion whilst giving effective immunotherapy was required in order to be able to answer the central hypothesis. Thus, an aim for this project was to develop a Ab9 treatment protocol which allowed for effective plaque burden reduction within the 4 week time window.

As a weekly treatment of 8 weeks resulted in a significant reduction in plaque number and amyloid burden as previously shown (Figure 11). I reasoned that an equal dosage of antibodies administered over a shorter period of time would result in similar plaque reduction in interventional treatment of APPS1 mice.

Hence, APPS1 mice were treated with biweekly injections (twice a week, 34mg/kg/week) of Ab9 for four weeks (Fig 13), and this treatment round was compared with one weekly injection of Ab9 for four weeks (17mg/kg/week, Fig 13). The control mice were treated with unspecific IgG with the same dose.

To our surprise, inspite of the comparable total quantity of antibody administered into the animals, the efficacy of a biweekly treatment of 4 weeks was not as significant as when a weekly injection was spanned over 8 weeks (Figure 13). Amyloid burden was reduced, yet

overall Abeta load did not change.

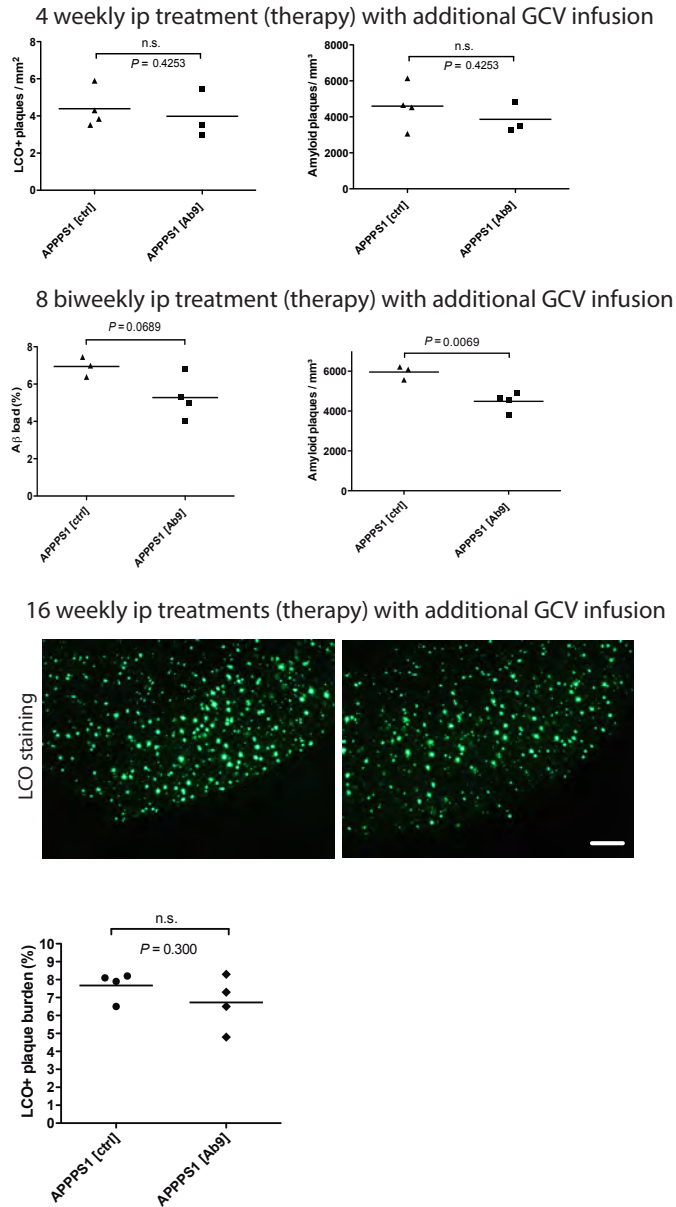


Figure 13 High dosing studies in APPS1 mice did not confer greater efficacy.

LCO or 4G8-stained Abeta burden was assessed for cortical coverage and/or population. Amyloidosis was assessed by counting the number of deposit sites per area of neocortex. Abeta load was not significantly different when a biweekly injection of Ab9 was administered

when compared to control ( $P>0.05$ ). However, there was a significant reduction in amyloid burden upon treatment in this treatment protocol ( $P<0.05$ ), which was similar to the 8 week treatment results (Figure 13).

Extending the biweekly treatment period by another two weeks for a total period of 6 weeks also resulted in a slight reduction in plaque burden (Figure 14) in the hippocampus but not in the neocortex (Figure 14).

6 weekly ip treatment (therapy) with no additional manipulations

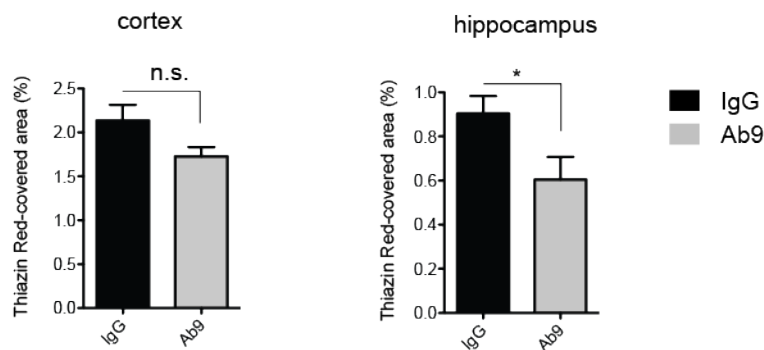


**Figure 14** 6 week long biweekly treatment in APPPS1 mice as a therapeutic paradigm confers efficacy in the hippocampus but not in the cortex.

Increasing the dose even further was attempted, aimed to achieve significant plaque removal upon Ab9 treatment. Mice were treated with 68mg/kg/week equaling 4 weekly ip injections. Surprisingly, even this dose failed to result in a significant reduction in plaque burden in APPPS1 mice in 4 weeks (Figure 13).

Taken together, we concluded that APPPS1 mice are not easily amenable to Ab9 treatment.

#### *4. Microglial depletion.*

A significant microglial depletion efficacy was required to answer the central hypothesis of the question. This depleted state had to be sustained within the duration of immunotherapy. To this end we aimed to establish a robust depletion protocol for a time window equal to, or longer than the shortest immunotherapy treatment window that showed a significant alleviation on plaque burden. (This was 4 injections/ 4 weeks in APP23 or Tg2576 mice as published in a prior study (97), and 8 weeks in APPPS1 mice (Figure 13.)

The titration experiments for a robust depletion protocol were carried out based on previously published results (88). HSV-TK responds to nucleoside analog ganciclovir, and three versions of this compound were at our disposal: ganciclovir, ganciclovir sodium (iv formulation), and prodrug valganciclovir (Figure 15). Additionally, ACV/acyclovir was tested as an alternative option on the grounds of being a conventional HSV medication in patients.

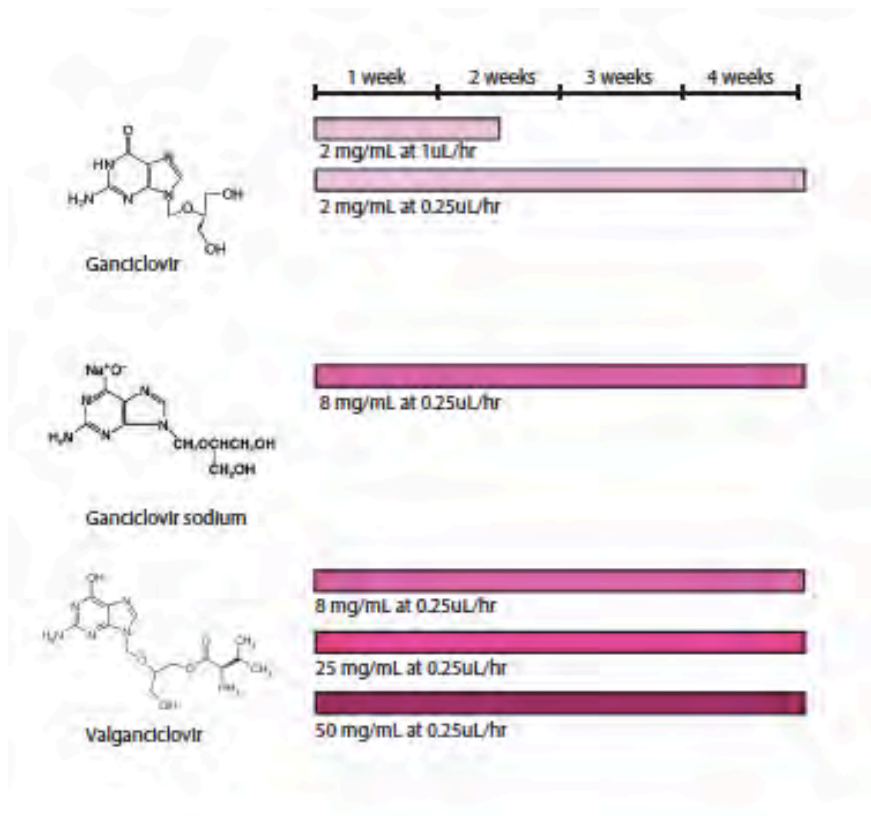


Figure 15 different ganciclovir derivatives and their concentrations tested. The drug names are given below their molecular structure (source: Roche material data sheet) on the left-hand column, and a timeline of different treatment protocols are depicted as a bar. The concentration and flow rate is shown below each bar.

Here, we aimed to test various depletion protocols in order to investigate whether (1) it was possible to dose the drug lower in order to circumvent observed/published microhemorrhage and frequently observed lethality, (2) it was possible to extend the published depletion period to over 4 weeks in order to observe long term changes to plaque pathology in the context of Abeta immunization. We aimed for a targeted approach by delivering the drug GCV directly into the brain parenchyma using a mini osmotic pump, allowing the direct infusion into the tissue. We focused on this delivery method as it had given us the greatest depletion efficacy in the past.

A 10 day intracerebral infusion of 2mg/mL GCV at a relatively high flow rate of 1ul/hr resulted in a significant and robust depletion in the cortex and in the hippocampal area, as seen with immunohistochemistry of various microglia- associated markers (Figure 16). Moreover, the

lethal phenotype seen in higher concentrations of ganciclovir were absent when using this dosage of GCV.

A 10 day infusion of 10mg/mL Cymevene (GCV sodium) with the flow rate of 1ul/hr resulted in a significant and robust depletion in the cortex as well (Figure 18).

In order to extend this effective protocol over an extended period of 30 days, we utilized a 30 day miniosmotic pump which by manufacturer's design delivers the drug at a slower rate. This flow rate of the pump was limited by the manufacturer's model and thus not adjustable.

Variable results were observed when trying out different conditions (including drug derivative type and concentration) to mimic the 10 day depletion efficacy (Figure 20). Overall the viability of the treated animals was significantly lower (Figure 17).

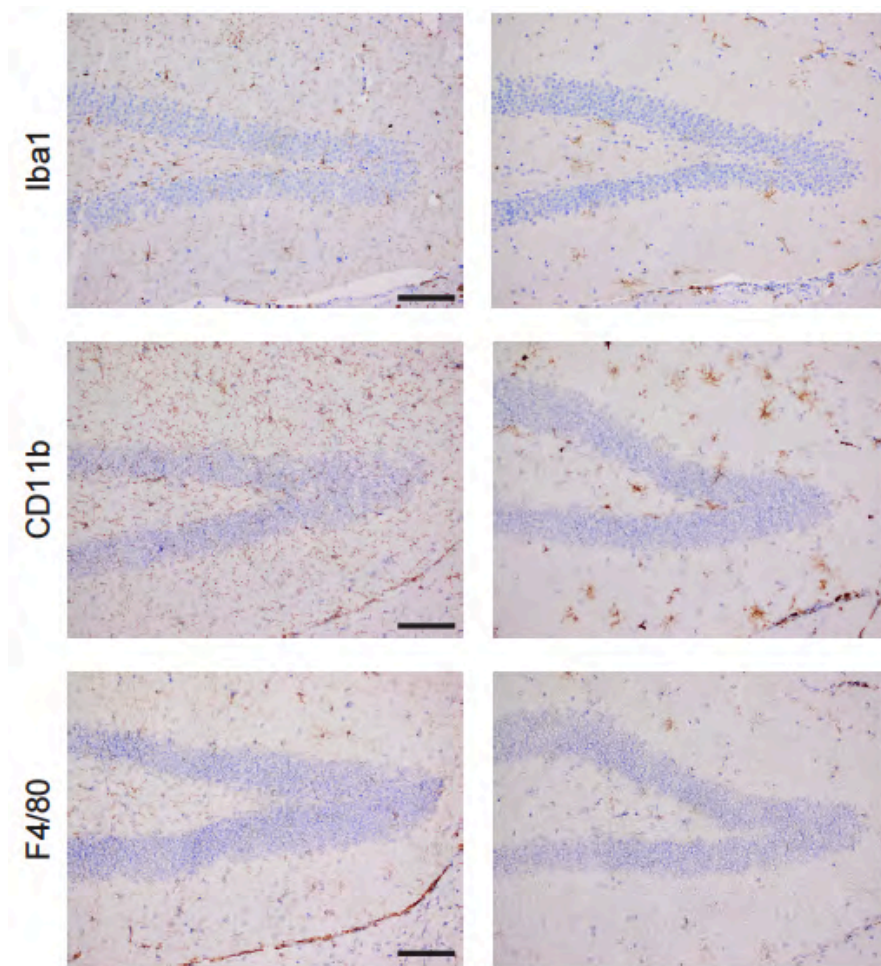


Figure 16 10 day depletion with ganciclovir confirmed by several microglia-associated markers. Three markers were used to confirm microglial depletion: Iba1, CD11b, F4/80.

High lethality often accompanied a high microglial depletion efficacy in 30 day depletion trials similar to what has been previously reported(88). These high drop-out rates were seen particularly in Valganciclovir at 50mg/mL (which has been published), as well as Valganciclovir at 25mg/mL. Cymevene treatment at 8mg/mL resulted in a slight increase in lethality as well.

In some areas of the brain in these mice (treated for 4 weeks), a previously reported patch of morphologically distinct Iba1 immunopositive cells were seen (Figure 19). These were consistent with newly infiltrating cells thought to arise from the periphery as previously postulated to repopulate the deprived brain environment(88).

Infiltrating cells were observed as a “united front” with higher density and less arborized processes with a larger cell body. These cells could morphologically be clearly distinguished from resident cells(98).

In conclusion, it was not possible to completely mimic the robust 10 day depletion protocol for 30 days. Survival rates and other side effects still occurred as published, even when the dosage or derivative substance was altered.

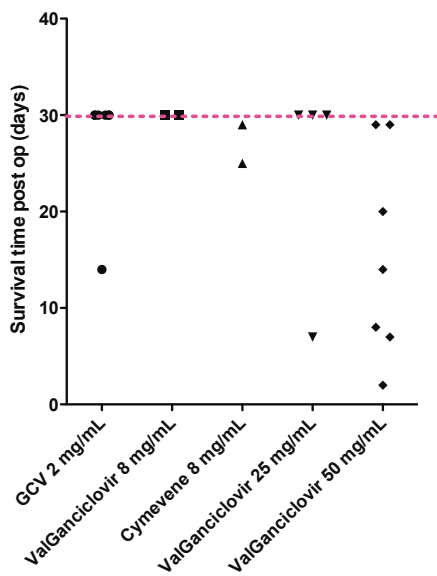


Figure 17 Survival time of CD11b-HSVTK mice with different dosages of ganciclovir derivatives aimed to treat for 4 weeks.

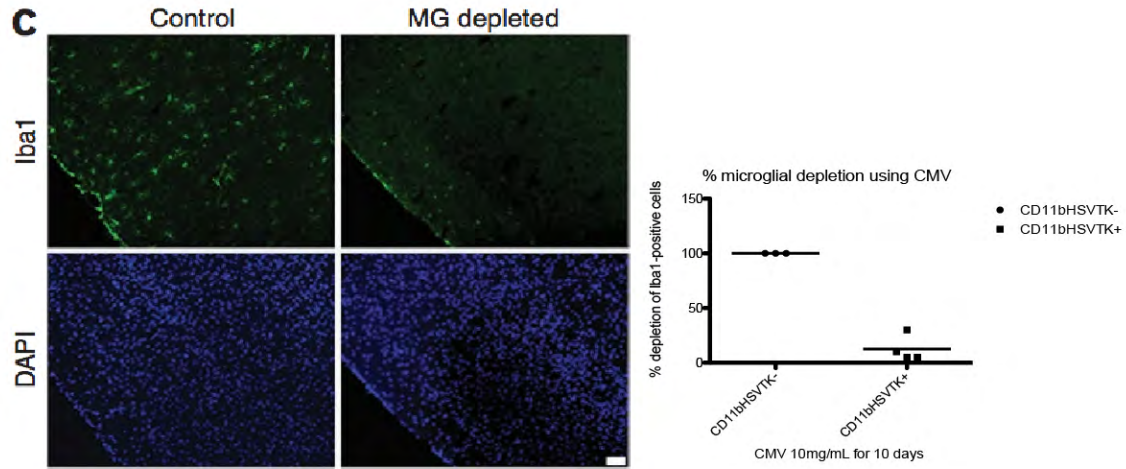


Figure 18 cortical depletion in CD11b-HSVTK construct-carrying transgenic mice (Lehmann et al 2012)

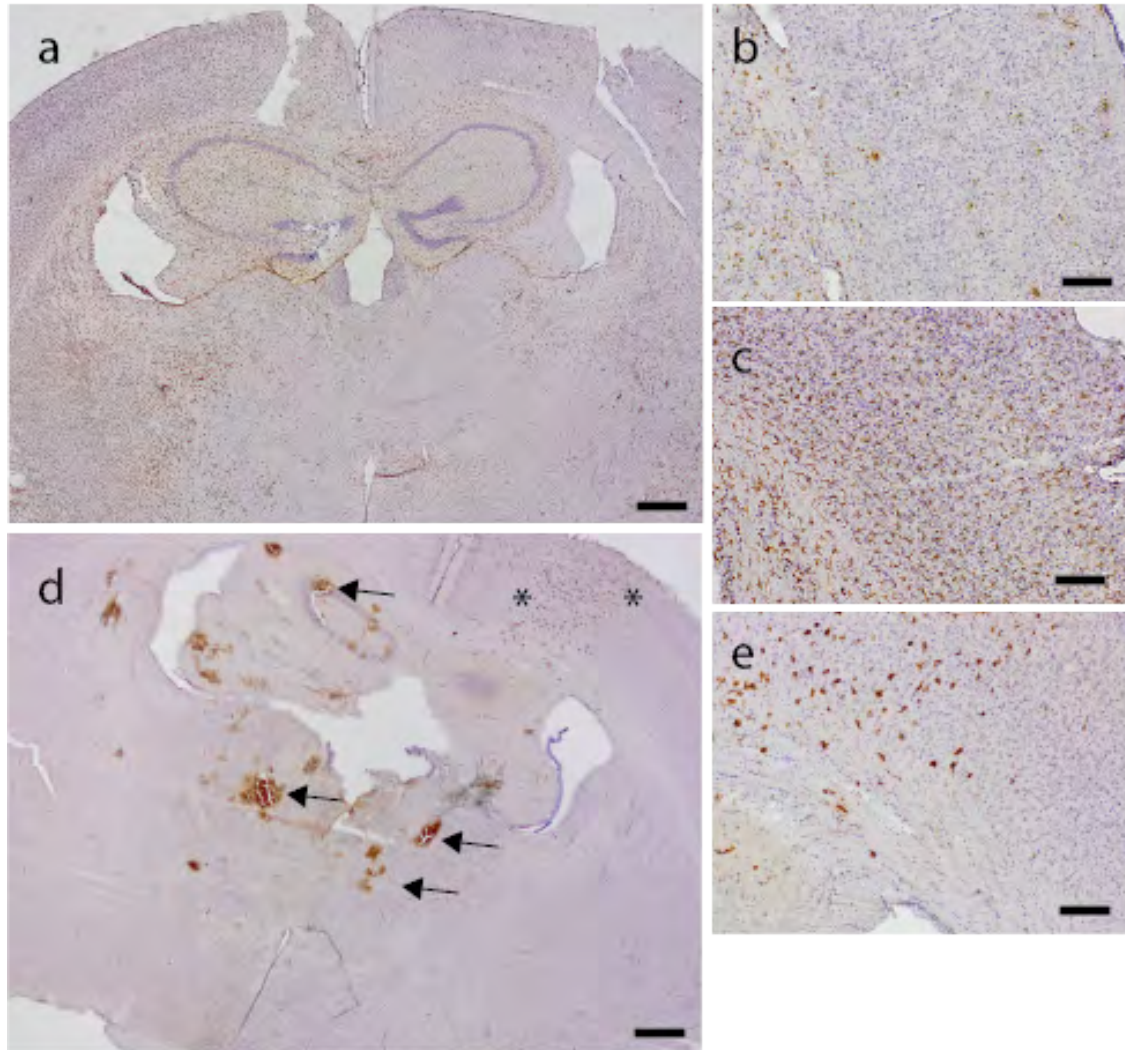


Figure 19 Depletion efficacies can vary and result in bleeding. a. Iba1-immunohistological staining of CMV treated CD11b-HSVTK mouse after 30 days. Partial depletion is observed in the contralateral side of the infusion site of the CMV (a, b) while the contralateral side seems to have inefficient depletion of microglia (a, c). (d) a VGCV treated TK mouse with obvious signs of bleeding (Iba1 immunohistochemistry, black arrows). In some regions, morphologically distinct Iba1-immunopositive cells are seen in a clustered patch. These cells are non-ramified and display an amorphous, non-circular cell body (e). Scale bar: 50um for a and d, 200 um for b, c, e.

<b>Drug</b>	<b>Concentration</b>	<b>Intracerebral infusion rate</b>	<b>Duration</b>	<b>Depletion outcome</b>	<b>Mouse line</b>	<b>Health status (tolerability)</b>
GCV	2mg/mL	1ul/hr	10 days	70-90% depletion	HSVTK	+++
GCV	2mg/mL	0.25ul/hr	30 days	30-40% depletion; Rep	HSVTK APP23;TK APP5;TK	++
GCV	2mg/mL	0.25ul/hr	60days	Rep	HSVTK	++
GCV:Na (Cymevene)	10mg/mL	1uL/hr	10 days	90%+ depletion	HSVTK	++
GCV:Na (Cymevene)	20mg/mL	0.25ul/hr	30 days	70-90% depletion	HSVTK	+/- high lethality
Valganciclovir	20mg/mL	0.25ul/hr	30 days	30-90% depletion	HSVTK	++ high lethality
Valganciclovir	50mg/mL	0.25ul/hr	30 days	30-90% depletion; rep	HSVTK APPS;TK (ref Grath)  APP23;TK (ref Grathw)	+/- high lethality
ACV	50mg/mL	0.25ul/hr	30 days	15-30% depletion	HSVTK	+++

Table 8 Depletion protocol titrations (Legend: +++ effective depletion of microglia, ++ moderate depletion of microglia, + little depletion of microglia).

### *5. Effect of microglial depletion on neuronal physiology:*

We had to consider any gross functional alterations in brain physiology upon microglial depletion. In particular, we focused in on neuron health and their aptitude to perform their day-to-day function of signal transmission.

Since the transgenic APP construct in APP23 and APPS1 mice is expressed in neurons, we wanted to ensure the additional manipulation of microglial depletion was not resulting in a shift in basic neuronal functional properties. We thus checked a battery of tests as a benchmark indicator of basic neuronal health and aptitude, which when altered could be interpreted to have a general shift in its functional profile.

Any such shifts could putatively affect the APP gene expression & secretion as well, and thereby falsely influencing the main pathological read-out– namely plaque burden.

Using Paxinos Mouse Brain Atlas, we depleted microglia in adult mice using the most reliable protocol (Figure 21). The mouse strain available to us for this experiment was CD11b-HSVTK (not crossed to AD mice).

We utilized our most robust model of microglia depletion (with the most reliable depletion efficacy), in order to detect any subtle changes in brain physiology in this setting. Mice were treated with ganciclovir for 10 days (Fig 21), and acute hippocampal slices were generated for recording from hemispheres by my colleague.

A battery of electrophysiological assays was carried out on the Schafer collateral pathway by my colleague Ismini Papageorgiou. Some of the results are included in this thesis as a representation of the test battery she conducted on these in vivo microglia-deprived hippocampal slices.

Firstly, stimulation response of principal neurons was measured by recording the excitatory

postsynaptic field potential (fEPSP) of the stratum radiatum in CA1 upon stimulation of CA3 with different voltage strengths. Measured fEPSP slopes from single traces were plotted against the voltage of initial stimulus in CA3, resulting in a stimulation response curve. This curve was not significantly different when comparing GCV-treated wild type mice with GCV-treated CD11b-HSVTK mice (Figure 20a).

Stimulation response was also measured by assessing synchronous action potentials in the stratum pyramidale of CA1. Population spike (fPop spike) intensity was plotted to its corresponding stimulation strength. There was no significant difference in synchronous firing activity detected in CA1 principal neurons between GCV-treated wild type and CD11b-HSVTK mice (Figure 20b).

Coupling the two parameters confirmed the lack of a significant shift in signal transmission upon stimulus in the Schaffer collateral pathway (Figure 20c). fEPSP-dependent fPop spiking seems to have no significant difference between the two groups.

Kinetics of the coupling ratio between fEPSP and fPop spiking seemed to show no significant deviation either, as the coupling plot over a span of varying potentiation strengths showed no significant difference. Both groups of GCV-treated mice displayed the typical sigmoid curve also seen in wild type adult mice which received no manipulation.

A careful dissection of the curve for any differences in  $S_{max}$ ,  $EC_{50}$ , and hill slope between the two groups of mice reaffirmed a lack of significant difference in the fEPSP-Spike coupling of neurons in CA1 (Figure 20d).

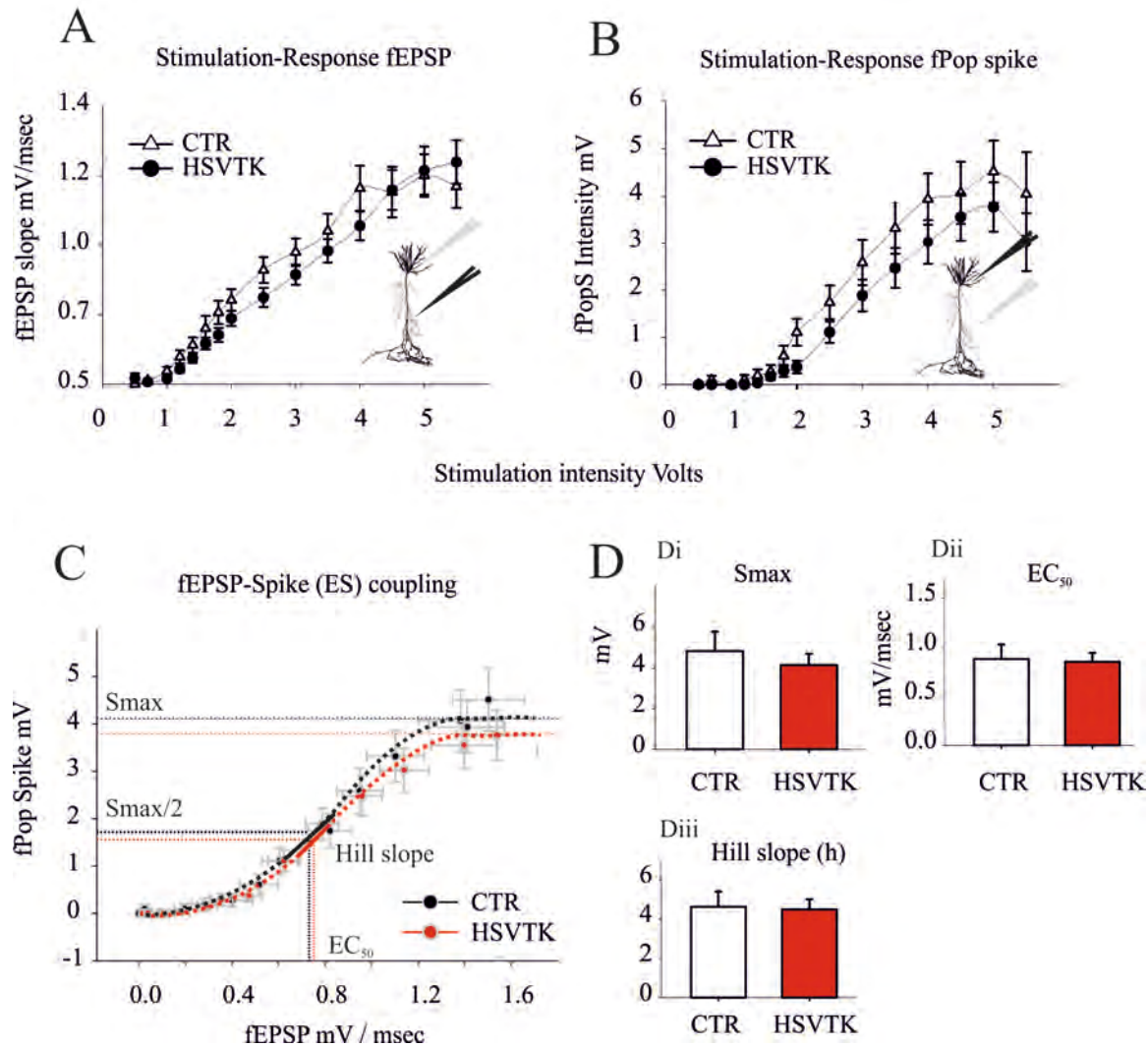
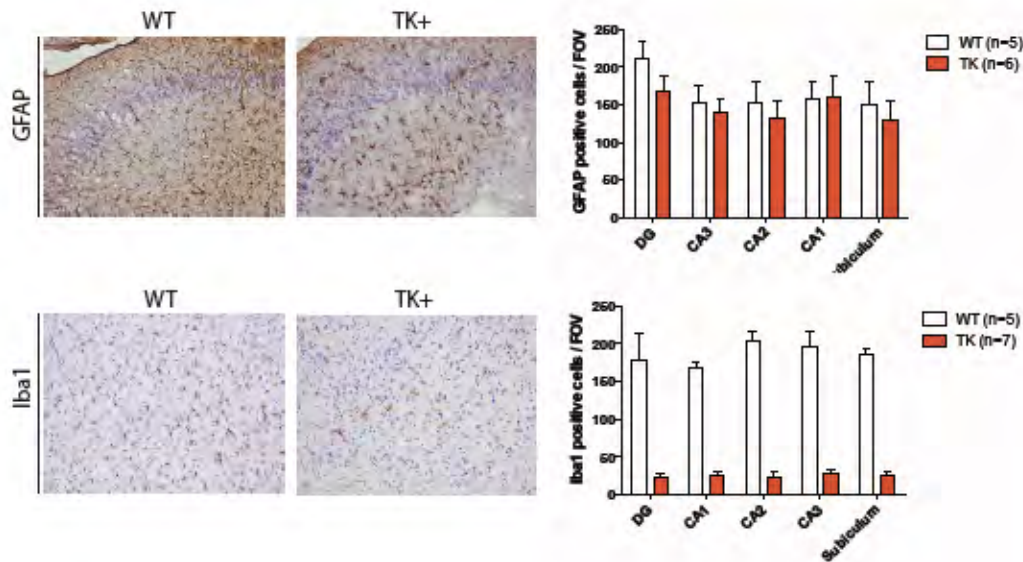


Figure 20 stimulation response curve of CA1 principal neurons

I wanted to confirm a successful in vivo depletion of microglia in one group (the CD11b-HSVTK mice with ganciclovir) but not in the other (WT treated with GCV) in the hippocampal slices used in electrophysiological recordings.

Histological quantification of microglia was done by immunostaining sections of recorded slices and by dividing the hippocampus into its anatomical subregions. Microglia was quantitated by manual counting in each subregion as defined by Paxinos mouse atlas and the Hippocampus book (Figure 21 b).

I saw a significant depletion of microglia in the GCV-treated CD11bHSVTK slices that were recorded, when compared to GCV-treated WT slices. In particular, there was a trend for the depletion to be greater around the CA2 and CA3 area, whereas depletion efficacy was the lowest in CA1 (Figure 21, lower panel). These differences in regional depletion efficacy were not statistically significant.



**Figure 21 recorded sections assessed for microglia and astroglia population. Upper panel – two dimensional quantitation of astrocytes by GFAP immunohistochemical staining. Lowerpanel – two dimensional quantitation of microglia by Iba1 staining.**

It has been previously shown that there was a large and significant astrogliosis following microglial depletion. To this end I also quantitated astrocyte population in the same fashion as microglia in recorded hippocampal sections. Paradoxically, I did not see a significant difference in astrocyte population, and rather saw a more profoundly visible astrogliosis in wildtype mice rather than microglia-depleted mice, in terms of GFAP-immunopositive cell population. This trend was not statistically significant, however.

In order to test functional parameters associated with astrocyte function, extracellular potassium activity was measured in both the axonal and cell body region of CA1 upon Schafer collateral stimulation (data not shown). While there was a statistically significant difference in the potassium curve architecture analysis in terms of its curvature and kinetics, this difference

was only visible upon delayed time lapse (3.0 seconds, data not shown) after simulation of the SC and thus less physiologically relevant. It thus suggested subtle changes in potassium buffering upon microglia depletion in the hippocampus.

In order to assess the inflammatory microenvironment of the hippocampus, which may influence electrical recordings of the parameters assessed in this study (references!), we measured a panel of cytokines in the absence or presence of microglial cells under the same in vivo microglial ablation protocol as our recorded mice. We quantified message expression (mRNA) of proinflammatory cytokines TNFalpha and IL6, as well as Iba1 and GFAP as an indicator of inflammatory environment in lieu of microglial depletion. Interestingly, Iba1 mRNA expression was not decreased in the 10 day depleted hippocampus (Fig 21, Figure 22). Histology of the same animal was qualitatively assessed for Iba1 protein, and there was significantly visible depletion in neighbouring regions of where mRNA quantification was done, confirming no error due to experimental set up (data not shown). TNFalpha, IL6 and GFAP expression all *tended* to be higher in microglia depleted group, but were not significant statistically (Figure 22 a, c).

Protein secretion was assessed of TNFalpha in order to affirm message expression (Figure 22 d). I also saw no statistically significant difference in secreted protein levels of TNFalpha. Overall the detectable TNFalpha levels in the hippocampal microenvironment were relatively low when compared to LPS treated hippocampus read at 8 hours post exposure.

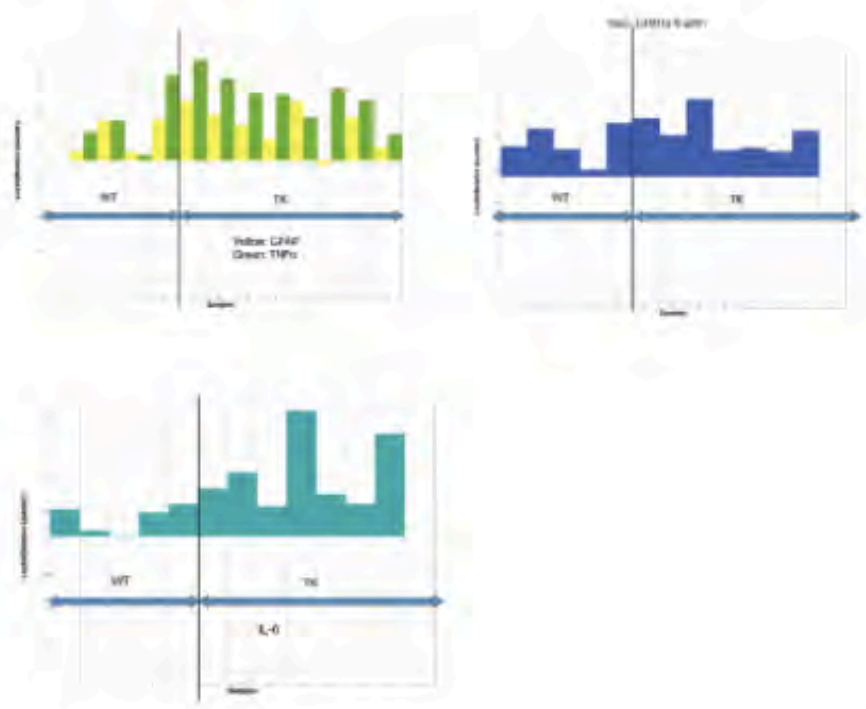
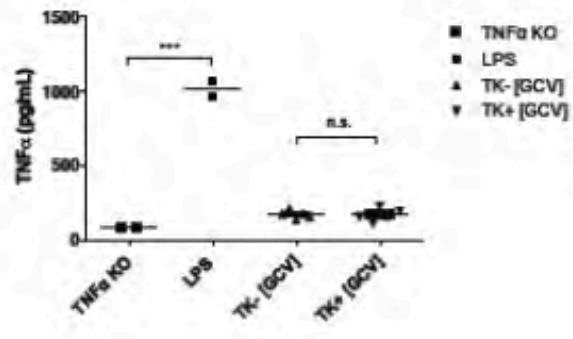


Figure 22 Hippocampal microenvironment upon microglial depletion.

## 6. Role of microglia upon AD immunotherapy (in APP23;TK mice)

As the longest robust protocol for microglia depletion lasted 30 days, and since APPS1 mice were difficult to immunize in that time frame - both in prevention and intervention of plaque pathology (Figure 1-5), we resorted to another transgenic murine models of AD. Available for this experiment were 19 month-old APP23-TK mice, which have been reported to be amenable to Abeta directed antibody treatment in previous studies (cite, cite).

Double transgenic *APP23;TK+* mice were generated by crossing the *APP23* mouse model of cerebral amyloidosis to CD11b-HSVTK mice, allowing removal of microglia. These mice at 19 months were then treated intracerebroventricularly (icv) with ganciclovir (GCV) using Alzet® miniosmotic pumps as described previously. Single transgenic littermate *APP23;TK-* mice were used as controls. In parallel all mice received a passive vaccination regimen of weekly intraperitoneal (ip) injections of either Ab9 or nonspecific IgG antibody ("ctrl").

After four weeks of icv GCV and antibody treatment, stereomorphometric analysis revealed a significant reduction of Iba1-immunopositive cortical microglia by 40% (Fig 23 a, b) in Ab9 treated *APP23;TK+* mice when compared to *APP23;TK-* control mice. This depletion of microglia was confirmed qualitatively by a second histological marker (isolectin B4, data not shown).

Notably, antibody treatment and icv GCV administration did not affect microglia numbers in *APP23;TK-* mice compared to age-matched non-treated controls (Fig. 23a, b). Upon observation in Ab9 treated *APP23;TK-* mice, microglia appeared to surround plaques more "tightly", with the processes polarized more frequently towards the center of the plaques. This morphological observation in Ab9 treated *APP23;TK-* mice differed from the control treated mice and from microglia-depleted mice, where microglial processes flared in multiple directions in spite of cells being clustered around the plaques.

Microglia depletion seemed to be less efficacious in control IgG treated *APP23;TK+* mice when compared to Ab9 treated *APP23;TK+* mice, as there was no statistically different microglial population between control treated *APP23;TK-* and *APP23;TK+* mice (Figure 23b). Upon

qualitative observation, however, Iba1 immunohistochemistry confirmed that ctrl/GCV treated APP23;TK+ assumed the distinctive morphology undergoing the depletion process.

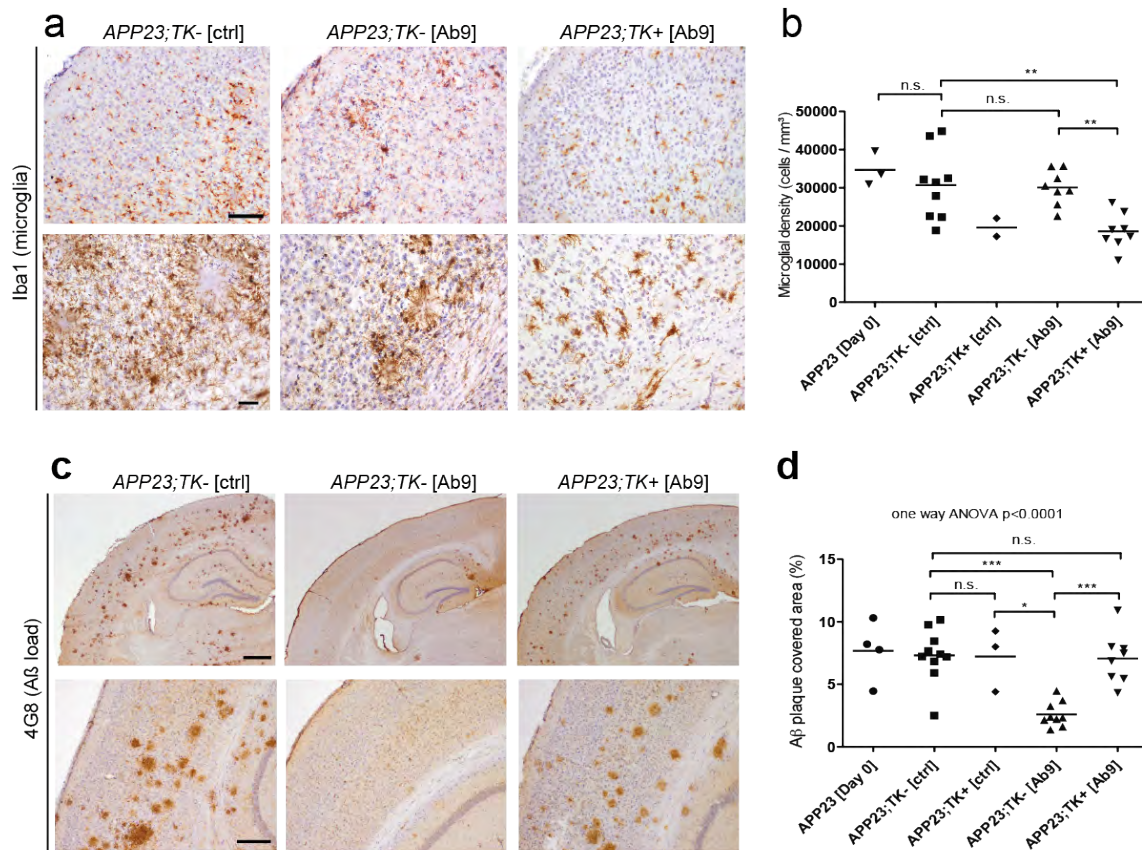


**Figure 23** Depletion of microglia neutralizes therapeutic efficacy of A $\beta$ -targeted antibody treatment in APP23 mice. (a, b) Microglial density in aged APP23;TK- and APP23;TK+ mice treated intracerebroventricularly (icv) with ganciclovir (GCV; 2mg/mL at a flow rate of 0.25 $\mu$ l/h) for 4 weeks and additional intraperitoneal (ip) injections of either control antibodies ([ctrl], n=9, left panel) or A $\beta$ -specific IgG2 $\alpha$  ([Ab9], APP23;TK-, n=8, middle panel; APP23;TK+, n=8, right panel) assessed by stereomorphometric quantification of Iba1-immunopositive cells in the neocortex ((b); one symbol represents the average cell density of one mouse). [pre-treatment] indicates untreated controls (n=3). Representative low (upper row; scalebar: 100  $\mu$ m) and high (lower row; scalebar: 25  $\mu$ m) magnification images are shown. (c) A $\beta$  plaque burden of the mice described in (a, b) was analyzed by stereomorphometric quantification of A $\beta$  (4G8)-stained brain sections (d; one symbol represents the average A $\beta$  burden of one mouse). Representative low (upper row; scalebar: 500  $\mu$ m) and high (lower row; scalebar: 100  $\mu$ m) magnification images are shown.

Importantly, we assessed plaque pathology in these mice. Congruent with other AD vaccination studies, immunotherapy in aged APP23;TK- mice using four weekly Ab9 injections led to a significant and visible reduction in A $\beta$ -plaque burden by 65% (Fig. 23c, d) when

compared to control-treated *APP23;TK-* mice (n=9 per group) and untreated *APP23* mice at Day 0/19 months of age (n=3).

However, when we immunized *APP23;TK+* mice with Ab9 in which microglia were substantially removed (Fig. 23a, b), cortical A $\beta$  plaque load was not reduced and remained at similar levels as the control-treated group (Fig. 23c, d).

While the overall A $\beta$  plaque load of Ab9-treated *APP23;TK+* mice were no different from the control treated *APP23 (TK-)* mice or the untreated *APP23;* mice, there was a qualitative difference in the plaque appearance. Qualitatively the plaques looked smaller and more numerous when compared to control treated *APP23;TK-* mice, but this observation was not statistically significant upon a thorough plaque size distribution analysis (Figure 27). Plaques of Ab9 treated *APP23;TK+* mice also appeared more round in shape, displayed a clear border (“less fuzzy”), and were more evenly distributed throughout the neocortical parenchyma when compared to the control treated *APP23;TK-* group (qualitative observation).

This lack of an efficacy of Ab9 treatment of microglia depletion was confirmed in the hippocampus, where a similar trend was observed when assessing the same parameters (data not shown).

We confirmed this striking effect of a lack of Ab9 treatment efficacy by measuring total A $\beta$  content biochemically (Fig. 24). Electrochemoluminescent immunosorbent assays (with greater sensitivity than conventional ELISAs) were utilized to measure total A $\beta$  content of the brains from treated *APP23;TK+* and *APP23;TK-* mice. We had fractionated brain homogenates in a sequential fashion, extracting most water-soluble proteins to most water insoluble to create altogether four fractions (TBS-soluble, Triton-X soluble, SDS soluble and 70% FA soluble). The total A $\beta$  (A $\beta$  40 + A $\beta$  42) quantity extracted from all four fractions recapitulated plaque pathology assessed by histological quantification (Figure 24c, Figure 23a).

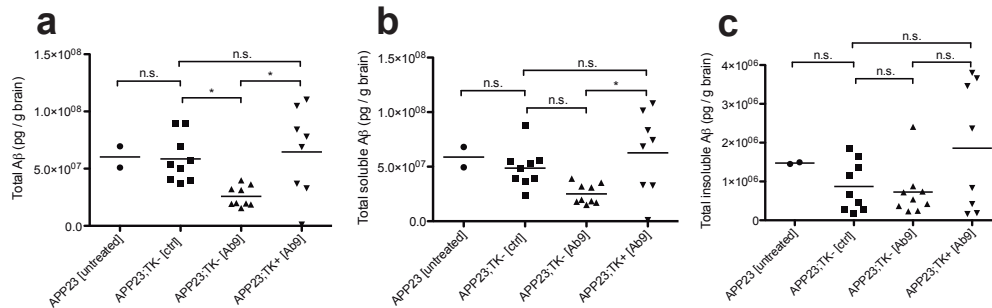


**Figure 24 (a) Total A $\beta$  (A $\beta$ 40 + A $\beta$ 42) brain content, (b) 2%-SDS soluble A $\beta$  (A $\beta$ 40 + A $\beta$ 42) brain content, and (c) 2%-SDS insoluble / 70% formic acid extracted A $\beta$  (A $\beta$ 40 + A $\beta$ 42) brain content determined by electrochemoluminescent enzyme-linked immunosorbent assay (ELISA). \* P < 0.05, \*\*P < 0.01, \*\*\*P < 0.001 versus respective basal values using Bonferroni post-hoc test after one-way analysis of variance (ANOVA). (a-c): one symbol represents one mouse.**

When the first three soluble biochemical fractions were summed up for total “soluble” A $\beta$  species (both A $\beta$ 40 and A $\beta$ 42), there was no significant difference between any of the groups, except between Ab9 treated APP23;TK- and Ab9 treated APP23;TK+ mice, where APP23;TK+ mice had significantly higher soluble brain A $\beta$  content (P<0.05).

A more detailed biochemical analysis revealed a preferential reduction of the first and second most soluble A $\beta$ -species in Ab9 treated APP23;TK- mice compared to control treated APP23;TK- mice, while insoluble fractions of A $\beta$  were only slightly or not altered upon Ab9 treatment (Figure 25 a-h). Soluble A $\beta$ -species were in contrast not altered in microglia depleted and Ab9 treated APP23;TK+ mice compared to control treated control mice, while these mice revealed a trend towards higher levels of insoluble A $\beta$ -species (Figure 25).

In line with the lack of a significant change in insoluble A $\beta$  in the brain upon Ab9 treatment when compared to control, there was also a less impressive reduction of Congo red-positive plaques in Ab9 treated APP23;TK- mice compared to control treated mice (Figure 26).

Together these results indicate that the reduction of A $\beta$  from the brain observed during passive vaccination is largely mediated by microglial cells, but that a large portion of this A $\beta$  shift happens in the soluble fraction and not the insoluble A $\beta$  conformation.

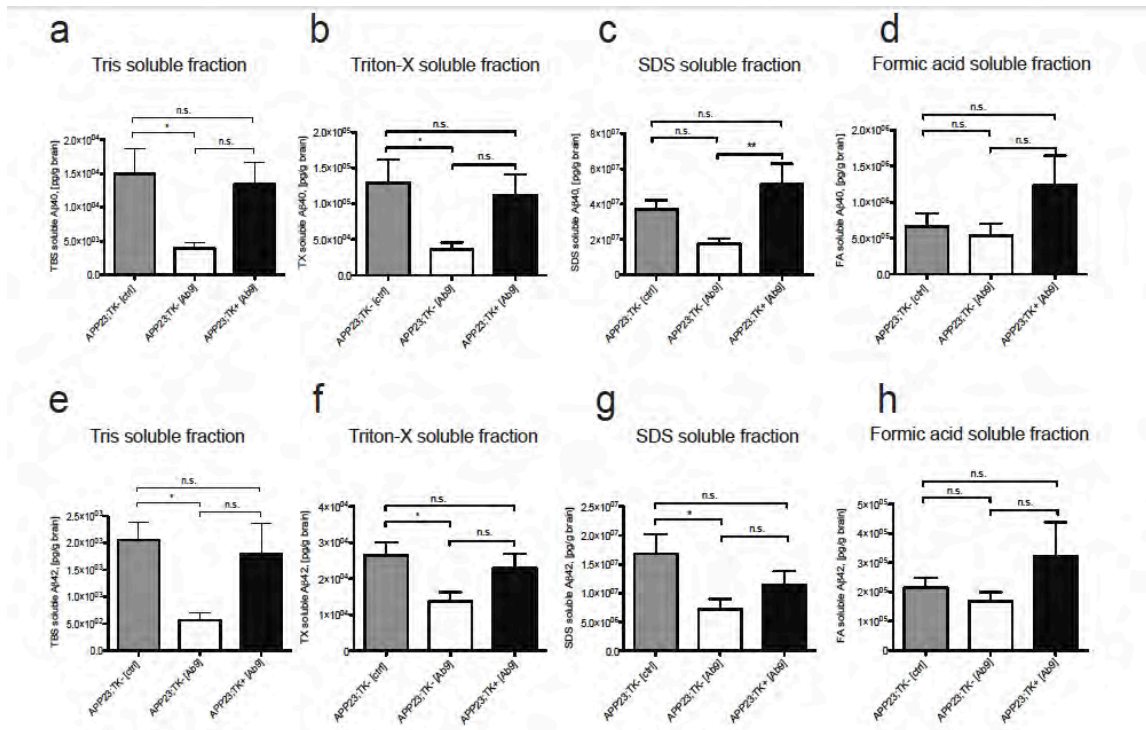


**Figure 25** 4-step sequential biochemical extraction of brain protein A $\beta$ 40 (a - d) and A $\beta$ 42 (e - f) content from four individual fractions from sequential brain protein extractions. Bars represent means of data + s.e.m, n=9 for control and Ab9-treated APP23;TK- mice and n=8 for Ab9-treated APP23;TK+ mice. Upper row = A $\beta$ 40, lower row = A $\beta$ 42. \* p<0.05, \*\*p<0.01 versus respective indicated reference values using Bonferroni post-hoc test after one-way ANOVA. p-values of one way ANOVA for each fraction: (a) p=0.0266 (\*) for A $\beta$ 40 and (e) p=0.0192 (\*) for A $\beta$ 42. (b) p=0.0122 (\*) for A $\beta$ 40 and (f) p=0.0299 (\*) for A $\beta$ 42. (c) p=0.0112 (\*) for A $\beta$ 40 and (g) p=0.0507 (n.s.) for A $\beta$ 42. (d) p=0.2992 (n.s.) for A $\beta$ 40 and (h) p=0.1767 (n.s.) for A $\beta$ 42. TBS = Tris buffered saline, TX = Triton-X, SDS = sodium dodecyl sulfate, FA = formic acid.

We asked whether there was a direct relationship between plaque burden and microglia density within our treated mice on a case by case basis. Microglia were less clustered around the remaining plaques of Ab9 treated APP23;TK+ mice, and this observation was obvious when a double immunofluorescent stain was performed, as there were surfaces of the plaques which were devoid of microglial contact. This observation was highly unusual as in comparison, Ab9 or control treated APP23;TK- mice had significant clustering of microglial processes around the plaque border.

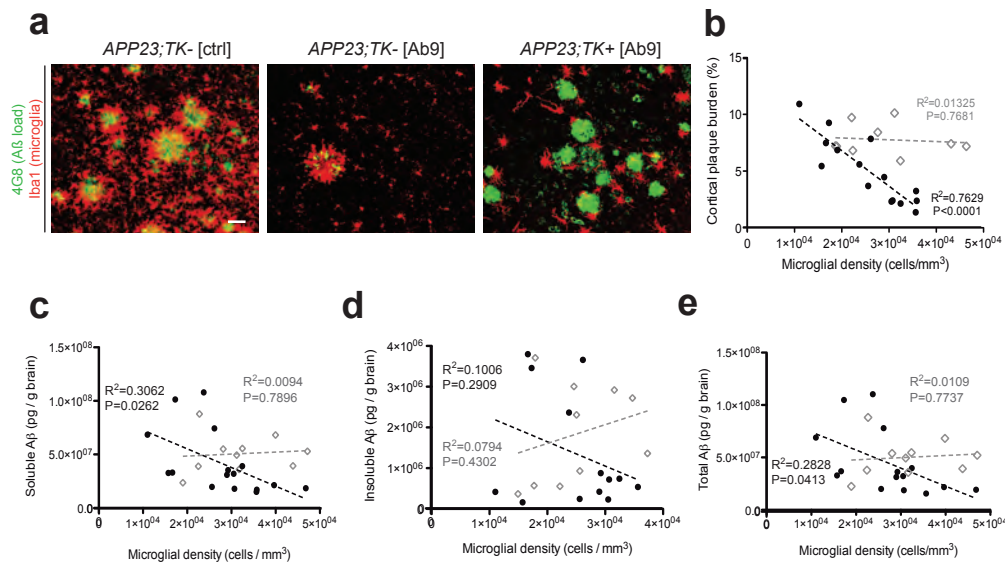


**Figure 26 Critical dependence on microglial effector function for lowering A $\beta$  burden in vaccinated APP23 mice. (a) Representative images of fluorescent double labeling with Iba1 antibodies (red) and anti-A $\beta$  antibodies (green; scale bar: 150  $\mu$ m) in mice described in Figure 1 A and B. (b) Correlation of microglial density and cortical A $\beta$  burden in control-treated APP23;TK- mice (grey symbols, [ctrl]) and A $\beta$ -vaccinated APP23;TK- and APP23;TK+ mice (black symbols, [Ab9]). (c) Correlation of microglial density and total soluble (buffer- or detergent- soluble) A $\beta$  burden (A $\beta$ 40+42) in control-treated APP23;TK- mice and A $\beta$ -vaccinated APP23;TK- and APP23;TK+ mice. (d) Correlation of microglial density and total insoluble (formic acid extracted) A $\beta$  burden (A $\beta$ 40+42) in control-treated APP23;TK- mice and A $\beta$ -vaccinated APP23;TK- and APP23;TK+ mice. (e) Correlation of microglial density and total A $\beta$  burden (A $\beta$ 40+42) in control-treated APP23;TK- mice and A $\beta$ -vaccinated APP23;TK- and APP23;TK+ mice. (b –e): one symbol represents one mouse, control treated APP23;TK- mice in grey symbols, [ctrl] and A $\beta$ -vaccinated APP23;TK- and APP23;TK+ mice in black symbols, [Ab9].**

We observed a striking inverse correlation between A $\beta$  plaque burden and microglial density in Ab9-treated mice regardless of genotype (*APP23;TK-* and *APP23;TK+* mice, Fig. 26), while notably there was no significant correlation between cortical plaque load and microglial density in control treated *APP23;TK-* mice (Fig. 26b, c, d, f). Similarly, there was a significant inverse correlation between biochemically measured total brain A $\beta$  content and microglial density, as well as soluble A $\beta$  content and microglial density in Ab9-treated mice regardless of genotype (Figure 26, c,d). Notably this significance was not seen when correlating insoluble A $\beta$  content in Ab9-treated (or control-treated) mice (Figure 26 e).

This finding further emphasized the critical dependency on microglia in anti-A $\beta$  antibody-mediated reduction of A $\beta$  plaque load.

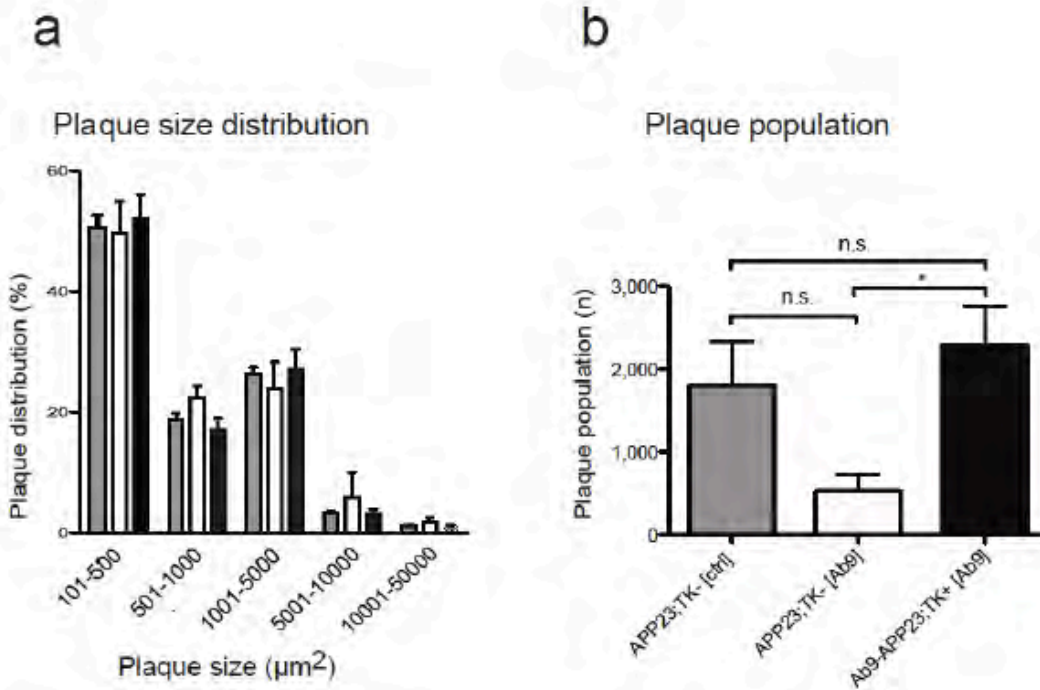


**Figure 27** Size distribution and population of plaques. (a) plaque size distribution between control-treated APP23;TK- (grey), Ab9-treated APP23;TK- (white), and Ab9 treated APP23;TK+ (black) mice (n=5 per group). No statistical significance was observed. Bars represent means of data + s.e.m per group. (b) Plaque number from 30 corticla brain images. See methods for detail. Bars represent means of data + s.e.m. per group (n=5 per group), \*P<0.05 versus indicated reference group using Bonferroni post-hoc test after one way ANOVA (P=0.0405).

As previously mentioned, plaque size distribution (Figure 27) was not significantly altered between experimental groups in spite of the significant differences in plaque burden (Figure 23). Thus, antibody-mediated removal of existing plaques appeared to go along with prevention of new plaque formation in Ab9-treated mice in a relatively distributed fashion, not significantly favouring one process over another in this treatment set-up.

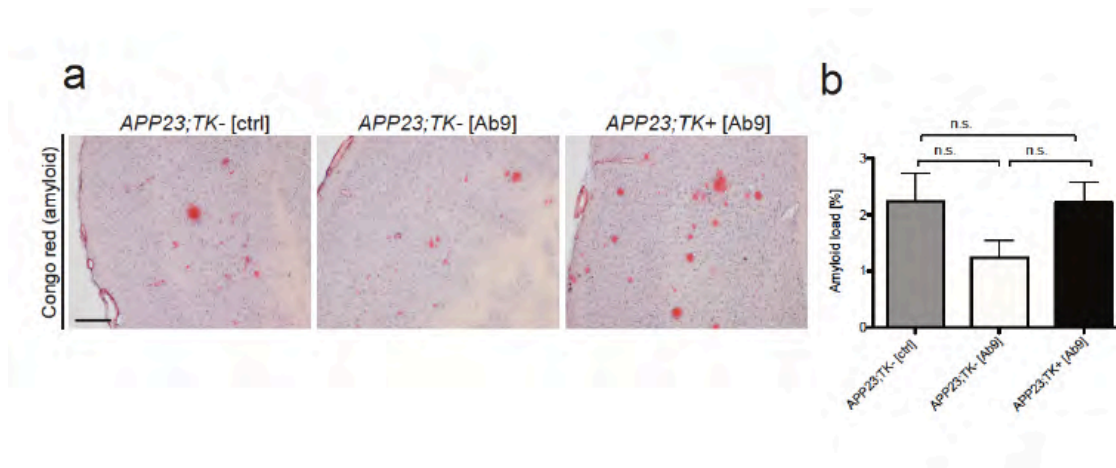


**Figure 28 Inefficient amyloid clearance in APP23 mice treated with antibodies in the absence and presence of microglia. (a) Representative images of Congo red staining (scale bar: 100um) are shown. (b) Quantitation of amyloid burden by cortical area covered by Congo red positivity (n=6-7 per group). Bars represent means of data + s.e.m. and statistical comparison between each group using Bonferroni post-hoc test after one-way ANOVA (P=0.1613).**

While there was no significant shift in amyloidosis during this four-week treatment window, we assessed vascular pathology with great interest in these mice. The vascular parameter was of particular interest in APP23 mice at this age of 20 months, as they are known to have an onset of cerebral amyloid angiopathy and spontaneous microhemorrhage.

Since vasogenic edema and microhemorrhage have been observed upon anti-A $\beta$  immunotherapy both in experimental animals(96) and AD patients(49), we analyzed vascular pathology in our experimental setup in detail.

Cortical vessels were assessed in a systematic fashion and scored for severity of amyloid pathology using criteria adapted from previous patient and murine studies (Methods and Materials of this thesis). Surprisingly, there were no differences in CAA severity (Figure 29a) or CAA score (Figure 29b) between the treated groups, nor was there a significant difference in frequency of the individual CAA classes between the treated groups (Figure 29c, d, e).

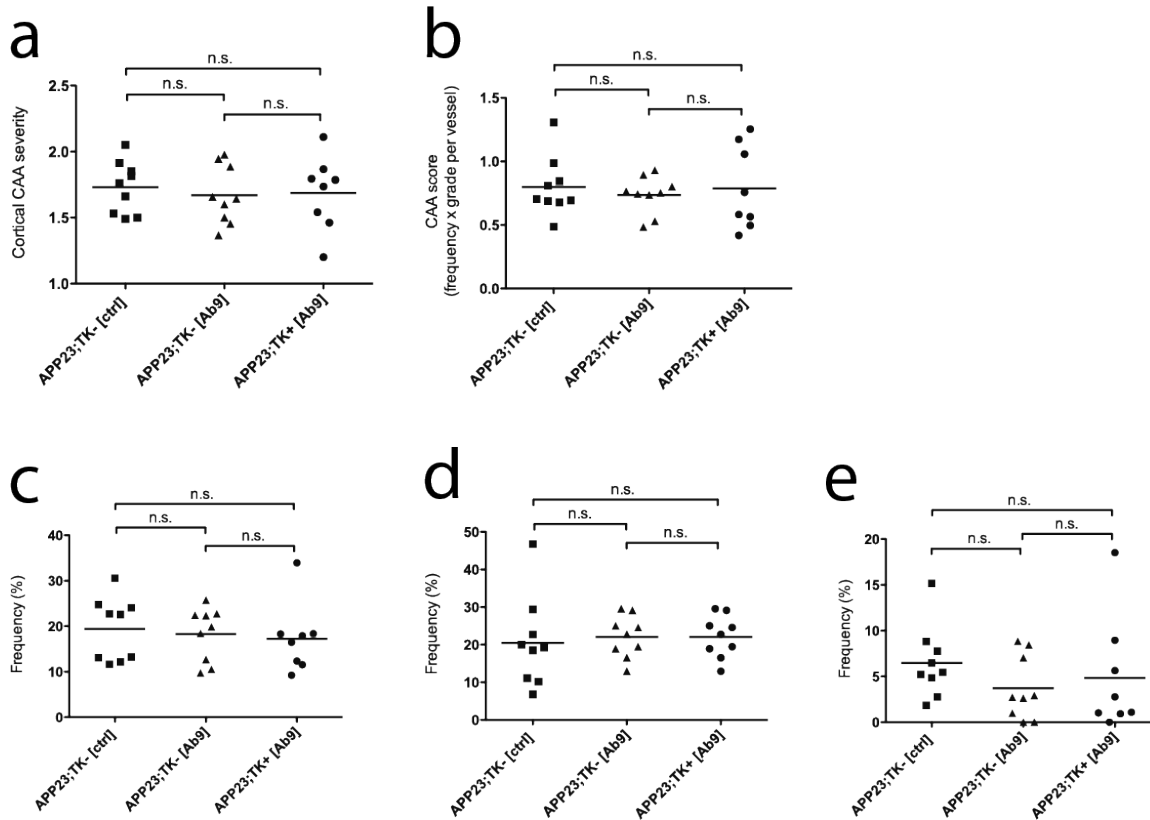


**Figure 29 Assessment of cerebral amyloid angiopathy. a. overall CAA severity, b. quantification of CAA scores. c – d individual frequencies of CAA grades.**

In conclusion, we found that frequency and severity of cerebral amyloid angiopathy (CAA) were not altered between experimental groups (Fig. 29).

Several reports showed an increase in microhemorrhage upon immunotherapy in AD patients and murine models of AD (cite). We analysed the number of bleeds per section and the severity of microhemorrhage and found no difference between the treated groups (Figure 30 a, b). While we saw a trend in an increase in microhemorrhage frequency upon Ab9 treatment in APP23;TK- mice but not in Ab9 treated APP23;TK+ mice, and this trend was not significant in our treatment set-up (Figure 30a, b).

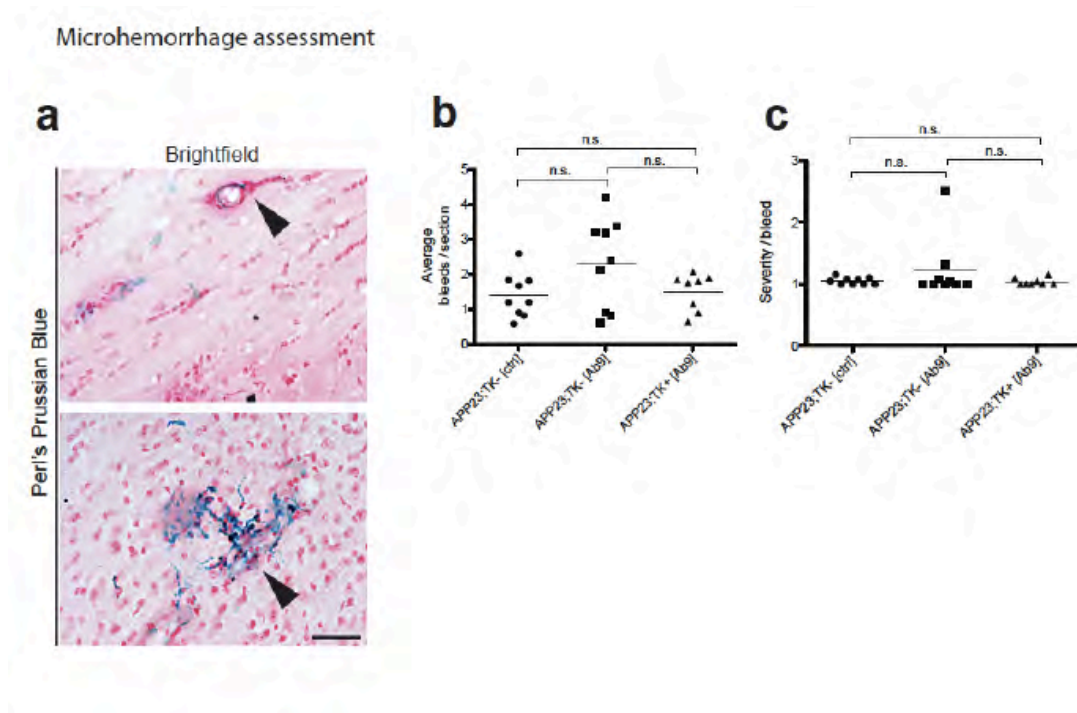


**Figure 30 vascular pathology as assessed by hemosiderin stain. a. representative image of a grade 1 (upper panel) and grade 3 (lower panel) bleed. b. quantitation of average number of bleeds and c. ratio of severity of bleeds/section.**

Overall, our study on vascular pathology revealed that within this 4 week period of Ab9 versus control antibody treatment in APP23 mice, there was no significant alteration on existing vascular pathology (Figure 29, Figure 30), eventhough there was a clear change in overall A $\beta$  pathology upon treatment (Figure 23).

Taken together, our data demonstrate that microglial density determines the efficacy of A $\beta$ -specific immunotherapy.

As we saw a clear effect in the brain (Figure 23) in terms of shift in A $\beta$  pathology upon Ab9 treatment in APP23;TK- mice when compared to controls, we next asked whether we could show that the antibody Ab9 had reached the brain. Thus we attempted to measure A $\beta$  specific antibody titres in the brain homogenates from treated animals. Using various treatment conditions in an A $\beta$  antibody capture ELISA, we were unable to detect any A $\beta$  antibodies in any of the brain homogenate fractions (data not shown). This was likely due to a sensitivity issue of the assay, as positive controls (homogenates spiked with Ab9) were unable to yield high signal (data not shown).

As an additional evidence of antibody presence in the brain, we measured complement levels in the TBS fraction (most water soluble fraction) of brain homogenates of treated APP23 mice. We found a statistically significant difference in Ab9 treated APP23;TK- and APP23;TK+ mice (Figure 31 c), but there was no difference between control treated and Ab9 treated APP23;TK- mice (Figure 31 c).

Besides a central mechanism of plaque reduction via microglia, increased peripheral drainage of A $\beta$  has been cited as a mechanism of A $\beta$  immunotherapy. We analysed plasma A $\beta$  titres using the electrochemoluminescent assay system. Neither A $\beta$ 40 nor A $\beta$ 42 were significantly elevated in plasma taken after 4 weeks of Ab9 treatment when compared to control treatment in APP23 mice (Figure 31 a, b)

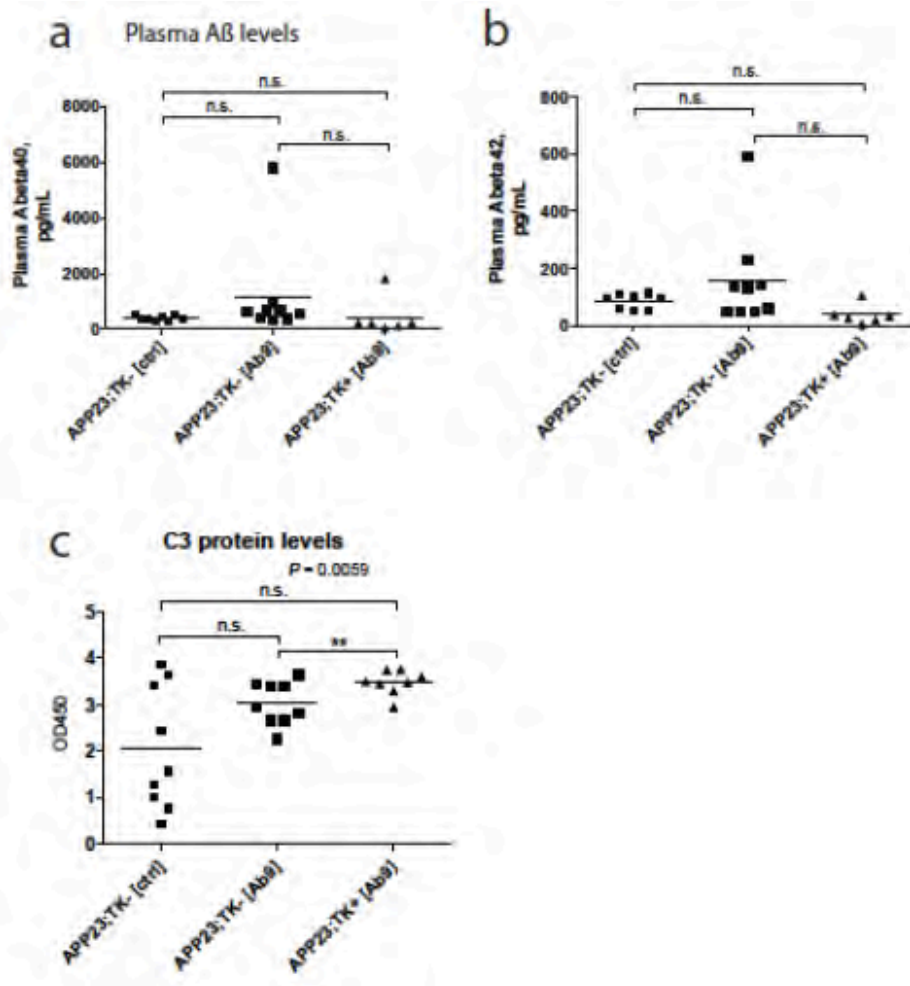


**Figure 31** peripheral Abeta detection in plasma. Central C3 levels from TBS fraction of brain homogenates of treated APP23 mice.

Taken together, Ab9 treatment in APP23;TK- mice seemed to manipulate largely cortical Aβ plaques but not vascular amyloid pathology nor the peripheral Aβ titers upon treatment. A depletion of cortical microglia in APP23;TK+ mice seemed to disable the antibody Ab9's ability to reduce plaque pathology, suggesting microglia are a key player in conferring treatment efficacy of Aβ antibodies.

## **Discussions:**

In the midst of anticipated results of continuously refined clinical trials of immunotherapy in AD, how these anti-A $\beta$  antibody regimens mediate relief of A $\beta$  burden in the diseased AD brain remains inconclusive to this date. Elucidating the mechanism of this treatment would enable modification strategies with greater finesse and predicting contraindications for the individual patient.

Putative mechanisms of A $\beta$  immunotherapy have included microglial involvement in phagocytosis or other forms of internalization of plaque A $\beta$ , supported by their clustering around plaque moieties and their observed upregulation of inflammatory markers (CD45, CD68)(99,100). At the very least, current evidence seems to suggest some sort of unique response by microglia to this treatment that differs from untreated patients.

In order to address this point directly, we utilized our unique murine models of AD with possible inducible ablation of microglia. Our strategic approach was simple: deprive the AD brain of myeloid cells while treating with A $\beta$  antibody and see if the treatment still works without these cells.

We first established treatment protocols specifically catering to our mouse models and our experimental set-up. The protocols we established had to fulfill the following criteria:

- 1) Selection of an appropriate transgenic murine model of AD for administering an anti-A $\beta$  antibody treatment protocol which would yield a clear and discernible reduction in A $\beta$  load from the brain (>30%). Such a murine model was required in order to anticipate kinetic changes in plaque pathology, upon microglia depletion in follow-up experiments.
- 2) The reduction in A $\beta$  load from immunotherapy had to occur within a timeframe that was compatible with a robust depletion protocol of microglia in our model.
- 3) Minimal perturbation on neuronal function was desired upon microglia depletion, in order to avoid offsetting overall brain physiology inadvertently. This outcome was desired to avoid falsely influencing pathological read out (introducing an error from the artificial effect of microglial depletion).

Only when these conditions were met would it be possible to assess the plaque burden upon microglia depletion in immunotherapy treated transgenic murine AD brains. Thus, technical titrations were a prerequisite part of our vaccination studies.

APPPS1 mice have a robust plaque burden with minimal gender difference, and early onset of plaque burden of 4 to 6 weeks with fulminant plaque pathology at 4 months of age. This expedited plaque deposition relative to other murine models makes it a very attractive model in a research setting, having relatively short waiting period until onset of a reliable pathological read out.

It was for these reasons that we first chose to establish a treatment protocol in APPPS1 mice. We first wanted to see whether Ab9 antibody was able to prevent or delay the onset of plaque pathology and thus applied the antibody as a prophylactic treatment in comparison with control treatment (unspecific antibody). We also wanted to see whether Ab9 was able to reduce existing plaque pathology by treating older animals.

As APPPS1 mice have a rapid and aggressive onset of plaque production at 6 weeks of age, we began treatment in 3-week-old animals on a weekly basis (n=7 Ab9, n=6 control) before any plaques had formed in the brain. This weekly intraperitoneal treatment continued until the animals were 4 months of age, where plaque burden was robust.

This was a total of 13 weeks of continuous treatment, and after this extensive treatment period we were surprised to find that there was no difference in overall plaque burden when assessed as area covered by A $\beta$ , or area covered by fibrillar A $\beta$  using novel chemoluminescent probe pFTAA. It was only when assessing total plaque population in terms of numeration in the cortex when a significant reduction was seen. This seemed to suggest that there was an overall increase in the size of plaques, as the deposits had decreased.

This observation warranted further investigation of plaque size analysis by breaking down the plaques into different class sizes and looking at the proportion of plaques per class comparing Ab9 and control treated groups.

Congruent with the overall plaque analysis there was a significant increase in the number of larger plaques in Ab9 treated groups when compared to control ( $P < 0.05$ ). There was also a significant decrease in the number of smaller plaques ( $P < 0.05$ ), confirming an overall shift in plaque types.

This shift can be explained when taking into account current literature on plaque formation, particularly in this specific murine model(101). Smaller plaques were shown in in-vivo studies to be newer plaques, while larger ones are older (cite). The current shift we see upon Ab9 treatment when compared to control may be due to a change in the type of plaques which are seen in Ab9 treated brains – as plaques become dissolved from Ab9 treatment (through a process of affinity competition between  $A\beta$  to existing plaques and to Ab9), the smaller plaques are more likely to dissolve and disappear, while the larger plaques remain. This would explain the decrease in the smallest plaque numbers. However, with the current data it is not possible to discern whether Ab9 in the brain is actually causing the dissolution of existing plaques or preventing the formation of new plaques, as both processes would result in a decreased number of small plaques in this mouse strain.

The increase in larger sized plaques could be due to an ongoing dissolution process of older plaques. This process would involve the gradual resolution of denser cores, where it is feasible that such a process would result in a larger surface area taken up by  $A\beta$ . Further supporting this notion is the observed decrease in amyloid burden in brains treated with Ab9 compared to controls, indicating the denser core comprised of amyloid structure is being removed. An intermediate step of amyloid dissolution could very well be an increased surface area as shown in a previous in vitro study(102,103), as amyloid is unwinding and dissolving.

Taken together, we concluded that this lengthy Ab9 prophylactic treatment alters plaque pathology and initiates a process of plaque removal in the early onset of plaques. We further concluded that this treatment is not sufficient to prevent plaque formation and that Ab9 treatment this early in APPPS1 mice was not an adequate treatment set-up for our study on

the role of microglia in immunotherapy.

Efficacy of Ab9 Treatment					
Timepoint	Plaque formation (early)			Plaque maintenance (late)	
Strain tgAD	Weekly dosing	GCV	Efficacy assessment	Weekly dosing	GCV
<i>APPS;TK-</i>	17mg/kg 13 weeks	no	slight	17mg/kg 8 weeks	yes
<i>APPS;TK-</i>				17mg/kg 4 weeks	yes
<i>APPS;TK-</i>				34mg/kg 4 weeks	yes
<i>APPS;TK-</i>				34mg/kg 6 weeks	no
<i>APPS;TK-</i>				68mg/kg 4 weeks	yes
<i>APP23;TK-</i>				17mg/kg 4 weeks	yes

Table 9 Efficacy of Ab9 treatment in two different transgenic AD mouse strains.

Previous studies have shown that any given anti-A $\beta$  antibody is either effective in intervention or prevention, but rarely in both. Thus we postulated that Ab9 might be effective in interventional treatment, since it was not impressive in preventing A $\beta$  plaque production.

We devised a treatment protocol that was shorter than the 13 weeks prevention study, by treating 8 month old APPS;TK- animals weekly with either Ab9 or vehicle control for 8 weeks (total 8 injections). In addition we wished to test whether or not ganciclovir infusion into the

brain (a necessary additional manipulation for our subsequent microglia study) would hinder treatment efficacy.

As interventional treatment for 8 weeks resulted in a significant reduction in plaque numbers, amyloid load and deposit numbers, but not overall A $\beta$  plaque load, we concluded that Ab9 was slightly better in this later treatment setting to reduce pathology.

As an additional read-out we assessed reported side effect of increased microhemorrhage incidence in these treated APPS-TK- mice. Upon qualitative assessment rendered no visible microhemorrhage in any of the mice that were treated with either Ab9 or vehicle. This is likely due to the fact that there is little vascular pathology present in this model, rather than an antibody effect, as control animals were also unaffected by cerebral bleeding.

While an 8 week treatment protocol showed a clearer reduction in plaque burden than a prevention study in younger APPS1 animals, we still did not see any reduction in overall A $\beta$  burden in the older treated mice. Thus we wanted to increase the antibody dose and work with a shorter time frame of treatment that was also compatible with a microglial depletion protocol of 4 weeks. Surprisingly, we encountered a ceiling effect, as even a four-times increased dose of antibody treatment did not render any significant treatment efficacy in a time period of 4 weeks (Figure 5). Titrating antibody dosage upwards within a restricted time frame seems to have no therapeutic effect, suggesting that the clearance system is already saturated (at capacity) with the lowest dose we tried out. After a certain dose of antibody, increasing therapeutic efficacy can thus only be achieved by increasing the treatment duration, and increasing the dose cannot compensate for this duration.

As 8 weeks of Ab9 treatment had given us the greatest treatment efficacy (greatest plaque reduction) thus far, we tried to match this time window with a microglia depletion protocol for the same duration. Table 10 summarizes our findings.

Previous studies had only cited 30 days of microglial depletion when administering the inductive drug GCV directly into the brain of our murine models (harbouring the CD11b-HSVTK construct). We wanted to extend this to double the time period in order to accommodate for a possible Ab9 treatment efficacy.

At our disposal was a plethora of ganciclovir derivations: the pure form itself (ganciclovir), ganciclovir sodium which was an infusion form, prodrug valganciclovir, and an entirely different antiviral drug acyclovir. In order to achieve the longest possible microglia depletion protocol, I opted to try all drugs for the purpose of this project. Each drug had their unique properties when tried as the inducer for microglial ablation in our CD11b-HSVTK mouse model.

Every form of GCV was able to ablate microglia in TK mouse brains, while acyclovir had no effect on microglia (data not shown). Titrating out various concentrations and flow rates of different GCV derivatives showed various depletion efficacies. GCV (pure form) was able to robustly deplete microglia in 10 days by about 80-90% in the hippocampus, while GCV sodium could be concentrated higher and thus achieved an even greater depletion rate (95%+) during that time window.

Extensive work had been done using prodrug Valganciclovir, reporting high depletion efficacy in 4 weeks. The work had not been tested beyond 30 days and thus warranted further tests in that direction. We encountered a significantly higher drop-out rate in valganciclovir-treated mice than pure GCV treated mice at 30 days and decided not to extend the treatment in the surviving mice. Post mortem brain analyses revealed a significant depletion as reported (>95%) but there was also a frequent incidence of bleeding in the mid brain area.

As VGCV could be concentrated 25 times higher than its pure GCV form, too high of a concentration may result in adverse side effects as observed. Similar effects of high drop out rates, high microglia depletion was seen in the intravenous derivative GCV sodium. However, in these treated mice no bleeding was observed. Pure GCV infusion cerebrally in CD11b-HSVTK mice for 30 days seemed to result in a modest depletion, but sometimes some morphologically distinct Iba1 immunopositive cells were visible in clusters, suggesting an occurrence of compensating myeloid cells (in spite of an incomplete depletion).

We thus concluded that it was challenging to achieve a depletion protocol for over 4 weeks without running into issues of drug tolerability (high lethality) or an occurrence of

compensating Iba1 immunopositive myeloid cells. We were restricted within our treatment set-up to a maximum of 30 days, and it was in the interest of having a higher survival rate and overall health of the animals to infuse ganciclovir at a lower concentration than the previously published dose of 50mg/mL(88).

It was pertinent for our study to have a minimal impact on neurons when microglia were depleted from their environment. We used electrophysiological measures as an indicator to ensure their functional capacity remained intact. The battery of tests administered shows that in spite of microglial depletion, there was no significant shift in basic neuronal firing properties, indicating their basic integrity as maintained. Taken together, there seems to be no drastically significant shift in neuronal functional properties when microglia are depleted from the microenvironment. More fine tuned tests such as assays for short term and long term plasticity have to be undertaken for a more detailed study on the effect of microglia on neuronal function in the healthy adult setting, but this biological question was outside of the scope of this study.

In summary, we were unable to find an Ab9 treatment protocol in APPPS1 mice that was compatible with a microglia depletion protocol as the time frames did not fit together. The Ab9 treatment in APPPS1 mice required a longer treatment duration than 8 weeks, while the microglial depletion protocol could not be extended beyond 4 weeks. We were in a position to either switch to another anti-A $\beta$  antibody and titrate out its therapeutic efficacy in APPPS1 (and APPS;TK) mice, or utilize another murine model of AD. We decided to attempt treatment in a second murine model, which only harboured the APP Swedish mutation and did not have the PS1 mutation. The PS1 mutation is known to accelerate plaque production and shift the production to aggregate prone, fibril-forming A $\beta$ 42 species. The absence of the PS1 in a murine model delays time of onset of production and results in “softer” plaques being produced. We reasoned that such a model would be more treatable within the restricted time frame we had to work with.

APP23;TK mice were available to us for this project. Continuous infusion of GCV and weekly ip injections of either control antibody or Ab9 for four weeks conferred both significant

microglia depletion and significant efficacy in plaque reduction. Microglial depletion seemed to work better in Ab9 treated APP23;TK+ mice than control treated APP23;TK+ mice. This speaks to a specific stimulation of microglia by Ab9 in a way that renders them more responsive to GCV. As the presence of A $\beta$  specific antibodies are likely to complex in the brain with A $\beta$ , forming immune complexes, it is likely that this immune complex formation somehow induces a greater or more specific activating stimulus to microglial cells resulting in an upregulation of CD11b. This CD11b-driven expression of viral kinase could very well induce a greater depletion, as there is a gene dosed increase in sensitivity to GCV. Evaluation of brain soluble C3 supports this notion, showing significant elevation of C3 in Ab9 treated APP23;TK+ mice, suggesting that clearance of this protein and downstream processing is dependent on microglial cells and is elevated in the absence of these effector cells in the formation of immune complexes.

Control treated APP23;TK+ mice in turn may have lower concentration of immune complexes forming in the brain, thus resulting in a lower activation pattern, or an activation pattern that is different and involves relatively lower expression of CD11b (and lower viral kinase expression). This would explain the lack of a significant reduction in microglial density in this group. Morphological examination however confirmed that the cells were undergoing depletion; it is possible that the depletion process is slower in these mice with control treatment than their Ab9 treated counterpart.

Previous studies had reported specific proliferation of microglial cells around plaques in APP23 mice (cite), suggesting plaque-associated microglia to be specifically activated. Interestingly, Ab9 treated APP23;TK- mice did not have a higher microglia density in the cortex (anatomic region with the highest plaque burden in this model) when compared to control treated APP23;TK- mice. Eventhough Ab9 treatment conferred a higher microglial depletion rate when compared to control treatment and eventhough microglia seemed to be indispensable for Ab9 treatment efficacy, immunotherapy in APP23 mice did not seem to involve a higher proliferation rate of microglia. Admittedly we did not quantify the number of microglia per plaque, to assess crowding instead of proliferation, as it is feasible that existing microglia concentrated around plaques (migrated from non-plaque regions) rather than

plaque associated microglia proliferating. Further analyses are required to address this topic in order to assess more subtle changes.

In aged APP23;TK- mice, our Ab9 treatment regimen was able to significantly relieve plaque burden in just four weeks, demonstrating greater amenability to immunotherapy than APPPS1 mice. While APPPS1 mice and APPS;TK- showed a reduction in plaque pathology by 25-30% in over 8 weeks, APP23 mice showed therapeutic efficacy by 65% at 4 weeks when compared to control. Furthermore, our therapeutic timing in APP23 mice recapitulated geriatric settings, during which interventional therapy for AD can occur in the clinic. Overall, APP23;TK mice were more suitable for our study.

We assessed therapeutic efficacy of A $\beta$  immunotherapy when microglia were removed by quantifying plaque burden in vaccinated APP23;TK+ histologically and biochemically.

Strikingly, therapeutic efficacy of the treatment regimen was completely obliterated and remained at pathological control treated A $\beta$  burden when the microglial compartment was curtailed by induced depletion. Depletion of microglia in APP23;TK+ mice treated with control antibodies also remained at control treated levels of plaque burden in APP23;TK- mice. In other words, plaque burden reduction was only possible when there was (1) A $\beta$  specific antibodies used as treatment (as supposed to nonspecific control antibodies and (2) the microglial compartment was not altered. In other words, microglia seemed to be indispensable effector cells in the context of A $\beta$  specific immunotherapy.

On a separate note, the plaque burden assessed in the control treated APP23;TK+ showed that there was no significant change from their APP23;TK- counterpart, confirming several previous findings on the role of microglia in AD in general that there is a limited effect of microglia in AD setting in the absence of an additional stimulus to these cells such as A $\beta$  specific antibodies.

There was a lack of treatment efficacy of Ab9 on amyloid burden, and this differed from our findings in APPPS1 mice. As roughly 50% of A $\beta$  plaques in APPPS1 mice contain amyloid in their core, it is not surprising that there is an effect on these plaques overall when treated for

an extended period of time. In our treatment setting in APP23 mice, we treated for a shorter duration and APP23 mice have less than 25% amyloid structure containing A $\beta$  plaques. Thus, it is feasible that Ab9 treatment would preferentially target “softer” A $\beta$  (ie those in non-amyloid form). This finding was also confirmed when assessing only the insoluble A $\beta$  fraction in biochemistry studies. However, previous studies treating APP23 mice over 5 months showed a modest (15%) reduction in amyloid burden with another A $\beta$  specific antibody. This modest effect was likely due to the five-times longer treatment period than our study.

Overall biochemical analyses of total A $\beta$  brain content also confirmed the histological assessment, rendering confirmation in our findings of microglia dependent therapeutic efficacy of A $\beta$  antibodies. Therapeutic efficacy of Ab9 on APP23;TK- mice seemed to be mainly significant in the more soluble fractions, whereas the microglia-depleted fraction had more insoluble A $\beta$  content in spite of Ab9 treatment.

This dependency on microglia on Ab9 treatment efficacy was even more apparent when doing a correlative analysis of plaque burden reduction and microglial density in Ab9 treated individual mice. The inverse correlation was striking and furthermore supported with biochemical values of A $\beta$  content. It was clear from our findings that there was an important effector function of microglia in this specific treatment context.

Our findings support a previous study of ours whereby microglia function was assessed in the presence and gradual onset of plaques as APPPS1 mice were aged. Canonical functions such as ability to migrate towards injury sites and phagocytic capacity were measured in a longitudinal fashion over different ages of APPPS1 mice (Krabbe et al 2013 PLoS One). The study showed clearly that canonical microglial function declines in correlation with plaque pathology accumulation in the brain in APPPS1 mice. When relieving plaque burden with Ab9 antibody, these functions in microglia were restored to full capacity to the level of age-matched wild type (non plaque harbouring) mice.

Patient data has shown increasingly frequent transient changes in MRI depending on the dosage of antibody treatment, suggesting vascular damages leading to increased vasogenic edema and microhemorrhage. Vascular pathology assessment in our model did not result in

detectable differences in cerebral amyloid angiopathy. We reasoned this was possibly due to the subtle transient nature of any potential changes “flare-ups” which were undetectable post mortem.

We considered microhemorrhage as another parameter of vascular pathology. Although we didn't see any significant alteration in microhemorrhage, this could again be due our short treatment period. Other studies have shown an increase in microhemorrhage frequency upon anti-A $\beta$  antibody treatment when compared to control (Wang et al 2011, Pfeiffer et al 2001). Nevertheless, we also did not see any significant amelioration of vascular pathology upon microglia depletion, demonstrating that removal of immune effector cells from the AD brain environment does not protect the brain from such side effects; ie. there may be other cascades that are independent of microglia which induce and/or exacerbate microhemorrhage and CAA.

It has been shown that anywhere between 0.02% to 0.1% of total administered anti-A $\beta$  antibody reaches the brain(97). We were unable to detect Ab9 in the brain by immunohistochemistry, immunofluorescence, or ELISA method. It is likely that our methodology was not sensitive enough to detect such low fraction of antibodies in the brain, and radiolabelling or biotinylation would have given us a more sensitive read out. It is feasible that a higher percentage of antibody was able to reach the brain due to the physical injury we induced by the miniosmotic pump insertion, conferring an unusually high rate of A $\beta$  clearance from the brain. This would explain why our treatment duration of 4 weeks worked better than previously published studies which took at least 6 weeks.

It has been argued that this small amount of antibodies reaching the brain acts as a catalyst for shifting the equilibrium from aggregated A $\beta$  to its dissolution and eventual exodus(99).

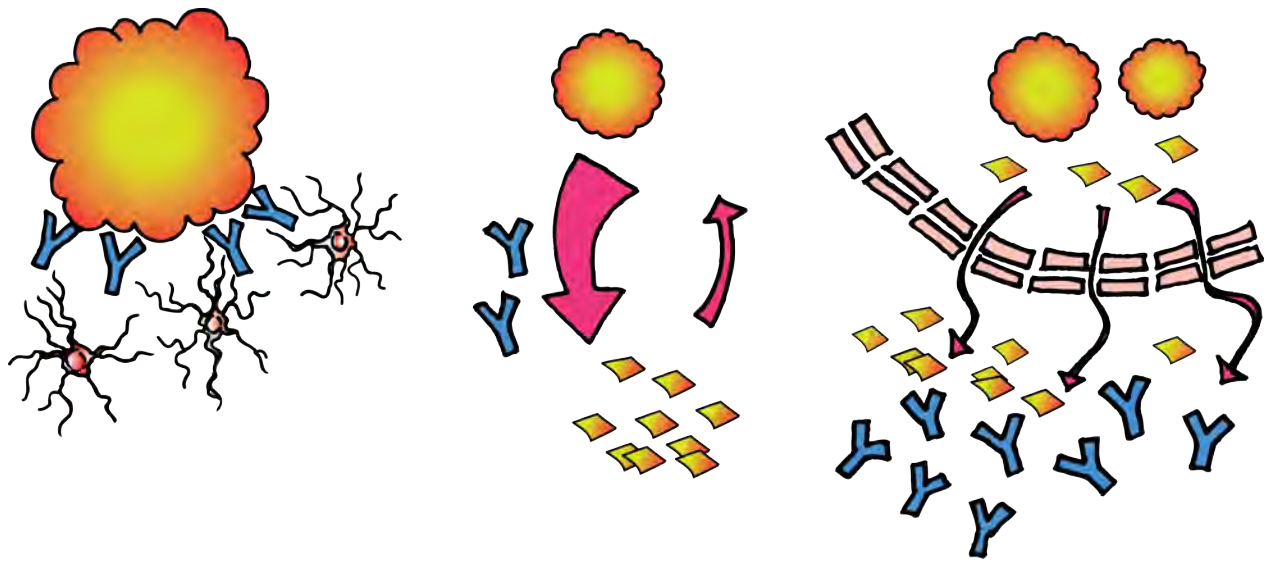


Figure 32 Putative mechanisms of A $\beta$  specific antibody treatments in AD. Left: antibodies specific to A $\beta$  reach the brain and cover A $\beta$  plaques. Microglia subsequently get activated by the immune complex and opsonize the A $\beta$  target. Centre: A $\beta$  plaques get dissociated by antibodies skewing the equilibrium from aggregation to dissociated state by some form of affinity competition with A $\beta$  itself. Right: the “peripheral sink” hypothesis stating that the antibodies with high affinity towards A $\beta$  create a high efflux of A $\beta$  out of the brain and into the periphery. Each of the three mechanisms has supporting evidence (Citron et al 2010).

An immediate rise in plasma A $\beta$  upon targeted antibody treatment elicited the peripheral sink hypothesis that stated the increased shuttling of A $\beta$  out of the brain due to intra- A $\beta$  aggregation affinity yielding to a higher affinity of the antibody to its target. This theory is thought to have some validity due to its observation in both patients and murine model upon treatment, however this spike in plasma A $\beta$  has been shown to return back to baseline levels within days of a single injection. While the half-life of an antibody in the periphery is up to three weeks(97), detectable A $\beta$  in the plasma is much shorter. It is possible that A $\beta$  complexed to the antibody is eliminated rapidly, as immune complexes are known to be recycled quickly in the spleen and in the lymph nodes via macrophages. In our study, we were unable to detect a rise in plasma A $\beta$  at the end of treatment. While there was no significant evidence for peripheral sink effect at this late timepoint, we did not check early and acutely after injection (within 24 hours, which has been reported to be a peak period for plasma A $\beta$ ). Nevertheless, we saw a significant 65% reduction in brain plaque burden, suggesting that the effect of the antibody on the brain did result in plaque removal. Thus, it is possible that any A $\beta$  that exits the brain is in a complexed state that is undetectable by ELISA. Alternatively, it

could be so rapidly recycled that there is no probably time window for capturing the process with our current readout, as the efficiency A $\beta$  clearance is not detectible.

A $\beta$  mediated abrogation of long term potentiation (LTP) in the hippocampus is a known experimental read out of synaptic damage upon AD. A $\beta$  specific antibodies have been shown to rescue this damaged LTP, leading to a theory that antibodies also block the synaptotoxicity of the A $\beta$  oligomers. Here, we did not check for functional outcome in these mice such as behavioural alterations. We also did not check electrophysiological parameters to assess plaque pathology as a functional read out.

However other studies showed that both our murine AD models also have behavioural phenotypes and that A $\beta$  antibody treatment relieves them(28,100).

The process of plaque dissolution may or may not involve facilitation by microglial cells; up until this point, the data has been contradictory. The hardest evidence for microglial involvement has been histological and confocal evidence of juxtaposition and increased internalization of plaque particles in microglial processes upon treatment. However, are microglial cells necessary for plaque removal upon immunotherapy? Up until this current work, there has been no evidence demonstrating indispensability in this context. In fact, an attempt to chemically deplete microglia while treating the AD brain with A $\beta$  antibody yielded no change in therapeutic efficacy –plaques were still removed by the same degree(80). This suggested that in vivo, there was rather lacking evidence for an importance of microglia in this treatment setting. Rather, the evidence supporting a microglial role in immunotherapy in AD has come forward overwhelmingly from in vitro studies, which their known limited translational value (100,104,105).

These numerous vitro studies have nevertheless supported the notion of microglia effector functioning in immunotherapy in AD. It has been shown that microglia cell lines and primary cultures are internalizing more A $\beta$  peptide when pre-incubated with antibodies against the peptide(100,104,105). This observation has been repeatedly reported from different groups over the years using different antibodies against A $\beta$ , suggesting some sort of effective stimulus on A $\beta$  upon treatment.

Beyond in vitro studies specifically testing this function, ex vivo observations on post mortem tissue has suggested a specific antibody activation of microglia in treated AD patients and murine models. CD68 is upregulated around the vicinity of the plaques in increased frequency upon immunization, especially when normalized to plaque burden(100), and confocal ex vivo examination of treated murine AD tissue has shown that there is increased A $\beta$  internalization inside microglia when compared to control.

It has been shown that there is a transient upregulation of Fc $\gamma$  receptors upon immunotherapy – a subset of receptors that engages the Fc portion of an antibody once it is complexed with its antigen (forming an immune complex). This observation was significantly different during the first few weeks of antibody treatment when compared to control (vehicle) treatment.

It has been shown that mononuclear phagocytes beyond the brain demonstrate enhanced engulfment of pathogens and other antigens upon complexing with a targeted antibody.

This process called opsonization has been demonstrated in the context of bacterial infections and other various contexts such as elimination of old, defunct cells (106). In terms of evolution, this process makes sense as the invaded host has an advantage upon increased elimination of target with the help of antibody complexing, and dispatching the professional phagocytes makes sense in order for quick efficient removal of unwanted targets to occur. The same concept applies to old cells (such as red blood cells) which are no longer functional and thus can be recycled in the liver.

Taken together it is tempting to draw the conclusion that antibody mediated A $\beta$  removal happens more efficiently via microglia when compared to non-treated settings.

Surprisingly however, enzymatic removal of the Fc portion from the antibodies, and treatment of tgAD mice with just these (Fc deprived) F(ab)<sub>2</sub> region of the antibody nevertheless conferred therapeutic efficacy, albeit to a lower extent as the whole immunoglobulin. Furthermore, an Fc $\gamma$ -receptor knockout mouse crossed to tgAD mouse was still treatable with anti- A $\beta$  antibodies and significantly conferred treatment efficacy murine models of AD (107).

The receptor repertoire and downstream signalling pathways involved in phagocytosis is poorly described and remains an ongoing subject of research.

Therefore, the degree to which microglia contribute to A $\beta$  antibody efficacy in vivo remains controversial and far from clear.

Here, our study shows clearly that at least in this specific treatment setting, microglia are indispensable effector cells in this treatment class in vivo. To my knowledge this is the first study showing this effect in vivo, and it supports the various in vitro studies mentioned previously. However, this finding begs the question why our data differed from previous attempts to paralyse microglial function in vivo and treat with A $\beta$  antibodies(80,107). Two prominent in vivo studies came to different conclusions from ours at first glance.

First, one group reported using genetic deletion of Fc $\gamma$ R receptors in the context of AD. Tg2576 crossed to Fc $\gamma$ R knockout mice were compared to single mutant Tg2576 mice upon concurrent vaccination and control treatment. Both mouse strains had significant reduction of plaque burden in the brain upon vaccination. The baseline plaque burden and its degree of removal were almost identical when comparing both mouse strains in their treatment arms of vehicle control and vaccination.

In this study, their approach was long-term active immunization for 3 months using A $\beta$ 42 peptide with incomplete and complete Freund's adjuvant. While their treatment approach was different from ours in that they actively vaccinated while we gave passive transfer of antibody alone, their data seems to support the notion that active vaccination with A $\beta$  is completely independent of the Fc $\gamma$ R receptor gene. Active vaccination is thought to utilize both the humoral immune component involving antibodies and the cellular component utilizing memory and cellular effector functions. In the context of AD, it is tempting to think that the antibodies raised against immunogen A $\beta$ 42 play a key role in reducing plaques from the brain, and therefore their finding may seem surprising and appear as though Fc $\gamma$ R receptors are completely dispensable. However, this would be a misleading conclusion.

An important confounder of this study is the incomplete knockout of the Fc $\gamma$ R receptor

repertoire. The redundancy of the FcG receptor system seems to be even more complex than previously thought: a new receptor subtype has been discovered only recently and after the publication of the aforementioned report(106) and in addition several subtypes of FcG receptors are known to be expressed independently of the FcG receptor gene. Admittedly the original nomenclature of this gene seems to misleadingly suggest a general knockout of all FcG receptor types. In fact, this knockout mouse strain only targets half of the repertoire of known FcG receptors, leaving the other half of the receptors intact and possibly even overexpressed as a compensatory response. It is unclear from this study therefore which exact receptor subclass activity was suppressed.

Quantitative real time PCR of FcG receptor types in these double mutant mice would have revealed more information, however this data was not included in their report. Previous studies have shown that this particular strain of knockout likely affects surface expression of FcGR type III almost completely, and partially suppresses effector functions of FcGR type I. FcGR II and FcGR IV are expressed independently of the deleted gene. While IgG1 interacts almost exclusively with FcGR type III, IgG2a can interact with all activating FcG Receptors (I, III and IV) and IgG2b interacts with FcGR type III and IV. Thus, an active vaccination paradigm which elicits the full range of antibody classes against the immunogen has several antibody species which can still interact with their effector receptors efficiently. This provides a plausible explanation as to why A $\beta$  vaccination efficiency was intact in spite of FcG receptor gene deletion.

In a second study, two chemical approaches were used to destroy microglial cells and directly injecting antibody against A $\beta$  into the transgenic AD mouse brain. The read-out of this study was 2-photon imaging at 3 and 7 days post injection of antibody. The injection resulted in a clear removal of plaques from the cortex in their region of interest. For chemical microglial inhibition, the investigators used minocycline and Mac1 saporin, but statistical analyses showed no significant removal of microglial cells upon stereological quantification compared to control mice.

While their chemical depletion approach did not reach significant reduction in microglial population, our microglia ablation using GCV inducible CD11b-HSVTK construct (a

pharmacogenetic depletion) seemed to be more effective as we had significant removal of these cells throughout the entire cortex. Minocycline is a general drug which has broad immunosuppressive function, and therefore a slightly different approach from ours. While Mac1 saporin is another approach to chemically ablate microglia, in this context there was no significant reduction in cell number.

They found that there was no significant difference in the degree of plaque burden reduction upon the additional treatment of either minocycline or Mac1 saporin. Interestingly, even though there was no significant inhibition of microglial cells according to statistical cell quantitation, there was still a trend for a higher plaque burden upon chemical treatment (both minocycline and Mac1 saporin) in antibody treatment. This study therefore cannot necessarily speak strongly against our findings, as they were unable to achieve a significant reduction of microglial cells upon stereological quantitation.

The antibody used in their study was 10D5, an IgG1 isotype. Much discussion and supporting data has been brought forward on the merits of taking the IgG subclass into account. An earlier study has suggested that the majority of antibodies directed against A $\beta$  work the most efficacious when on an IgG2a background. It has been speculated (but not demonstrated directly) that this IgG2a subtype most effectively engages Fc receptors expressed on microglial cells (97,108,109).

An additional aspect to consider is the application route of the antibody, as previous studies showed a minute percentage (less than 0.1%) of plasma IgGs intercalate into the brain and are detectable over time. Direct antibody application into the brain allows for an artificially high amount of antibody into the brain which may directly interact with the plaques and A $\beta$  rather than take microglial activation or programming into account. High doses of antibodies directly applied to the brain may enrich different mechanisms of plaque resolution than the physiologically intact context of peripheral administration (mimicking clinical settings). This would also explain the quick reduction in plaque burden the study observed – 40% within 3 to 7 days post application of antibody. Our laborious titrations suggest peripheral administration needs at least 4 weeks to mimic that effect in a “softer” AD mouse model (APP23) than their APP/dE9 murine model. It is therefore not surprising that this study setting

of direct cerebral injection of antibody is less dependent on microglial function, especially during the early stages post injection.

Much like the relevance of FcG receptor subtype and their different roles in an immune context, antibody subtype plays a significant and different role in immunodulation on a global scale. Th1/Th2 or M1/M2 activation phenotypes have been used as rough designations to describe a certain immune state. While this designation is short sighted and has severe limits in its subtle context dependent cases of pathology on an individual basis, it is a useful paradigm to think about on a global and general scale, as long as one appreciates that there is a graded response which spans different degrees from each extremes. Here, I argue that the subtype of IgG engineered against A $\beta$  relevantly modulates plaque pathology by means of manipulating the immune system distinctly.

Ab9 is our antibody of choice for this current study, and it was of subclass IgG2a. While not functionally demonstrated until this current work, speculative evidence had been brought forward supporting maximal microglial effector function of this subtype in line with our findings (97,108,109). An interesting outlook would be to repeat these experiments with Ab3, an IgG1 with the same epitope specificity raised in parallel as Ab9. A side-by-side comparison of Ab9 IgG2a versus other isotypes alongside microglia depletion would yield valuable information to which degree microglia mediate their effector functions. A comparison of IgG2a and IgG1 A $\beta$  antibodies in their effect on microglial activation pattern would further elucidate which receptors and pathways (even beyond FcG receptor paradigm) are specifically engaged.

While the mechanism of action is still an ongoing field of research, clinical trials have continued. 2012 brought a series of set backs in clinical trials of passive immunization strategies. Two treatments in Phase III failed to meet their clinical endpoints, Bapineuzumab (IgG1 against A $\beta$  1-5) and Solanezumab (IgG1 against A $\beta$  16-23). Nonetheless there was a silver lining in that Solanezumab kept cognitive stabilization in the mildly cognitively impaired patient arm, but this stabilization was not seen in the moderately impaired patient cohort. This spoke to the possibility that trials on antibodies were started "too little too late", and that it was in the interest of patients to be treated early. Such an effort would have to be met with

earlier diagnostic tools, and accordingly there is a rejuvenated push to establish faithful biomarkers for the early detection and accurate diagnosis of AD.

There has been discussion on the role of microglia contributing to vascular alterations observed in trial results. These concerns arose from early studies showing increased microhemorrhage in A $\beta$  antibody treated mice, and more recently from Bapineuzumab trials showing increased frequency of vascular related imaging abnormalities in patients with the highest antibody dose(49).

3D6, the murine analog of Bapineuzumab is an antibody when crystalized shows an unusual A $\beta$  conformation that is helical and abnormally sticky(110). This possibly suggests that the bioengineering of antibodies has to be investigated in greater detail to ensure A $\beta$  conformation upon binding is not inappropriately folded to be more harmful. These antibody A $\beta$  interactions and their effect on vascular pathology are independent on microglia and merit their own intensive investigation.

Whether microglia are involved in vascular alterations observed in A $\beta$  antibody treatment and in AD in general has to be investigated in more detail. In fact, there is currently very little evidence on how these imaging abnormalities come about in patients (or how the vascular pathological changes in murine models come about). An unbiased study beyond the role of microglia will have to be carried out carefully. While it is possible that microglia contribute to microhemorrhage in the context of immunotherapies, it could also be various other inflammatory factors independent of microglia, such as complement proteins which are also secreted by other glial cells.

Here we have shown that microglia are programmed in a way to remove plaque pathology effectively, as their cell specific depletion failed to confer any treatment efficacy of Ab9. Whether or not microglia contribute towards vascular pathology with adverse side effects was unclear, mostly due to the short treatment window we were confined to. Our finding lends support of maximal antibody efficacy with subtype IgG2a.

A prospective study should be conducted investigating the in vivo activation pattern of microglia upon A $\beta$  antibody treatment in AD murine models. Identifying molecular markers involved in potential side effects (if any) and discerning them from important effector molecules and pathways conferring treatment efficacy, could result in combination therapy which would enable maximal therapeutic benefit in the future.

Current treatment strategies try to circumvent microglial involvement by mutating Fc receptor (AAB 003, Ponezumab, GSK). Two of these trials already failed in early stages as there was insufficient treatment efficacy. Perhaps these strategies are misplaced in an overly conservative effort to avoid any inflammatory response speculated to come from Fc receptor engagement, and speaks to a more nuanced assessment of the role of microglia in AD immunotherapy.

## **Summary**

We have identified microglia as indispensable effector cells in the context of AD immunotherapy. These cells can play an essential role especially when the A $\beta$  antibody is of subtype IgG2a (known to be the most effective subtype to clear A $\beta$ ). While our findings do not rule out any other mechanisms of action to play in cohesion, we are able to place microglia as the forefront player in conferring therapeutic benefit of this drug class. Current translational medicine should strive for treatment strategies bioengineering effective engagement of microglial cells, not altogether circumvent their activation.

## References:

1. Reitz C, Brayne C, Mayeux R. Epidemiology of Alzheimer disease. *Nature reviews Neurology*. 2011 Mar;7:137–52.
2. Querfurth HW, LaFerla FM. Alzheimer's disease. *The New England journal of medicine*. 2010 Jan 28;362:329–44.
3. Selkoe DJ. Preventing Alzheimer's disease. *Science*. 2012 Sep 21;337:1488–92.
4. Callaway E. Alzheimer's drugs take a new tack. *Nature*. 2012 Sep 6;489:13–4.
5. Reports | Alzheimer's Association [Internet]. [cited 2013 Aug 7]. Available from: [http://www.alz.org/alzheimers\\_disease\\_21590.asp](http://www.alz.org/alzheimers_disease_21590.asp)
6. Hu WT, Holtzman DM, Fagan AM, Shaw LM, Perrin R, Arnold SE, et al. Plasma multianalyte profiling in mild cognitive impairment and Alzheimer disease. *Neurology [Internet]*. 2012 Aug 1; Available from: <http://www.ncbi.nlm.nih.gov/pubmed/22855860>
7. Benjamin R, Leake A, McArthur FK, Ince PG, Candy JM, Edwardson JA, et al. Protective effect of apoE epsilon 2 in Alzheimer's disease. *Lancet*. 1994 Aug 13;344(8920):473.
8. Rhinn H, Fujita R, Qiang L, Cheng R, Lee JH, Abeliovich A. Integrative genomics identifies APOE  $\epsilon$ 4 effectors in Alzheimer's disease. *Nature*. 2013 Aug 1;500(7460):45–50.
9. Fagan AM, Watson M, Parsadanian M, Bales KR, Paul SM, Holtzman DM. Human and murine ApoE markedly alters A beta metabolism before and after plaque formation in a mouse model of Alzheimer's disease. *Neurobiol Dis*. 2002 Apr;9(3):305–18.
10. Verghese PB, Castellano JM, Garai K, Wang Y, Jiang H, Shah A, et al. ApoE influences amyloid- $\beta$  ( $A\beta$ ) clearance despite minimal apoE/ $A\beta$  association in physiological conditions. *Proc Natl Acad Sci U S A*. 2013 May 7;110(19):E1807–1816.
11. Fryer JD, Taylor JW, DeMattos RB, Bales KR, Paul SM, Parsadanian M, et al. Apolipoprotein E markedly facilitates age-dependent cerebral amyloid angiopathy and spontaneous hemorrhage in amyloid precursor protein transgenic mice. *J Neurosci Off J Soc Neurosci*. 2003 Aug 27;23(21):7889–96.
12. Henderson AS, Eastel S, Jorm AF, Mackinnon AJ, Korten AE, Christensen H, et al. Apolipoprotein E allele epsilon 4, dementia, and cognitive decline in a population sample. *Lancet*. 1995 Nov 25;346(8987):1387–90.

13. Izaks GJ, Gansevoort RT, van der Knaap AM, Navis G, Dullaart RPF, Slaets JPJ. The Association of APOE Genotype with Cognitive Function in Persons Aged 35 Years or Older. *PLoS ONE*. 2011 Nov 14;6(11):e27415.
14. Small GW, Mazziotta JC, Collins MT, et al. APOlipoprotein e type 4 allele and cerebral glucose metabolism in relatives at risk for familial Alzheimer disease. *JAMA*. 1995 Mar 22;273(12):942–7.
15. Morris HR, Steele JC, Crook R, Wavrant-De Vrièze F, Onstead-Cardinale L, Gwinn-Hardy K, et al. Genome-wide analysis of the parkinsonism-dementia complex of Guam. *Arch Neurol*. 2004 Dec;61(12):1889–97.
16. Naj AC, Jun G, Beecham GW, Wang L-S, Vardarajan BN, Buross J, et al. Common variants at MS4A4/MS4A6E, CD2AP, CD33 and EPHA1 are associated with late-onset Alzheimer's disease. *Nat Genet*. 2011 May;43(5):436–41.
17. Guerreiro R, Wojtas A, Bras J, Carrasquillo M, Rogaeva E, Majounie E, et al. TREM2 variants in Alzheimer's disease. *N Engl J Med*. 2013 Jan 10;368(2):117–27.
18. Jonsson T, Stefansson H, Steinberg S, Jonsdottir I, Jonsson PV, Snaedal J, et al. Variant of TREM2 associated with the risk of Alzheimer's disease. *N Engl J Med*. 2013 Jan 10;368(2):107–16.
19. Jonsson T, Atwal JK, Steinberg S, Snaedal J, Jonsson PV, Bjornsson S, et al. A mutation in APP protects against Alzheimer's disease and age-related cognitive decline. *Nature*. 2012 Aug 2;488(7409):96–9.
20. Wilson RS, Hebert LE, Scherr PA, Barnes LL, Mendes de Leon CF, Evans DA. Educational attainment and cognitive decline in old age. *Neurology*. 2009 Feb 3;72(5):460–5.
21. Bero AW, Yan P, Roh JH, Cirrito JR, Stewart FR, Raichle ME, et al. Neuronal activity regulates the regional vulnerability to amyloid- $\beta$  deposition. *Nat Neurosci*. 2011 Jun;14(6):750–6.
22. Salmon DP, Thomas RG, Pay MM, Booth A, Hofstetter CR, Thal LJ, et al. Alzheimer's disease can be accurately diagnosed in very mildly impaired individuals. *Neurology*. 2002 Oct 8;59(7):1022–8.
23. Jack CR, Albert M, Knopman DS, McKhann GM, Sperling RA, Carillo M, et al. Introduction to Revised Criteria for the Diagnosis of Alzheimer's Disease: National Institute on Aging and the Alzheimer Association Workgroups. *Alzheimers Dement J Alzheimers Assoc*. 2011 May;7(3):257–62.
24. Klunk WE, Engler H, Nordberg A, Wang Y, Blomqvist G, Holt DP, et al. Imaging brain amyloid in Alzheimer's disease with Pittsburgh Compound-B. *Ann Neurol*. 2004 Mar;55(3):306–19.

25. Zeng F, Goodman MM. Fluorine-18 radiolabeled heterocycles as PET tracers for imaging  $\beta$ -amyloid plaques in Alzheimer's disease. *Curr Top Med Chem*. 2013;13(8):909–19.
26. Jack CR, Knopman DS, Jagust WJ, Shaw LM, Aisen PS, Weiner MW, et al. Hypothetical model of dynamic biomarkers of the Alzheimer's pathological cascade. *Lancet Neurol*. 2010 Jan;9(1):119.
27. Schilling S, Zeitschel U, Hoffmann T, Heiser U, Francke M, Kehlen A, et al. Glutaminy cyclase inhibition attenuates pyroglutamate A $\beta$  and Alzheimer's disease-like pathology. *Nat Med*. 2008 Oct;14(10):1106–11.
28. Citron M. Alzheimer's disease: strategies for disease modification. *Nat Rev Drug Discov*. 2010;9:387–98.
29. Bateman RJ, Xiong C, Benzinger TLS, Fagan AM, Goate A, Fox NC, et al. Clinical and biomarker changes in dominantly inherited Alzheimer's disease. *N Engl J Med*. 2012 Aug 30;367(9):795–804.
30. Reitz C. Alzheimer's Disease and the Amyloid Cascade Hypothesis: A Critical Review. *Int J Alzheimers Dis* [Internet]. 2012 [cited 2013 Aug 8];2012. Available from: <http://www.ncbi.nlm.nih.gov/pmc/articles/PMC3313573/>
31. Nalivaeva NN, Turner AJ. The amyloid precursor protein: a biochemical enigma in brain development, function and disease. *FEBS Lett*. 2013 Jun 27;587(13):2046–54.
32. Schwab C, McGeer PL. Inflammatory aspects of Alzheimer disease and other neurodegenerative disorders. *J Alzheimers Dis JAD*. 2008 May;13(4):359–69.
33. McGeer EG, McGeer PL. Neuroinflammation in Alzheimer's disease and mild cognitive impairment: a field in its infancy. *J Alzheimers Dis JAD*. 2010;19(1):355–61.
34. Mawuenyega KG, Sigurdson W, Ovod V, Munsell L, Kasten T, Morris JC, et al. Decreased clearance of CNS beta-amyloid in Alzheimer's disease. *Science*. 2010 Dec 24;330(6012):1774.
35. Taylor CJ, Ireland DR, Ballagh I, Bourne K, Marechal NM, Turner PR, et al. Endogenous secreted amyloid precursor protein-alpha regulates hippocampal NMDA receptor function, long-term potentiation and spatial memory. *Neurobiol Dis*. 2008 Aug;31(2):250–60.
36. Needham BE, Wlodek ME, Ciccotosto GD, Fam BC, Masters CL, Proietto J, et al. Identification of the Alzheimer's disease amyloid precursor protein (APP) and its homologue APLP2 as essential modulators of glucose and insulin homeostasis and growth. *J Pathol*. 2008 Jun;215(2):155–63.

37. Jucker M. The benefits and limitations of animal models for translational research in neurodegenerative diseases. *Nat Med*. 2010 Nov;16(11):1210–4.
38. Bondolfi L, Calhoun M, Ermini F, Kuhn HG, Wiederhold KH, Walker L, et al. Amyloid-associated neuron loss and gliogenesis in the neocortex of amyloid precursor protein transgenic mice. *The Journal of neuroscience : the official journal of the Society for Neuroscience*. 2002 Jan 15;22:515–22.
39. Radde R, Bolmont T, Kaeser SA, Coomaraswamy J, Lindau D, Stoltze L, et al. A $\beta$ 42-driven cerebral amyloidosis in transgenic mice reveals early and robust pathology. *EMBO Rep*. 2006 Sep;7(9):940–6.
40. Oddo S, Caccamo A, Shepherd JD, Murphy MP, Golde TE, Kaye R, et al. Triple-Transgenic Model of Alzheimer's Disease with Plaques and Tangles: Intracellular A $\beta$  and Synaptic Dysfunction. *Neuron*. 2003 Jul 31;39(3):409–21.
41. Duff K, Suleman F. Transgenic mouse models of Alzheimer's disease: how useful have they been for therapeutic development? *Brief Funct Genomic Proteomic*. 2004 Apr;3(1):47–59.
42. Doody RS, Raman R, Farlow M, Iwatsubo T, Vellas B, Joffe S, et al. A phase 3 trial of semagacestat for treatment of Alzheimer's disease. *N Engl J Med*. 2013 Jul 25;369(4):341–50.
43. Schenk D, Basi GS, Pangalos MN. Treatment strategies targeting amyloid  $\beta$ -protein. *Cold Spring Harb Perspect Med*. 2012 Sep;2(9):a006387.
44. Loeffler DA. Intravenous immunoglobulin and Alzheimer's disease: what now? *J Neuroinflammation*. 2013 Jun 5;10:70.
45. Schenk D, Barbour R, Dunn W, Gordon G, Grajeda H, Guido T, et al. Immunization with amyloid-beta attenuates Alzheimer-disease-like pathology in the PDAPP mouse. *Nature*. 1999 Jul 8;400:173–7.
46. Nicoll JA, Wilkinson D, Holmes C, Steart P, Markham H, Weller RO. Neuropathology of human Alzheimer disease after immunization with amyloid-beta peptide: a case report. *Nature medicine*. 2003 Apr;9:448–52.
47. Gandy S, Heppner FL. Breaking up (amyloid) is hard to do. *PLoS Med*. 2005 Dec;2(12):e417.
48. Moreth J, Mavoungou C, Schindowski K. Passive anti-amyloid immunotherapy in Alzheimer's disease: What are the most promising targets? *Immun Ageing*. 2013 May 11;10(1):18.
49. Sperling R, Salloway S, Brooks DJ, Tampieri D, Barakos J, Fox NC, et al. Amyloid-related imaging abnormalities in patients with Alzheimer's disease treated with bapineuzumab: a retrospective analysis. *Lancet Neurol*. 2012;11:241–9.

50. Adolfsson O, Pihlgren M, Toni N, Varisco Y, Buccarello AL, Antonello K, et al. An Effector-Reduced Anti- $\beta$ -Amyloid (A $\beta$ ) Antibody with Unique A $\beta$  Binding Properties Promotes Neuroprotection and Glial Engulfment of A $\beta$ . *J Neurosci Off J Soc Neurosci*. 2012;32:9677–89.
51. Reichert JM. Which are the antibodies to watch in 2013? *MAbs*. 2013 Feb;5(1):1–4.
52. Prinz M, Priller J, Sisodia SS, Ransohoff RM. Heterogeneity of CNS myeloid cells and their roles in neurodegeneration. *Nat Neurosci*. 2011 Oct;14:1227–35.
53. Davies LC, Rosas M, Jenkins SJ, Liao C-T, Scurr MJ, Brombacher F, et al. Distinct bone marrow-derived and tissue-resident macrophage lineages proliferate at key stages during inflammation. *Nat Commun*. 2013 May 21;4:1886.
54. Hashimoto D, Chow A, Noizat C, Teo P, Beasley MB, Leboeuf M, et al. Tissue-resident macrophages self-maintain locally throughout adult life with minimal contribution from circulating monocytes. *Immunity*. 2013 Apr 18;38(4):792–804.
55. Shornick LP, Wells AG, Zhang Y, Patel AC, Huang G, Takami K, et al. Airway epithelial versus immune cell Stat1 function for innate defense against respiratory viral infection. *Journal of immunology*. 2008 Mar 1;180:3319–28.
56. Gordon SB, Read RC. Macrophage defences against respiratory tract infections The immunology of childhood respiratory infections. *Br Med Bull*. 2002 Mar 1;61(1):45–61.
57. Ginhoux F, Lim S, Hoeffel G, Low D, Huber T. Origin and differentiation of microglia. *Front Cell Neurosci*. 2013;7:45.
58. Gomez Perdiguero E, Schulz C, Geissmann F. Development and homeostasis of “resident” myeloid cells: The case of the microglia. *Glia*. 2013 Jan;61(1):112–20.
59. Gautier EL, Shay T, Miller J, Greter M, Jakubzick C, Ivanov S, et al. Gene-expression profiles and transcriptional regulatory pathways that underlie the identity and diversity of mouse tissue macrophages. *Nat Immunol*. 2012 Nov;13(11):1118–28.
60. Chow A, Brown BD, Merad M. Studying the mononuclear phagocyte system in the molecular age. *Nat Rev Immunol*. 2011 Nov;11(11):788–98.
61. Greter M, Merad M. Regulation of microglia development and homeostasis. *Glia*. 2013 Jan;61(1):121–7.
62. Geissmann F, Manz MG, Jung S, Sieweke MH, Merad M, Ley K. Development of monocytes, macrophages, and dendritic cells. *Science*. 2010 Feb 5;327(5966):656–61.

63. Kohyama M, Ise W, Edelson BT, Wilker PR, Hildner K, Mejia C, et al. Role for Spi-C in the development of red pulp macrophages and splenic iron homeostasis. *Nature*. 2009 Jan 15;457(7227):318–21.
64. Den Haan JMM, Kraal G. Innate immune functions of macrophage subpopulations in the spleen. *J Innate Immun*. 2012;4(5-6):437–45.
65. Ransohoff RM, Perry VH. Microglial physiology: unique stimuli, specialized responses. *Annu Rev Immunol*. 2009;27:119–45.
66. Nimmerjahn A, Kirchhoff F, Helmchen F. Resting microglial cells are highly dynamic surveillants of brain parenchyma in vivo. *Science*. 2005 May 27;308(5726):1314–8.
67. Hanisch UK, Kettenmann H. Microglia: active sensor and versatile effector cells in the normal and pathologic brain. *Nature neuroscience*. 2007 Nov;10:1387–94.
68. Stewart CR, Stuart LM, Wilkinson K, van Gils JM, Deng J, Halle A, et al. CD36 ligands promote sterile inflammation through assembly of a Toll-like receptor 4 and 6 heterodimer. *Nat Immunol*. 2010 Feb;11(2):155–61.
69. Halle A, Hornung V, Petzold GC, Stewart CR, Monks BG, Reinheckel T, et al. The NALP3 inflammasome is involved in the innate immune response to amyloid-beta. *Nat Immunol*. 2008 Aug;9(8):857–65.
70. Heneka MT, Kummer MP, Stutz A, Delekate A, Schwartz S, Vieira-Saecker A, et al. NLRP3 is activated in Alzheimer's disease and contributes to pathology in APP/PS1 mice. *Nature*. 2013 Jan 31;493(7434):674–8.
71. Yasojima K, Schwab C, McGeer EG, McGeer PL. Up-regulated production and activation of the complement system in Alzheimer's disease brain. *Am J Pathol*. 1999 Mar;154(3):927–36.
72. Wyss-Coray T, Yan F, Lin AH-T, Lambris JD, Alexander JJ, Quigg RJ, et al. Prominent neurodegeneration and increased plaque formation in complement-inhibited Alzheimer's mice. *Proc Natl Acad Sci U S A*. 2002 Aug 6;99(16):10837–42.
73. Vom Berg J, Prokop S, Miller KR, Obst J, Kälin RE, Lopategui-Cabezas I, et al. Inhibition of IL-12/IL-23 signaling reduces Alzheimer's disease-like pathology and cognitive decline. *Nat Med*.
74. Mildner A, Schlevogt B, Kierdorf K, Bottcher C, Erny D, Kummer MP, et al. Distinct and non-redundant roles of microglia and myeloid subsets in mouse models of Alzheimer's disease. *The Journal of neuroscience : the official journal of the Society for Neuroscience*. 2011 Aug 3;31:11159–71.

75. Krstic D, Madhusudan A, Doehner J, Vogel P, Notter T, Imhof C, et al. Systemic immune challenges trigger and drive Alzheimer-like neuropathology in mice. *J Neuroinflammation*. 2012;9:151.
76. Krstic D, Knuesel I. Deciphering the mechanism underlying late-onset Alzheimer disease. *Nat Rev Neurol*. 2013 Jan;9(1):25–34.
77. Zhang B, Gaiteri C, Bodea L-G, Wang Z, McElwee J, Podtelezchnikov AA, et al. Integrated systems approach identifies genetic nodes and networks in late-onset Alzheimer's disease. *Cell*. 2013 Apr 25;153(3):707–20.
78. Fan R, Xu F, Previti ML, Davis J, Grande AM, Robinson JK, et al. Minocycline Reduces Microglial Activation and Improves Behavioral Deficits in a Transgenic Model of Cerebral Microvascular Amyloid. *J Neurosci*. 2007 Mar 21;27(12):3057–63.
79. Dunston CR, Griffiths HR, Lambert PA, Staddon S, Vernallis AB. Proteomic analysis of the anti-inflammatory action of minocycline. *Proteomics*. 2011 Jan;11:42–51.
80. Garcia-Alloza M, Ferrara BJ, Dodwell SA, Hickey GA, Hyman BT, Bacskai BJ. A limited role for microglia in antibody mediated plaque clearance in APP mice. *Neurobiol Dis*. 2007;28:286–92.
81. Jung S, Aliberti J, Graemmel P, Sunshine MJ, Kreutzberg GW, Sher A, et al. Analysis of fractalkine receptor CX(3)CR1 function by targeted deletion and green fluorescent protein reporter gene insertion. *Mol Cell Biol*. 2000 Jun;20(11):4106–14.
82. Diwan M, Misra A, Khar RK, Talwar GP. Long-term high immune response to diphtheria toxoid in rodents with diphtheria toxoid conjugated to dextran as a single contact point delivery system. *Vaccine*. 1997 Dec;15(17-18):1867–71.
83. Gowing G, Vallières L, Julien J-P. Mouse model for ablation of proliferating microglia in acute CNS injuries. *Glia*. 2006 Feb;53(3):331–7.
84. Heppner FL, Greter M, Marino D, Falsig J, Raivich G, Hovelmeyer N, et al. Experimental autoimmune encephalomyelitis repressed by microglial paralysis. *Nature medicine*. 2005 Feb;11:146–52.
85. Janoly-Dumenil A, Rouvet I, Bleyzac N, Bertrand Y, Aulagner G, Zobot M-T. Effect of duration and intensity of ganciclovir exposure on lymphoblastoid cell toxicity. *Antivir Chem Chemother*. 2009;19(6):257–62.
86. Ajami B, Bennett JL, Krieger C, Tetzlaff W, Rossi FMV. Local self-renewal can sustain CNS microglia maintenance and function throughout adult life. *Nat Neurosci*. 2007 Dec;10(12):1538–43.

87. Sturchler-Pierrat C, Staufenbiel M. Pathogenic mechanisms of Alzheimer's disease analyzed in the APP23 transgenic mouse model. *Ann N Y Acad Sci.* 2000;920:134–9.
88. Grathwohl SA, Kalin RE, Bolmont T, Prokop S, Winkelmann G, Kaeser SA, et al. Formation and maintenance of Alzheimer's disease beta-amyloid plaques in the absence of microglia. *Nature neuroscience.* 2009 Nov;12:1361–3.
89. Vloeberghs E, Van Dam D, Coen K, Staufenbiel M, De Deyn PP. Aggressive male APP23 mice modeling behavioral alterations in dementia. *Behav Neurosci.* 2006 Dec;120(6):1380–3.
90. Huttner KM, Pudney J, Milstone DS, Ladd D, Seidman JG. Flagellar and acrosomal abnormalities associated with testicular HSV-tk expression in the mouse. *Biol Reprod.* 1993 Aug;49(2):251–61.
91. Breeding Strategies for Maintaining Mice Colonies [Internet]. Jackson Laboratories; Available from: <http://jaxmice.jax.org/manual/>
92. Bondolfi L, Calhoun M, Ermini F, Kuhn HG, Wiederhold K-H, Walker L, et al. Amyloid-associated neuron loss and gliogenesis in the neocortex of amyloid precursor protein transgenic mice. *J Neurosci Off J Soc Neurosci.* 2002 Jan 15;22(2):515–22.
93. Olichney JM, Hansen LA, Galasko D, Saitoh T, Hofstetter CR, Katzman R, et al. The apolipoprotein E epsilon 4 allele is associated with increased neuritic plaques and cerebral amyloid angiopathy in Alzheimer's disease and Lewy body variant. *Neurology.* 1996;47:190–6.
94. Kawarabayashi T, Younkin LH, Saido TC, Shoji M, Ashe KH, Younkin SG. Age-dependent changes in brain, CSF, and plasma amyloid (beta) protein in the Tg2576 transgenic mouse model of Alzheimer's disease. *J Neurosci Off J Soc Neurosci.* 2001;21:372–81.
95. Aslund A, Sigurdson CJ, Klingstedt T, Grathwohl S, Bolmont T, Dickstein DL, et al. Novel pentameric thiophene derivatives for in vitro and in vivo optical imaging of a plethora of protein aggregates in cerebral amyloidoses. *ACS chemical biology.* 2009 Aug 21;4:673–84.
96. Pfeifer M, Boncristiano S, Bondolfi L, Stalder A, Deller T, Staufenbiel M, et al. Cerebral hemorrhage after passive anti-Abeta immunotherapy. *Science.* 2002;298:1379–1379.
97. Levites Y, Das P, Price RW, Rochette MJ, Kostura LA, McGowan EM, et al. Anti-Abeta42- and anti-Abeta40-specific mAbs attenuate amyloid deposition in an Alzheimer disease mouse model. *J Clin Invest.* 2006;116:193–201.

98. Varvel NH, Grathwohl SA, Baumann F, Liebig C, Bosch A, Brawek B, et al. Microglial repopulation model reveals a robust homeostatic process for replacing CNS myeloid cells. *Proc Natl Acad Sci U S A*. 2012 Oct 30;109(44):18150–5.
99. Wilcock DM, Munireddy SK, Rosenthal A, Ugen KE, Gordon MN, Morgan D. Microglial activation facilitates Aβ plaque removal following intracranial anti-Aβ antibody administration. *Neurobiology of disease*. 2004 Feb;15:11–20.
100. Wang A, Das P, Switzer RC, Golde TE, Jankowsky JL. Robust amyloid clearance in a mouse model of Alzheimer's disease provides novel insights into the mechanism of amyloid-beta immunotherapy. *J Neurosci Off J Soc Neurosci*. 2011;31:4124–36.
101. Hefendehl JK, Wegenast-Braun BM, Liebig C, Eicke D, Milford D, Calhoun ME, et al. Long-term in vivo imaging of β-amyloid plaque appearance and growth in a mouse model of cerebral β-amyloidosis. *J Neurosci Off J Soc Neurosci*. 2011 Jan 12;31(2):624–9.
102. Solomon B. Intravenous immunoglobulin and Alzheimer's disease immunotherapy. *Current opinion in molecular therapeutics*. 2007 Feb;9:79–85.
103. Arbel M, Solomon B. Immunotherapy for Alzheimer's disease: attacking amyloid-beta from the inside. *Trends in immunology*. 2007 Dec;28:511–3.
104. Brazil MI, Chung H, Maxfield FR. Effects of incorporation of immunoglobulin G and complement component C1q on uptake and degradation of Alzheimer's disease amyloid fibrils by microglia. *J Biol Chem*. 2000 Jun 2;275(22):16941–7.
105. Bohrmann B, Baumann K, Benz J, Gerber F, Huber W, Knoflach F, et al. Gantenerumab: a novel human anti-Aβ antibody demonstrates sustained cerebral amyloid-β binding and elicits cell-mediated removal of human amyloid-β. *J Alzheimers Dis JAD*. 2012;28:49–69.
106. Nimmerjahn F, Lux A, Albert H, Woigk M, Lehmann C, Dudziak D, et al. FcγRIV deletion reveals its central role for IgG2a and IgG2b activity in vivo. *Proc Natl Acad Sci U S A*. 2010 Nov 9;107(45):19396–401.
107. Das P, Howard V, Loosbrock N, Dickson D, Murphy MP, Golde TE. Amyloid-beta immunization effectively reduces amyloid deposition in FcRγ-/- knock-out mice. *J Neurosci Off J Soc Neurosci*. 2003 Sep 17;23(24):8532–8.
108. Bard F, Barbour R, Cannon C, Carretto R, Fox M, Games D, et al. Epitope and isotype specificities of antibodies to beta -amyloid peptide for protection against Alzheimer's disease-like neuropathology. *Proc Natl Acad Sci U S A*. 2003;100:2023–8.
109. Demattos RB, Lu J, Tang Y, Racke MM, DeLong CA, Tzaferis JA, et al. A plaque-specific antibody clears existing β-amyloid plaques in Alzheimer's disease mice. *Neuron*. 2012 Dec 6;76(5):908–20.

110. Miles LA, Crespi GAN, Doughty L, Parker MW. Bapineuzumab captures the N-terminus of the Alzheimer's disease amyloid-beta peptide in a helical conformation. *Sci Reports* [Internet]. 2013 Feb 18 [cited 2013 Aug 8];3. Available from: <http://www.ncbi.nlm.nih.gov/pmc/articles/PMC3575012/>

„Ich, Gina Dji-In Eom versichere an Eides statt durch meine eigenhändige Unterschrift, dass ich die vorgelegte Dissertation mit dem Thema: “Manipulating microglia in Alzheimer’s disease” selbständig und ohne nicht offengelegte Hilfe Dritter verfasst und keine anderen als die angegebenen Quellen und Hilfsmittel genutzt habe.

Alle Stellen, die wörtlich oder dem Sinne nach auf Publikationen oder Vorträgen anderer Autoren beruhen, sind als solche in korrekter Zitierung (siehe „Uniform Requirements for Manuscripts (URM)“ des ICMJE [www.icmje.org](http://www.icmje.org)) kenntlich gemacht. Die Abschnitte zu Methodik (insbesondere praktische Arbeiten, Laborbestimmungen, statistische Aufarbeitung) und Resultaten (insbesondere Abbildungen, Graphiken und Tabellen) entsprechen den URM (s.o) und werden von mir verantwortet.

Meine Anteile an etwaigen Publikationen zu dieser Dissertation entsprechen denen, die in der untenstehenden gemeinsamen Erklärung mit dem/der Betreuer/in, angegeben sind. Sämtliche Publikationen, die aus dieser Dissertation hervorgegangen sind und bei denen ich Autor bin, entsprechen den URM (s.o) und werden von mir verantwortet.

Die Bedeutung dieser eidesstattlichen Versicherung und die strafrechtlichen Folgen einer unwahren eidesstattlichen Versicherung (§156,161 des Strafgesetzbuches) sind mir bekannt und bewusst.“

Datum

Unterschrift

"Mein Lebenslauf wird aus datenschutzrechtlichen Gründen in der elektronischen Version meiner Arbeit nicht veröffentlicht."





## Publikationsliste Gina Dji-In Eom:

1.  
Functional impairment of microglia coincides with Beta-amyloid deposition in mice with Alzheimer-like pathology.  
Krabbe G, Halle A, Matyash V, Rinnenthal JL, **Eom GD**, Bernhardt U, Miller KR, Prokop S, Kettenmann H, Heppner FL.  
*PLoS One*. 2013;8(4):e60921.
2.  
An unconventional role for miRNA: let-7 activates Toll-like receptor 7 and causes neurodegeneration.  
Lehmann SM, Krüger C, Park B, Derkow K, Rosenberger K, Baumgart J, Trimbuch T, **Eom G**, Hinz M, Kaul D, Habel P, Kälin R, Franzoni E, Rybak A, Nguyen D, Veh R, Ninnemann O, Peters O, Nitsch R, Heppner FL, Golenbock D, Schott E, Ploegh HL, Wulczyn FG, Lehnardt S.  
*Nat Neurosci*. 2012 Jun;15(6):827-35.
3.  
Essential role of interleukin-6 in post-stroke angiogenesis.  
Gertz K, Kronenberg G, Kälin RE, Baldinger T, Werner C, Balkaya M, **Eom GD**, Hellmann-Regen J, Kröber J, Miller KR, Lindauer U, Laufs U, Dirnagl U, Heppner FL, Endres M.  
*Brain*. 2012 Jun;135(Pt 6):1964-80.
4.  
A circadian clock in macrophages controls inflammatory immune responses.  
Keller M, Mazuch J, Abraham U, **Eom GD**, Herzog ED, Volk HD, Kramer A, Maier B.  
*Proc Natl Acad Sci U S A*. 2009 Dec 15;106(50):21407-12.

### Publication in revision:

Microglia are indispensable effector cells in AD immunotherapy.  
Eom GD, Prokop S, Heppner FL.  
*Sci Transl Med*. *In revision*

# Acknowledgements

“Bernard of Chartres used to say that we are like dwarfs on the shoulders of giants, so that we can see more than they, and things at a greater distance, not by virtue of any sharpness of sight on our part, or any physical distinction, but because we are carried high and raised up by their giant size.” *Metalogicon* (1159, John of Salisbury)

Frank L Heppner, for his tireless enthusiasm for my projects. You have an incredible intuition for scientific questions and I hope you will continue to follow them. I owe you much of my career, I know it's more than what I can fathom right now.

Stefan Prokop for his structure, for driving the projects forward and for his expertise in Alzheimer's disease and his brilliant scientific aptitude.

Roland E Kälin for his mentorship during my first year in the lab, his insurmountable help setting up day to day tools which everyone now relies on.

My parents for their substantial support. My brother for his kindness and support, and my cousins Tony and Iris. *An Manfred: vielen Dank für Deine Unterstützung während meiner Promotion.*

Pam Glowacki, who navigates the challenges of red tape with such grace and jubilee.

Everyone in my lab. Notably: Alex for taking care of every little ordering detail, Kerstin and Anja for taking care of the “little” but so *not* little things, Josefine Radke for our lab talks late at night, Johannes von Büren for our lab talks even later at night, Nicole Hentschel for your extreme kindness and gentle spirit. Josephin Held for being the best desk-neighbour I could ever wish for, Elif Gül for your infectious eagerness to learn new things, Gordon Wilke for ping-ponging immunology ideas back and forth on a frequent basis. Kelly R Miller for her memorable standard in professionalism with which she speaks about each coworker.

A special thank-you to Sarah Starossom for encouraging & inspiring me to stay in science and providing me with a much needed female role model in the lab. Golo Kronenberg for his personal counsel when I needed it the most.

Dr. Helmut Kettenmann and Dr. Ulrich Dirnagl for giving me the opportunity to be part of the Berlin community and their leadership of the program. Thank you for always championing Medical Neuroscience and inviting me to be part of it.

My dearest friends: you were my family in Berlin. I want to thank Ivo for when times were so rough; you prevented me from getting lost. Francesco for the countless coffee breaks and tireless fun. Anna for keeping things lighthearted and for bringing us all together. Ryan, our exciting discussions and debates which sometimes lasted days. Tatiana my kindred spirit. Julia Nichtweiss, my sweetest friend. My Luxembourg family for giving me respite, especially Ainsley – I thank you in every language that you and I speak together.

Last but not least Ken L, my higher conscience, my anchor, my soul mate, my everything. I cannot wait to live in a time zone closer to you again.